Cumulative Author Index 1995

Abdelouahab, F. B., 3231
Abi-Aad, E., 99, 3299
Aboluwoye, C. O., 2095
Aboukaïs, A., 99, 1025, 3299
Aboulayt, A., 2913
Abras, A., 3511
Abushamleh, A. S., 1607, 3309
Acharya, A. N., 1715
Achouri, M. E., 4105
Ackermann, M., 1625
Adams, D. J., 3303
Ågren, H., 4729
Ahmad, I. K., 2989
Ahmed, O., 603, 3795
Ai, X., 4121
Aich, S., 1593
Aihara, J-i., 237, 1563, 4349
Aika, K-i., 1805
Airoldi, G., 3969
Aïssi, F. C., 1025
Alagia, M., 575
Al-Akl, A., 3585
Alderson, A., 2671
Aliev, A. E., 2017, 3167
Allen, G. C., 2767, 3717
Alleres, D. R., 3357
Allgaier, J. B., 2403
Allott, R. M., 1297
Al-Obaidi, A. H. R., 411
Aloisi, G. G., 3117
Altricher, B., 1155
Amada, I., 2751
Ambrosone, L., 1339
Ameen, A. P., 1363, 2051, 3907
Amemiya, Y., 473, 1081
Amine, K., 4451
Amorelli, A., 517
Amos, Y. D., 517
Anderson, R. F., 2115
Ando, T., 3209
André, J-M., 1641
André, J. J., 1025
Andrés, E., 1217
Andrews, S. R., 1181, 1901
Andrzejewska, E., 2339
Anpo, M., 4279
Antos, G., 3933
Aoyama, E., 4139
Arabindoo, B., 4471
Arai, S., 597
Aramaki, K., 1477
Aravindakumar, C. T., 615
Aravindan, P., 2743
Arcoya, A., 1679
Arey, J., 3033
Armes, S. P., 905
Arriortua, M. I., 423
Arthur, N. L., 3367
Artizzu, P., 3263
Asakura, K., 4161
Aschmann, S. M., 3033
Ashfold, M. N. R., 773, 2715, 3327, 3339
Ashtekar, S., 1045
Ashton, L., 1631
Aslin, H. D., 2349
Asmus, K-D., 1923
Asscher, M., 3655
Atilgan, A. R., 2483
Atkinson, P. J., 2847
Atkinson, R., 3033
Attard, G., 3585
Auroux, A., 3263
Aveyard, R., 175, 2681
Avron, J. E., 4037
Axford, S. D. T., 827, 835
Babalola, J. O., 2095
Babu, G. P., 3983
Bach, J., 1229
Bachelier, J., 2907
Bacskay, G. B., 1587
Bagchi, S., 631
Bahar, İ., 2483
Bain, C. D., 1281
Baird, T., 3219
Balaji, S., 3949
Baldovino, D., 323
Bales, B. L., 2863
Balint, I., 1805
Balucani, N., 575
Bandosz, T. J., 493, 2929
Banerjee, D., 631
Banham, S. F., 4005
Baonza, V. G., 59
Barbaux, Y., 2899
Barbouth, N., 569
Barlow, S., 3303
Barnes, A. J., 3111
Barnes, J. C., 2149
Barrabass, S., 637
Barr-David, G., 1207
Barron, L. D., 2087
Barry, B. W., 3883
Bartels, D. M., 3127
Barthomeuf, D., 3281, 3291
Barton, S. S., 1529
Bartoszak, E., 87
Bartoszewicz, J., 2207
Basu, S., 1191, 1593
Basu Roy, M., 1191
Batamack, P., 3933
Batey, A. D., 2053
Battin-Leclerc, F., 1313
Bauer, C., 2053
Baumgartel, H., 3073
Baur, W. H., 2217
Bautista-Toledo, I., 3213
Baysal, C., 2483
Beadle, C. A., 887
Beamson, G., 3495
Becerra, R., 2723
Beck, A. J., 3907
Beer, P. D., 295, 4331
Beeston, M. A., 899, 1407
Beguin, F., 493
Behal, S. K., 2855
Belkoura, L., 3385
Bell, S. E. J., 411
Bellatreccia, M., 2045
Belletête, M., 2133
Belton, P. S., 1459
Bengtsson-Kloo, L., 4223
Benítez, J. J., 4477
Ben Maimoun, I., 493
Bennani, A., 99, 3299
Bensalem, A., 2185
Bent, B. E., 3645
Berclaz, T., 2155
Bergaoui, L., 2229
Berger, J., 4037
Bernardinelli, G., 2155
Bernazzani, L., 649
Berndt, H., 725
Berthier, Y., 569
Bertram, R., 1163
Bertrán, J., 1451
Beruto, D., 323
Beutl, M., 3639
Bhat, A. N., 3983
Bhat, R., 3983
Bhat, S. N., 681
Bhattacharyya, K., 1769
Bhattacharyya, M. M., 3373
Bhattacharyya, S. N., 1191
Bianchi, C. L., 3969
Bicerano, J., 2507
Bidoglio, G., 2275
Biehl, H., 3073
Bieske, E. J., 1
Biggs, P., 817, 3045
Biggs, S., 665, 2921
Bijma, K., 1229
Billing, R., 1625
Binder, K., 2369
Binet, C., 2913
Bisset, A., 499
Bitzer, T., 3627
Black, I. J., 4251
Blake, A. J., 2149
Blandamer, M. J., 1229, 4275
Bleha, T., 2465
Bloemink, H. I., 781, 1891, 2059
Błaszczak, Z., 2339
Boccuzzi, F., 3237
Boda, D., 889
Boddenberg, B., 163, 555
Bohmhammel, K., 3879
Boisdron, N., 2899
Bolis, V., 113
Bolton, R., 687
Bonifačič, M., 1923
Bonnelle, J-P., 99, 3299
Booth, C., 1357, 1491, 3461
Borade, R. B., 539
Bordiga, S., 525, 3285
Borg, H. J., 3679
Borodzinski, J. J., 2353
Borovkov, V. Yu., 2035
Borówko, M., 3195
Borzęcka-Prokop, B., 145
Boué, S., 3809
Bouih, H., 93
Bowker, M., 3663
Bowmaker, G. A., 133, 4149, 4321
Bozon-Verduraz, A., 2185
Bozon-Verduraz, F., 3291
Bradford, E. G., 2881
Bradley, R. H., 3201
Bradshaw, A. M., 3575
Bramley, R., 1207
Branton, P. J., 1139, 2041
Bräuer, P., 535
Braunschweig, T., 1091, 1539
Brevet, P. F., 1763
Brewbaker, J. L., 2507
Bridier, I., 3033
Briend, M., 3281, 3291
Briggs, B., 4275
Brint, P., 2699, 3083
Briscoe, B. J., 1787
Brocklehurst, B., 223
Brogan, M. S., 733
Brouwer, A. M., 2107
Brown, D. R., 1031
Brown, J. M., 2999
Brown, R., 1131
Brown, S. E., 1013, 4335
Brownsword, R. A., 191
Brückner, A., 725, 1173
Brumby, S., 1207
Brun, A. M., 4047
Brzezinski, B., 3141
Buffon, R., 3511
Bui, V. T., 2797
Büker, K., 725
Bulthuis, J., 205
Buma, W. J., 773, 2715, 3339
Burford, M. D., 1333
Burgess, J., 1229
Burnell, E. E., 4127
Burrows, H. D., 3913
Busca, G., 1861
Bushev, V. Ph., 149
Buxton, G. V., 279, 1631, 3303
Buzza, M., 2403
Buzzoni, R., 525
Cabañas, A., 2779
Cabañas Galan, B., 1185
Cabani, S., 649
Cáceres, M., 59, 1941
Cai, S-H., 479
Cairns, J. A., 733
Calvaruso, G., 1075
Calvo, E. J., 2323, 4083
Calvo, R., 423
Campbell, K. C., 3219
Campbell, M. L., 3787
Campbell, S. A., 2331
Campelo, J. M., 1551, 4171
Camplin, J. P., 3563
Cané, E., 3741
Canevali, C., 3969
Canosa-Mas, C. E., 817, 2269, 3045
Cardozo, M. G., 2515
Care, C. M., 2593
Carl, W., 2525
Carley, A. F., 2167
Carlsson, M., 2081
Carrasco, N., 3839
Carrasco-Marín, F., 3519
Carrier, M., 1241
Carrington, A., 1887, 3725
Carrott, P. J. M., 2179
Carss, S. A., 3167
Carver, T. J., 3449
Casavecchia, P., 575
Casey, N. J., 3269
Castillo, J., 3809
Castner, E. S., 2655
Castner Jr., E. W., 867
Castro, G. R., 3639
Cataluña, R., 1679
Catlow, C. R. A., 3975
Cemič, F., 3633
Cerrato, G., 113, 125
Ceulemans, A., 3089
Chabanel, M., 4395
Chachaty, C., 3299
Chadwick, B. L., 1931
Chakrabarty, D. K., 1045
Champagne, B., 1641
Chan, R. K., 3063
Chan, W-T., 1717, 3747
Chandra, P., 23
Chang, T-h., 375
Chang, Z., 2319
Chao, K-j., 167
Chapman, R. G., 4127
Charara, M., 1207
Chartier, P., 1871
Chatterjee, A., 4313
Chen, C., 1179
Chen, F., 847
Chen, J-H., 3873
Chen, J-S., 469
Chen, K. Y., 2817
Chen, L-W., 3873
Chen, T. Y., 1787
Chen, Y., 381
Chen, Z., 295, 4331
Cheng, C-F., 2955, 3995
Chesters, M. A., 2191, 2203
Chi, Q., 1471
Chilukuri, S. V. V., 1045
Chinake, C., 1635
Cho, S. J., 3245
Choi, M. F., 881
Chopra, N., 4127
Chorkendorff, I., 1267
Chou, S-C., 949
Choudhary, V. R., 843, 2935
Chowdhury, R., 681
Christian, F. R., 2671
Chuang, Y-F., 4127
Chudek, J. A., 2149
Chun, W-J., 4161
Cifra, P., 2465
Clark, D. C., 1991
Clark, G. R., 1523
Claxton, T. A., 3015
Clearfield, A., 539
Cleaver, B., 3869
Cleland, G., 4001
Clifford, A. A., 1333
Clint, J. H., 175, 687, 2681
Coats, A. M., 3703
Codd, R., 1207
Coluccia, S., 2961
Compañ, V., 4235
Conesa, J. C., 1669, 1679
Connerton, J., 1841
Conti, F., 3813
Conti, G., 649
Contreras, R. H., 4031
Conway, B. E., 283
Cook, J. C., 3563
Cooke, S. A., 1891
Cooney, R. P., 133, 4149, 4321
Cooper, A., 2087
Cooper, D. L., 749, 3357, 3363, 3751, 4011
Cooper, E., 3703
Cooper, I. A., 3367
Corn, R. M., 1411, 2353
Cornec, M., 1991
Coronas, A., 2071
Correia, N. T., 2003
Corvaja, C., 3813
Coto, B., 273, 2779, 4381
Coulter, P. D., 2615
Coulthurst, S. J., 1751
Couris, S., 3083
Courtieu, J., 1371
Cowie, B. C. C., 3555
Cox, P. A., 2331
Cox, R. A., 3027, 4189
Cracknell, R. F., 1377
Creasey, J. C., 3073
Cremer, P. S., 3671
Cremonese, F., 3813
Cruzeiro-Hansson, L., 251, 1465
Cullis, P. M., 1229, 4275
Cunningham, T. P., 3357
Curro, J. G., 2427
Czarnecki, M. A., 697
da Costa Faro Jr, A., 741
Dai, S., 1179
Daïmellah, A., 3555
Damilano, N., 2961
Danilowicz, C., 4083
D'Aprile, F., 3969
Darling, G. D., 4199
Das, K., 1769
Das, S., 1769
Dash, A. C., 1715
Datta, K., 3095
David, E. F., 2411
Davidson, G., 3897
Davies, P. B., 2993
Davies, P. R., 2885
Davis, M. I., 2291, 3553
Davis, R. J., 1825
DeArmitt, C., 905
De Asha, A. M., 3611
de Boer, E., 1519
Dega-Szafran, Z., 87
de Lange, C. A., 773, 2715, 3339
Delichère, P., 2891
Della, E. W., 4031
Della Védova, C. O., 231
Delpuech, J-J., 2307
del Rio, J. M., 2805
De Maeyer, L., 303
Demontis, P., 525
Deng, N., 1357
Deng, Y., 4215
Denkov, N. D., 3415
Denny, W. A., 2115
De Robertis, A., 1619
Deronzier, A., 1241
D'Errico, G., 1339
de Segovia, J. L., 3569
Deshpande, D. K., 623
Desquilles, C., 1025
De Stefano, C., 1619
Devonshire, R., 1445
Dhariwal, H. S., 3569
Dharmalingam, P., 2743
Di Bella, S., 2709
Dickinson, E., 51, 2847, 4413
Dilger, H., 1935
Dines, T. J., 463, 499, 733
Dippel, O., 3633
Disdier, J., 2343

Disko, M., 2855
Dixon, R., 3495
Do, D. D., 1695
Doblhofer, K., 1949
Dobrokhotova, Zh. V., 703
Doherty, S., 1853
Doi, M., 1967, 4143
Dolling, S. J., 2059
Dong, S., 1471
Dorémieux-Morin, C., 3933
Dossi, C., 2045
Doubova, L. M., 3311
Doughty, A., 1587
Douhéret, G., 2291, 3553
Dourdin, M., 1025
Dozier, W. D., 2855
Drew, M. G. B., 3449
Drozdowski, M., 2339
Duarte, F., 1203
Duer, M. J., 559, 963
Duffy, J. A., 3485
Durocher, G., 2133
Dutta, R. K., 681
Dyson, P. J., 2149
Dziembowska, T., 77
Easton, C. J., 1013, 4335
Edwards, H. G. M., 1439, 1445, 3883
Egdell, R. G., 3495
Eguchi, T., 2949
Ehrensberger, K., 1935
Einicke, W-D., 535, 971
Elangovan, S. P., 4471
Eliet, V., 2275
Elimelech, M., 3389
Elisei, F., 3117, 3405
Elliott, A. J., 3659
Emanuele, A., 3803
Emerson, A. P. J., 3441
Engberts, J. B. F. N., 1229, 4275
Eriksson, L. A., 4343
Erman, B., 2483
Eskendirov, I., 991
Essassi, E. M., 4105
Estevão Candeias, A. J., 2179
Etchenique, R., 4083
Ettema, A. R. H. F., 3555
Evans, A. C., 4467
Evans, C., 1723
Evans, K. E., 2671
Fairbrother, D. H., 3619
Fan, G., 3475
Fantola Lazzarini, A. L., 419
Farbotko, M., 3481
Farrell, R. P., 1207
Farwell, D. W., 3883
Fattepur, R. H., 623
Faucheux, L. P., 3163
Fausto, R., 1571, 3755
Favaro, G., 3405, 4099
Fawcett, V., 1439, 1445
Fehér, M., 1063
Fendler, J. H., 673
Fereday, R. J., 1759
Ferino, I., 3263
Fernández, J., 2071
Fernando, K. R., 1759
Ferrarini, A., 3177
Ferreira, J. A., 3913
Ferro-García, M. A., 3213
Ferroni, L., 113, 125
Fidler, V., 867
Fields, M., 1445
Finocchio, E., 1861
Firth, S., 975
Fischel, L. B., 2381
Fischer, R., 1303
Fishtik, I., 259, 1325
Fitzsimons, N. P., 713, 719
Fleming, G. R., 867
Florêncio, M. H., 1203
Fluendy, M. A. D., 2249
Fontana, A., 3809
Ford, S. J., 2087
Fornasiero, D., 1997
Fornili, S. L., 3803
Forrest, B. M., 2355
Foti, C., 1619
Fowler, P. W., 1421, 2241, 3089
Fracheboud, J-M., 817, 3045
Fragalà, I. L., 2709
Fraissard, J., 1037, 3933
Franck, R., 2229
Franco, M. L. T. M. B., 3821
Franke, O., 937
Franks, F., 1511
Frederick, B. G., 3627
Freire, F. G., 2343
Freshwater, R. A., 3027
Frey, H. M., 2723
Fruböse, C., 1949
Fuess, H., 1813
Fujii, T., 4279
Fujii, Y., 2319
Fukuda, K., 1111, 1117, 1125
Furlong, D. N., 665, 3399
Furuta, T., 4139
Furuya, H., 983
Gabelica, Z., 2213
Gale, J. D., 3537
Galiatsatos, V., 2655
Galiazzo, G., 3117
Galiński, M., 1097
Gammie, D. I., 1887
Ganapathy, S., 3549
Gao, M., 4121
García, J., 2071
García-Antón, J., 1345
Gardner, P., 3575
Gatehouse, B., 3347
Gay, D. H., 925
Geobaldo, F., 3285, 4445
Geoffroy, M., 2155
George, A. R., 3975
Gerratt, J., 749, 3357, 3363, 3751, 4011
Gerry, M. C. L., 3347
Gianguzza, A., 1619
Gill, D. S., 2307, 2789
Gill, P. M. W., 4337
Gillespie, S. E., 4207
Gillies, D. G., 887
Girault, H. H., 1763
Giribet, C. G., 4031
Giuffrè, L., 3969
Gladden, L. F., 559, 963
Gläser, B., 971
Glasser, L., 991
Gloriozov, I. P., 3779
Godward, J., 1491, 3461
Gohshi, Y., 895
Goldbeck-Wood, G., 2587
Golman, B., 1391
Gonbeau, D., 93
Gonzalez, E. R., 1005
González-Lafont, A., 1451
González-Ureña, A., 389
Goodfellow, J. M., 251, 1465
Goodings, J. M., 2257
Goodman, D. W., 3709
Góralski, J., 3481
Gordon, M. S., 2723
Görgényi, M., 1303
Göritz, D., 2649
Görner, H., 3117
Goslar, J., 2207
Grady, A. S., 3015
Grange, P., 4477
Grech, E., 77
Green, D. A., 4467
Green, N. J. B., 223
Gregory, R. E., 451
Grenthe, I., 2275
Grice, S. T., 4355
Grieser, F., 665, 2843, 3399
Griffiths, J. A., 687
Griffiths, T. R., 3101
Grima, R., 1345
Grimmer, N. E., 1741
Gritzner, G., 875, 3843
Groen, C. P., 2107
Grofcsik, A., 1297
Grolier, J-P. E., 1941
Gu, G., 3021
Gualberto Volpi, G., 575
Gubbins, K. E., 1377
Guelton, M., 1025
Guglielminotti, E., 3237
Guillard, C., 1853
Guiñón, J. L., 1345
Guo, C. J., 1143
Guo, J., 1835
Guo, Q., 3663
Guo, X-C., 3685
Gutman, I., 259, 1325
Hadden, R. A., 3659
Hadjiivanov, K. I., 149
Hage, W., 2823
Hajji, M. S., 4105
Hakushi, T., 4079
Hall, C., 4423
Hall, P. G., 1139, 2041
Hallbrucker, A., 2823
Hallén, D., 2081
Halliday, I., 2593
Hamada, K., 1601
Hamakado, M., 4161
Hamakawa, S., 1655
Hamanoue, K., 607, 855
Hamilton, P. A., 2989, 2993
Hanabusa, K., 2877
Handford-Styring, S. M., 1431
Haneda, M., 4459
Hanken, D. G., 1411, 2353
Hanna, S., 2615
Hanson, G. R., 1207
Hao, L., 2837
Harada, S., 3525
Hardman, P. J., 3569
Harland, P. W., 4355
Harriman, A., 4047
Harris, F. M., 1181, 1901
Harris, K. D. M., 1497, 2017, 3167
Harris, K. R., 4071
Harris, R. K., 805, 1795, 3167
Harrison, C. C., 4287
Harrison, I. M., 3919
Harwood, M. H., 3027
Haselbach, E., 3123
Hashim, R., 2141
Haskard, C. A., 1013, 4335
Hasselbrink, E., 3633
Hatayama, F., 1557, 3505
Hattori, H., 2961
Haubtmann, C., 1025
Hawkins, P., 881
Hawthorne, S. B., 1333
Hayakawa, T., 1111, 1117, 1655
Hayashi, H., 31
Hayhurst, A. N., 827, 835, 2257
Hayhurst, D. T., 1143
Hayman, G. D., 1313, 1911
He, H., 77, 2955, 3925, 3995
Healy, A., 1735
Healy, T. W., 2921
Heatley, F., 1491, 3461
Hébert, P., 1763
Hecht, L., 2087
Heeribout, L., 3933
Hefter, G. T., 2789
Hegarty, J. N. M., 411
Heger, R., 3385
Heil, S. R., 1877
Heineking, N., 3347
Hensel, K. D., 2999
Henshaw, G. S., 3307, 4299
Herley, P. J., 713, 719
Herreros, B., 1147
Herrington, T. M., 4251
Herrmann, J-M., 2343, 3231
Hester, R. E., 411, 1751
Heuchel, M., 535, 971
Hewitt, D., 1997
Hey, M. J., 3897
Heyes, D. M., 687, 1975
Hibbs, D. E., 3925
Hibino, T., 1955, 4419
Higgins, D. A., 1411, 2353
Higgs, P. G., 2531
Hikosaka, M., 2573
Himo, F., 4343
Hinds, K., 1891, 2059
Hirai, K., 895
Hirai, M., 473, 1081
Hirai, T., 473
Hirao, H., 445
Hirst, D. M., 793, 2053, 3783
Hixson, H., 3593
Hoang, D. L., 4441
Hobdell, J. R., 2497
Hochard-Poncet, F., 2891
Hohm, U., 1277
Høiland, H., 2291, 3553
Hollas, J. M., 197
Holliman, P. J., 3219
Hölsä, J., 1503
Holz, M., 1877
Hong, P., 1179
Hopfinger, A. J., 2515
Horiai, K., 3007
Horn, A. B., 4005
Horne, D. S., 2847
Horrocks, B. R., 4001
Hörzenberger, F., 3843
Hosamani, M. T., 623
Hosoe, M., 2319
Houlton, A., 4001
Hounkonnou, M. N., 41
Howard, J. A., 17, 799
Howard, S. T., 3925
Howe, J. D., 773, 2715
Hoyle, R., 3219
Hsu, J-P., 1223, 4093
Huang, R-b., 987
Hubert, S., 2767
Hughes, C., 517
Hughes, N. P., 1407
Hughes, R. A., 2999
Hunger, M., 1813
Hunter, C. A., 2009
Hunter, G., 2149
Hursthouse, M. B., 3925
Husain, D., 811
Husband, F., 1991
Hussein, G. A. M., 1385
Hutchings, G. J., 141
Iglesias, E., 1349
Ikawa, S-i., 3379
Ikier, Ch., 3385
Ilczyszyn, M., 1611, 3859
Ilett, S. M., 3897
Imamura, S., 1261
Inglot, A., 145
Insausti, M., 423
Inui, T., 1103
Irwin, J. A., 1207
Ishchenko, S. Y., 3779
Ishida, M., 2663
Ishiguro, S-i., 2313, 3851
Ishikawa, Y., 597
Isoda, T., 3525
Ito, O., 2287
Ito, T., 1261
Iwade, T., 1801
Iwahara, H., 1955
Iwahashi, M., 697
Iwamoto, E., 627
Iwamoto, M., 767
Iwasaki, M., 983
Iwasawa, A., 445
Iwasawa, Y., 1663, 4161
Izatt, R. M., 4207
Izawa, K., 1103
Izumi, J., 767
Jackson, P., 805
Jackson, R. A., 4133
Jackson, S. D., 3269
Jagiełło, J., 493, 2929
Jain, A. N., 1871
Jakobsen, H. J., 4423
Jalowiecki-Duhamel, L., 2899
Jancke, K., 1155, 1163
Jaskólski, M., 87
Jeevarajan, A. S., 2881
Jehng, J-M., 953, 3245
Jenkin, M. E., 1911
Jerkiewicz, G., 2353
Ji, H-F., 2761
Ji, J-Y., 1207
Jiang, D-z., 1835
Jiang, M., 1845
Jimenez, R., 867
Jin, Y. S., 381
Jobic, H., 2891
Jochims, H. W., 3073
Johari, G. P., 329, 337, 343
Johnson, B. F. G., 2149
Johnson, D. F., 3695
Johnson, J. M., 2403
Joly, H. A., 799
Joly, J-P., 3213
Jones, F. R., 1363, 2051, 3907
Jones, J., 1587
Jones, J. P., 3147
Jones, M. J., 1497
Jones, M. N., 2805
Jones, R. G., 3555, 3603
Jones, R. L., 3027, 4189
Jones, W., 77, 713, 719
Jones, W. J., 1297, 3101
Jonnalagadda, S. B., 1635
Jonquières, A., 1247
Joyce, S. J., 2491
Joyner, R. W., 1497, 1841, 3663
Jung, C. G., 3809
Kabongo, B., 991
Kacker, N., 2457
Kacperska, A., 1229, 4275
Kaizu, Y., 437
Kakuta, N., 4459
Kameyama, T., 1111, 1117, 1125
Kamieńska-Piotrowicz, E., 71
Kamo, M., 3209
Kan, J., 1179
Kanai, H., 1261
Kanamura, K., 3469
Kaneko, K., 2161
Kanno, T., 1391
Kapteijn, G. M., 2009
Karadakov, P. B., 749, 3357, 3363, 3751, 4011
Karasawa, O., 437
Karge, H. G., 549, 1845, 2035
Kasprowicz, D., 2339
Kassner, D., 2217
Kastner, T. M., 1877
Katsanos, N. A., 485
Kaulgud, M. V., 999
Kavassalis, T. A., 2541
Kawaguchi, J-i., 1103
Kawai-Hirai, R., 1081
Kawakami, Y., 2515
Kawasaki, S., 3209
Kawashima, T., 4375
Kayakawa, T., 1125
Kazansky, V. B., 385
Keane, M., 905
Kępiński, L., 507
Kegley-Owen, C. S., 3055
Keller, A., 2573
Kelly, K. K., 3063
Kemball, C., 741, 1131
Kemp, T. J., 3893
Kendrick, J., 2609
Kennedy, J. C., 911
Kentgens, A. P. M., 1519
Kerkar, M., 3555
Kershaw, D., 1067
Kessling, G., 303
Kestilä, E., 1503
Kevan, L., 3987
Khodakov, A., 569
Khodakov, A. Yu., 385
Kholodenko, A. L., 2473
Khoo, K. H., 1759
Khoshtariya, D. E., 1625
Kijlstra, S., 3245
Kikuchi, Y., 643
Kilmartin, P. A., 4403
Kim, S-C., 2945
Kimura, K., 1237
Kimura, M., 1967, 4143
Kimura, T., 4079
Kinart, C. M., 65
Kinart, W. J., 65
King, F., 141
Kintscher, K., 1173
Kirtman, B., 1641
Kishore, N., 2101
Kispert, L. D., 2881

Kitchen, S. J., 1459
Kitching, X. J., 3627
Klein, H., 1813, 3385
Klein, M. L., 2633
Klinowski, J., 77, 1147, 2955, 3925, 3995
Klissurski, D. G., 149
Knoche, W., 637
Kobayashi, H., 3771
Kobayashi, K., 473, 1081
Kobayashi, M., 1391
Kobayashi, S., 2877
Kobayashi, T., 1271
Kocjan, D., 2811
Koda, S., 445
Koide, M., 2313, 3851
Komatsu, T., 3275
Kondo, S., 319
Kong, Y. C., 4261
Konishi, S., 1557
Kontturi, A-K., 3433
Kontturi, K., 3433
Kooreman, P. A., 1229
Kornatowski, J., 2217
Koronaios, P., 3869
Kotov, N. A., 673
Kourouklis, H. N., 3963
Kowalak, S., 385
Kowalewski, J., 215
Koyama, K., 1051
Koyama, T., 2877
Kozawa, M., 1103
Kozielski, M., 2339
Krägel, J., 1991
Kralchevsky, P. A., 3415
Kreitmeier, S. N., 2601
Krishnasamy, V., 4471
Kristl, A., 995
Krzyzanowska, E., 657
Kubinyl, M., 1297
Kuczkowski, R. L., 975
Kudo, Y., 4079
Kulbida, A., 1571, 3755
Kumamaru, T., 627
Kumar, S. K., 2457
Kunimori, K., 1801
Kuo, Y-C., 1223, 4093
Kurimura, Y., 2877
Kurzawaski, I., 1163
Kustov, L. M., 385
Kuwahara, Y., 1955, 4419
Kuzenkov, S., 2217
Kwok, E. S. C., 3033
Kyd, G. O., 3485
Kytökivi, A., 941
Laasonen, K., 2633
Lafont, F., 1551, 4171
Laha, A. K., 631
Lahiri, P., 3489
Lahousse, C., 2907
Lainez, A., 1941
Lajoie, P., 2291, 3553
Lam, H. N., 4071
Lamb, J. D., 4207
Lambert, J-F., 2229
Lamberti, C., 113
Lamont, C. L. A., 3575
Lancaster, N. M., 269
Lane, E., 3083
Langenfeld, J. J., 1333
Langer, S., 405
Langner, R., 3831
Lanza, G., 2709
Lasson, E., 3111
Latterini, L., 3117
Laurent, Y., 4477
Lavalley, J-C., 2907, 2913
Lay, P. A., 1207
Lazana, M. C. R. L. R., 3821
Lazzarini, E., 419
Lazzeretti, P., 4031
Leaist, D. G., 2837
Leaver, M. S., 4269
Le Bail, M., 1241
Lebeau, L., 4329
Lefley, C. R., 411
Legido, J. L., 2071
Legon, A. C., 781, 1881, 1891, 2059
Lei, J., 811
Lemański, D., 3925
Lenik, M., 3481
Lennon, D., 2191, 2203
Leofanti, G., 3263
Léonard, J., 2797
Leong, Y-K., 2921
Leontidis, E., 2355
Lepori, L., 431, 1885
Lesot, P., 1371
Levasseur, A., 93
Levendis, D. C., 1741
Lewandowski, A., 875, 1097
Lewis, D. W., 3537
Lewis, T. J., 3147
Lezama, L., 423
Li, H-f., 13
Li, H., 1271, 1357, 3021
Li, Y-W., 3255
Li, Y., 3663
Liang, G. L., 2601
Libchaber, A., 3163
Lieske, H., 4441
Lin, F-c., 987
Lin, J., 847
Lin, M. Y., 2855
Lin, S-H., 949
Lincoln, S. F., 1013, 4335
Lindblad, M., 941
Lineton, W., 905
Linney, R. E., 3015
Linse, P., 2081
Lippert, R., 971
Liszi, J., 889
Littlewood, D., 1407
Litvina, A. D., 703
Liu, C-W., 479
Liu, C-Y., 917
Liu, X., 759, 1567
Liu, Y., 697
Liu, Y. R., 2817
Liu, Z-T., 3255
Liu, Z-y., 987
Livneh, T., 3655
Ljungström, E., 405
Lloyd, F. R., 1357
Lluch, J. M., 1451
Lochert, I. J., 4031
Lochon, P., 1247
Loewenstein, M., 3063
Löffler, E., 1155, 1163
Lohse, U., 1155, 1163, 1173
López, E. R., 2071
Lopez, M. R., 1941
Lopez-Castañares, R., 3185
Lorimer, J. P., 1067
Loton, N., 4287
Lourenço, J. P., 2213
Lovell, M. R., 1783
Lowenstein, A., 1371
Łomnicki, S., 2207
Lu, X-J., 2009
Luan, Z., 2955
Lücke, B., 725
Luckham, P. F., 1787
Luckhurst, G. R., 2141, 3177
Luk, S. Y., 905
Ma, J., 1835
Macdonald, J. N., 789
Mack, H-G., 231
Mackie, J. C., 1587
Maclagan, R. G. A. R., 4355
Macmillan, M. G., 3157
Macpherson, J. V., 899, 1407
Madix, R. J., 3685
Mahdyarfar, A., 2017
Mahmood, Z., 3015
Maiti, N. C., 4369
Malagoli, M., 4031
Malatesta, V., 4099
Malikova, A. B., 13
Malone, T. M., 3303
Mamaev, V. M., 3779
Man, P. P., 1037, 3281
Mandal, P. C., 1191
Mandler, D., 1019
Mano, J. F., 2003
Manolopoulos, D. E., 1421
Mansani, R., 3263
Mansur, H. S., 665, 3399
Marchand, R., 4477
Marcus, Yizhak, 427
Mariani, M., 419
Marinas, J. M., 1551, 4171
Markoulides, T., 1741
Markwell, R. D., 3015
Marques, H. M., 1741
Marsicano, F., 1741
Marston, G., 1185, 3045, 4059
Martin, A., 725
Martin, P. A., 1063
Martin, R., 3575
Martinez-Arias, A., 1669, 1679
Martorana, V., 3803
Martra, G., 2961
Maruoka, S., 2877
Maruthamuthu, P., 2743
Marychurch, M. S., 665
Masegi, A., 1955
Mason, B. P., 2723
Mason, R. S., 1297
Mason, T. J., 1067
Massiani, P., 3291
Massucci, M., 269
Mataga, N., 4047
Mathes-Juventin-Andrieu, I., 1025
Matos, M. A. R., 1907
Matsuda, J., 1477
Matsumoto, A., 1707
Matteoli, E., 431, 1885
Mattice, W. L., 2435
Maugé, F., 2907
Maung, N., 3475
Mayadevi, S., 2935
Mayer, E., 2823
McCague, C., 799
McCann, G. F., 4321
McCash, E. M., 3563
McClean, R. E., 3787
McCoustra, M. R. S., 4005
McDougall, G. S., 1131
McGarvey, J. J., 411
McGimpsey, G., 17
McLeish, T. C. B., 2403
McNaughton, D., 1723
McTigue, P. T., 451
Meadows, J., 911, 3919
Meddour, A., 1371
Meenan, P., 4133
Mehrotra, S. C., 623
Meijers, S., 1861
Meldrum, F. C., 673
Melrose, J. R., 1975
Meltzer, S., 1019
Menduiña, C., 2779
Menetrier, M., 93
Merlet, D., 1371
Messina, G., 3263
Messow, U., 535
Mesuda, K., 1601
Metaxa, H., 485
Metson, J. B., 133, 4149
Mezyk, S. P., 3127
Mezzasalma, S., 323
Miguel, M. da G., 3913
Miki, S., 607
Miklavc, A., 2811
Milan, J. B., 773
Mile, B., 17, 3799
Milewski, M., 197
Millar, G. J., 133, 4149, 4321
Miller, D. J., 1333
Miller, R., 1991
Min, E-z., 1835
Minaev, B., 1729
Minagawa, K., 1051
Mioskowski, C., 4329
Misono, M., 367
Mita, S., 319
Mitchell, P. C. H., 749, 4467
Mitchell, P. J., 1975
Mitsuishi, M., 1601
Mittal, J. P., 615, 2121
Miyamura, K., 895
Miyanaga, T., 4389
Miyata, H., 1557, 3505
Mizuhata, M., 4451
Mizukami, F., 2161
Mizuno, M., 1955
Mizushima, T., 4459
Mjojo, C. C., 4009
Mo, Y., 241
Moen, A., 3189, 3529
Mogutnov, B. M., 703
Mohan, H., 615, 2121
Moise, A., 1425
Mollica, V., 649
Monnier, A., 2899
Montanaro, L., 113
Montejano, H. A., 1197
Montenegro, L., 1349
Moore, C., 3041
Moore, E. A., 1735, 2871
Moore, J. N., 411, 1751
Morais, V. M. F., 1907
Morales, C., 3185
Moraweck, B., 2891
Morazzoni, F., 3969
Morel, J-P., 2771
Morel-Desrosiers, N., 2771
Moreno-Castilla, C., 3213, 3519
Morgan, R. A., 773, 2715, 3327, 3339
Morley, C. P., 1901
Morley, J. O., 2067
Morrison, R. J. S., 1931
Morterra, C., 113, 125
Mortimer, M., 2871
Motheo, A. J., 1005
Moule, D. C., 399
Moura Ramos, J. J., 2003
Moutet, J-C., 1241
Mowbray, A. P., 3603
Moyer, B. A., 4215
Mukherjee, A. K., 3095
Müller, H. S. P., 3347
Müller, M., 2369
Mulvaney, P., 2843
Muñoz-Caro, C., 399
Munro, O. Q., 1741
Murtomäki, L., 3433
Murugesan, V., 4471
Muryn, C. A., 3569
Myshakin, E. M., 3779
Na, K., 367
Nagayama, K., 3415
Nagypál, I., 259, 1325
Nair, A. C., 23
Naito, S., 1967, 4143
Najbar, M., 145
Nakai, T., 1261
Nakamura, J., 1655
Nakamura, K., 1081
Nakamura, N., 607, 2949
Nakanishi, K., 31
Nakashima, N., 1775
Nakayama, H., 2949
Nakayama, T., 607, 855
Nalezinski, R., 3575
Narikiyo, Y., 1775
Nascimento, S. M., 3913
Nassar, A-E. F., 1775
Natarajan, S., 3537
Nath, D., 1769
Naujok, R. R., 1411, 2353
Navaratnam, S., 3133
Navarrini, W., 3813
Navez, P., 41
Nemoto, H., 473
Ng, T-L., 3475
Nicholson, D., 1377, 4261
Nicholson, D. G., 3189, 3529
Nicholson, T. M., 2623
Nielsen, C. J., 3111
Niemantsverdriet, J. W., 3679
Nieminen, J., 1571
Nigam, S., 2133
Niño, A., 399
Nishi, N., 4063
Nishihara, H., 1477
Nishimoto, J., 627
Nishimoto, S-i., 1103
Nix, R. M., 3611, 3963
Nogaj, B., 3925
Noid, D. W., 2601
Nomura, H., 445
Nomura, M., 2319
Nordio, P. L., 3177
Norman, P. R., 1795
Nortier, P., 3941
Noto, R., 3803
Núñez, J., 59, 1941
Ochiai, S., 4079
Odelius, M., 215
Odriozola, J. A., 4477
Oed, W., 2369
Ogata, Y., 983
Ogden, M. I., 295
Ogilvie, J. F., 3005, 3007
Ogryzlo, E., 3021
Oguro, K., 4451
Ohira, M., 1601
Ohno, T., 1557, 3505
Ohtani, B., 1103
Ohtsu, K., 4375
Okada, H., 2573
Okada, T., 4047
Okal, J., 507
Okino, F., 3209
Okonjo, K. O., 2095
Okuhara, T., 367
Okuyama, M., 3379
Olaj, O. F., 2551
Oliveira, F. L., 2877
Oliveira, M. E. C. D. R., 3913
Olivieri, A. C., 3167
Olsson, U., 4269
Omenetto, N., 2275
Onishi, H., 1663
Onyestyák, G., 1399
Orbis, F., 59
Orlandi, G., 1421
Orlando, J. J., 3055
Orlik, M., 875
Orr-Ewing, A. J., 3327, 3339
Ortica, F., 3405, 4099
Ösawa, E., 1563
Oscarson, J. L., 4207
Osguthorpe, D. J., 2491
Otani, A., 855
O'Toole, L., 1363, 2051, 3907
Otsuka, K., 3953
Ouchi, M., 4079
Oudar, J., 569
Oya, M., 1081
Oyama, N., 1547
Ozaki, Y., 697
Ozutsumi, K., 4375
Packer, K. J., 2191, 2203
Padgett, J. A., 2491
Padley, M. B., 141, 1841
Padovan, M., 3263
Palacios, J. M., 1217
Palivan, C., 2155
Palmer, R. E., 3633
Pando, C., 273, 2779, 4381
Paolo Cavasino, F., 1075
Parker, K., 251
Parker, S. F., 517
Parlitz, B., 1155, 1163, 1173
Parma, L., 2275
Parry, D. E., 1181, 1901
Parsonage, N. G., 2971, 4261
Parsons, B. J., 3133
Parthun, M. G., 329
Paryjczak, T., 3481
Pascheto, W., 343
Patel, K. B., 2115
Pathmanathan, K., 337
Patterson, P. M., 2257
Pattrick, G., 1741
Paul, M., 3717
Paunov, V. N., 3415
Payen, E., 4467
Peat, R., 4299
Peeters, F., 3809
Peiffer, D. G., 2855
Peltre, M-J., 3281
Pemble, M. E., 3627
Peng, X. D., 3619
Perez, E., 4329
Pérez, V., 1451
Pérez-Herranz, V., 1345
Perpête, É., 1641
Perrichon, V., 2185

Persson, K., 2863
Petch, B., 3751
Petrik, T., 2551
Pfister-Guillouzo, G., 93
Phillips, C., 1901
Phillips, L. F., 4363
Phillips, Y., 283
Pichat, P., 1853
Piekara-Sady, L., 2881
Piekarski, H., 2299
Pieper, G., 2217
Piers, A., 105, 359
Piers, A. S., 1253, 3309
Pijolat, M., 3941, 4431, 4437
Pilgrim, A. J., 4331
Pilling, M. J., 4179
Pilloud, D., 3123
Pilz, W., 2217
Pimblott, S. M., 223
Pincet, F., 4329
Pinna, F., 3237
Pintauro, P., 2827
Pizarro, J. L., 423
Plachkevytch, O., 1729
Plato, M., 2881
Pletcher, D., 457
Poels, E., 3245
Point, J-J., 2565
Pokale, W. K., 999
Polson, J. M., 4127
Ponec, V., 1861
Portela, M. F., 2343
Porter, N., 517
Portsmouth, R. L., 559, 963
Possemiers, K., 2173
Pottage, C., 1795
Prakes Ramalho, J. P., 2179
Pratash, A. M., 1045
Pratt, K. F. E., 1961, 3307, 4299
Preis, W., 2127
Previtali, C. M., 1197
Price, C., 1357
Price, G. J., 2491
Price, R., 3585
Prieto, G., 2805
Prime, A. F., 3569
Prin, M., 3941
Prisyajnyuk, A. V., 3779
Pritchard, H. O., 1425, 1717, 3747
Proffitt, M. H., 3063
Psaro, R., 2045
Putyera, K., 493, 2929
Puyuelo, P., 2715
Puzzarini, C., 3741
Qian, H-B., 13, 2993
Qian, S. Y., 283
Rabeony, M., 2855
Radhakrishnan, T. P., 2739
Radziejewski, P., 3141
Raimondi, M., 3357, 3363, 3751, 4011
Raja, T., 3949
Rajasekaran, J. J., 2427
Rajput, A. M., 843
Rajumon, M. K., 2167
Ralston, J., 1997
Ramaprabhu, S., 2155
Ramírez, C. B., 3839
Ramos, M. N., 1571
Ramsay, D. A., 2975
Rao, B. S. M., 615
Rao, K. C., 1229
Rao, R. R., 615
Raos, G., 4011
Raos, G. M., 749
Rapold, R. F., 2435
Rasanen, M., 1571
Rasmussen, P. B., 1267
Rastogi, S., 2573
Ratajczak, H., 1611, 3859
Ratcliffe, N. M., 2331
Rathouský, J., 937
Ratliff, J. L., 2291, 3553
Rattigan, O. V., 4189
Raval, R., 3703
Ravi, M., 2739
Ravikanth, M., 4369
Ravishankar, R., 3549
Recchia, S., 2045
Reed, C. L., 3327
Rees, L. V. C., 1399, 2027, 4309
Reijerse, E. J., 1519
Ren, X-M., 917
Rendulic, K. D., 3639
Renouprez, A. J., 2891
Renuncio, J. A. R., 273, 2779, 4381
Rey, F., 3537
Rezende, M. C., 3839
Rhodes, C. N., 1031
Ribeiro, F. R., 2213
Ribeiro, M. F., 2213
Ribeiro Carrott, M. M. L., 2179
Ribeiro-Claro, P. J. A., 197
Ribeiro da Silva, M. A. V., 1907
Ricchiardi, G., 3285
Richardson, N. V., 3627
Richardson, R. M., 2847
Richmond, W., 657
Rieley, H., 2349
Rivera-Utrilla, J., 3213
Robb, I. D., 3901, 3919
Robert, J-L., 2229
Roberts, K. J., 4133
Roberts, M. W., 2167
Robertson, E. G., 1723
Robertson, S. H., 4179
Robson, E., 2609
Rocha, J., 2213
Rochester, C. H., 105, 141, 359, 733, 1253, 3309
Rockland, U., 3073
Rodehüser, L., 2307
Rodger, P. M., 3449
Rodriguez, C., 3185
Roduner, E., 1935
Roessner, F., 1091, 1539
Roewer, G., 3879
Rohl, A. L., 925
Roizard, D., 1247
Rojo, T., 423
Roland, U., 1091, 1539
Román, E., 3569
Romano, S., 2141
Romanowski, S. J., 65
Romm, L., 3655
Rongère, P., 2771
Root, A., 941
Rosenthal, S. J., 867
Roser, S. J., 1783
Rosmus, P., 2053
Roubani-Kalantzopoulou, F., 485
Rouzaud, J-N., 493
Rowley, D. M., 3027
Rubini, P., 2307
Rubio, J. E. F., 59
Rubio, R. G., 273, 1941, 2779, 4381
Rudham, R., 1689
Ruiz de Azúa, M. C., 4031
Rull, F., 3883
Rusling, J. F., 1775
Russell, D. K., 3015
Russell, M. P., 1751
Rynkowski, J. M., 3481
Ryoo, R., 3245
Rżysko, W., 3195
Rønning, M., 3189
Sabulal, B., 2101
Sachleben, R. A., 4215
Sagara, T., 1775
Saito, K., 3795
Sakakini, B., 3659
Sakata, T., 603
Sakauchi, J., 1271
Sakka, T., 983
Sakuma, A., 4139
Salem, M., 4105
Salh, J. S., 191
Salim, P. H., 245
Salmon, G. A., 3303
Salzer, R., 1091
Samanta, A., 2739
Sammartano, S., 1619
Sanchez, V., 3185
Sano, T., 1533
Santhanalakshmi, J., 3949
Santos, Â., 1203
Saramago, B., 1203
Sarkar, N., 1769
Sarmiento, F., 2805
Sarpal, R. S., 2133
Sarre, P. J., 2053
Sartorio, R., 1339
Sasaki, Y., 2287
Sase, M., 2751
Sato, K., 1111, 1655
Sato, S., 4139
Sato, T., 3771, 4419
Sato, Y., 3209
Sauvage, A., 3291
Sawa, Y., 4389
Sawada, K., 643
Sayag, C., 3537
Sayle, T. X. T., 1465
Sbriziolo, C., 1075
Scales, P. J., 2921
Scarano, D., 3285, 4445
Scheier, E., 1163
Scherzo, K., 1303
Schiffrin, D. J., 3433
Schöllner, R., 535
Schöneich, C., 1923
Schoonheydt, R. A., 953, 3245
Schreier, E., 1155, 1173
Schrems, O., 1571, 3755
Schuchardt, U., 3511
Schuddeboom, W., 2107
Schulz, P., 569
Schulz-Ekloff, G., 937
Schuppert, A. A., 2629
Schwarz, J. A., 493, 2929
Schweiger, A., 177
Schweizer, K. S., 2411
Scragg, G., 3555
Seakins, P. W., 4179
Sekiguchi, S., 3379
Semmer, V., 3933
Sen, T., 3549
Senanayake, G., 2789
Senba, M., 1935
Sengupta, S. K., 3489
Seoane, X. L., 1679
Seres, L., 1303
Setser, D. W., 2979
Shah, D. B., 1143
Shalaev, E. Y., 1511
Shallcross, D. E., 817, 3045
Shannon, I. J., 1497
Shaw, A. M., 1887, 3725
She, Y., 847
Shen, D-L., 1425
Shen, D., 1399, 1717, 2027, 3747
Shen, J-p., 1835
Shen, J., 4121
Shen, P. K., 2817
Sheng, E., 3201
Sherman, J. C., 4127
Sherwood, P. M. A., 3593
Shi, W-G., 469
Shinkai, S., 1237
Shirai, H., 2877
Shizuka, H., 2751
Short, R. D., 1363, 2051, 3907
Shukla, N., 2885, 3627
Siddiqui, M. R. H., 1497
Signoretto, M., 3237
Sillman, P. D., 3799
Simha, R., 2443
Simon, S., 1519
Simoni, E., 2767
Simonyan, V. V., 3779
Simoyi, R. H., 1635
Sing, K. S. W., 2041
Singh, A. P., 2935
Singh, J., 2789
Singh, Pravinder, 2789
Singh, Pritam, 2789
Singh, R. N., 1871
Singleton, L., 2699
Siripittayananon, J., 2623
Sitte, W., 2127
Sivasanker, S., 3549
Skibsted, J., 4423
Smith, D. M., 3073
Smith, G., 3101
Smith, I. W. M., 191, 3041
Smith, J. R., 2331
Smith, N. J., 1483
Smith, S., 3461
Smyk, B., 789
Sohara, T., 643
Sokolovskii, V. D., 991
Soldi, L. G., 1229
Solinas, V., 3263
Sommer, J-U., 2649
Somorjai, G. A., 3671
Song, L., 3389
Sonnefeld, J., 2965
Sonntag, P., 2593
Sonoyama, N., 437
Sørensen, T. S., 4235
Soria, J., 1669, 1679
Sostaric, J. Z., 2843
Sotiropoulos, S., 457
Sotiropoulou, V., 485
Sotowa, C., 3795
Soujanya, T., 2739
Soustelle, M., 3941, 4431, 4437
Spells, S. J., 2593
Spinner, M. A., 2587
Spolaore, E., 3177
Spoto, G., 3285, 4445
Sprang, T., 163, 555
Ståhl, K., 4223
Stair, P. C., 3619
Stellnberger, K-H., 875
Stéphan, O., 1241
Stephenson, E. H., 789
Stepto, R. F. T., 2639
Stewart, P. A., 4337
Stickdorn, K., 637
Stimpfle, R. M., 3063
Stirling, D., 3219
Stokes, R. H., 1457
Stolte, S., 205
Stranges, D., 575
Stranix, B. R., 4199
Strey, R., 4269
Strnadová, K., 2217
Stuart, C. R., 279, 1631
Subha, M. C. S., 1229
Sueishi, Y., 603
Suffritti, G. B., 525
Suh, S-H., 2945
Sukumoda, A., 473
Sumitomo, Y., 627
Sun, L. M., 1695
Sundararajan, P. R., 2541
Suppan, P., 3123
Suquet, H., 2229
Surman, P. W. J., 1523
Sutcliffe, L. H., 887
Sutcliffe, R., 799
Suter, U. W., 2355
Sutherland, I., 3201
Suzuki, H., 3851
Suzuki, M., 697, 2877
Suzuki, T., 3499
Suzuki, Y., 627
Sway, M. I., 1607, 3309
Sychev, M., 2217
Szafran, M., 87
Szalai, I., 889
Szukalska, A., 1097
Szymanowski, J., 657
Tabatabaei, J., 3659
Tábora, J. E., 1825
Takada, K., 1547
Takahashi, N., 1271
Takahashi, O., 3795
Takahashi, S., 4063
Takamatsu, Y., 3209
Takayanagi, T., 3771
Takeda, Y., 4079
Takehara, Z-i., 3469
Takehira, K., 1111, 1117, 1125, 1655
Takenaka, H., 4451
Takimoto, J-I., 1051
Takizawa, T., 1081
Tamaura, Y., 1533
Tamburello Luca, A. A., 1763
Tanaka, F., 2663
Tanaka, H., 31, 4279
Tanaka, R., 3901
Tanida, H., 4389
Tanimoto, N., 3379
Tanizawa, Y., 3499
Tanodekaew, S., 3461
Tarroni, R., 3741
Tascón, J. M. D., 1217
Tatsuma, T., 1547
Taylor, D. J. R., 2639
Taylor, G. K., 2655
Taylor, M. J., 1523
Taylor, P. A., 1267
Taylor, S. E., 687
Taylor, S. M., 1887, 3725
Teixeira-Dias, J. J. C., 197
Telfer, G. B., 4133
Tempesti, E., 3969
Teplyakov, A. V., 3645
Theodorou, D. N., 2381
Thiyagarajan, P., 2855
Thomas, A. G., 3569
Thomas, G. P., 2699
Thomas, J. K., 759
Thomas, J. M., 3537, 3975
Thompson, A. E., 4355
Thompson, L., 4261
Thompson, T. V., 1795
Thomson, J., 155
Thoret, J., 1037
Thorn, J. C., 781, 1891
Thornton, G., 3569
Thrush, B. A., 13
Timothy, B., 3585
Tiwari, S. K., 1871
Tkaczyk, M., 2299
Toda, A., 2573, 2581
Togawa, T., 1533
Tokuhisa, H., 1237
Tomishige, K., 4161
Tondre, C., 657
Tortelli, V., 3813
Toshima, N., 4111
Touaj, K., 4395
Toufar, H., 549
Touhara, H., 3209
Touret, O., 3941
Trasatti, S., 3311
Trautenberg, H. L., 2649
Trebble, M. A., 245
Tregenna-Piggott, P. L. W., 1935
Treguer, M., 2041
Trenary, M., 3619
Trethewey, A. N., 1795
Trombetti, A., 3741
Truesdale, V. W., 863, 2269
Trümper, U., 1277
Trunschke, A., 4441
Truscott, T. G., 4059
Trushin, S. A., 597
Tse, J. S., 799
Tseung, A. C. C., 2817
Tsuboi, Y., 4047
Tsuji, H., 2961
Tsuji, M., 1533
Tsunashima, S., 3771
Tsunoda, T., 1111, 1117, 1125, 1655
Tsutsumi, K., 1707
Tuazon, E. C., 3033
Tuck, A. F., 3063
Tuckett, R. P., 3073
Tung, C-H., 2761
Turco Liveri, M. L., 1075
Turkewitsch, P., 4199
Turner, A. R., 3627
Turner, J. M. C., 1439
Turton, S., 3555
Tyndall, G. S., 3055
Tziraki, M., 3083
Uchijima, T., 1655
Uddin, Md. A., 3275
Uehara, H., 3007
Uekawa, N., 2161
Ueki, T., 473
Uemura, T., 1051
Uetsuka, H., 1801
Ulenikov, O. N., 13
Ulloa, J., 2291, 3553
Ulvenlund, S., 4223
Unwin, A. P., 2623
Unwin, P. R., 899, 1407, 3893

Urquhart, R. S., 665, 3399
Usanga, I. A., 2095
Ushiki, K-i., 1955, 4419
Ustynyuk, Y. A., 3779
Vago, E. R., 2323
Vairamani, M., 1901
Vajda, Š., 867
van der Pol, A., 1519
Van Der Voort, P., 353, 2173
van Dijk, S. I., 2107
van Eldik, R., 1625
van Hardeveld, R. M., 3679
van Koten, G., 2009
van Leuken, J. J., 205
van Moorsel, G-J. M. P., 1519
Vansant, E. F., 353, 2173
Vassilev, G. P., 485
Verhoeven, J. W., 2107
Vesnaver, G., 995
Vetrivel, R., 4313
Vetter, R., 389
Vincent, D. J., 2885
Vincze, L., 3893
Viner, H. E., 2191, 2203
Viricelle, J. P., 4431, 4437
Vitagliano, V., 1339
Vlaic, G., 2045
Vogt, F., 1155
Volta, J-C., 3231
Vomscheid, R., 3281
Vrancken, K. C., 353, 2173
Wachs, I. E., 953, 3245
Wada, K., 1647
Wada, Y., 1533
Wakisaka, A., 4063
Wales, N. P. L., 2715, 3339
Walker, I. C., 2249
Walker, R. W., 1431
Walsh, R., 2723
Walter, H., 3879
Walton, J. R., 517
Walz, J., 2827
Wandelt, B., 4199
Wang, C-r., 987
Wang, C., 4207
Wang, E., 1471
Wang, P., 4207
Wang, W., 847
Wang, Y., 3953
Ward, I. M., 2623
Warman, J. M., 2107
Warren, P., 3901
Watanabe, A., 2287
Watanabe, I., 4389
Watanabe, K., 1801
Watanabe, M., 2161
Watanabe, Y., 1647
Watkins, R. W., 2587
Watling, T. C., 4309
Waugh, K. C., 3659
Wayne, R. P., 817, 1185, 3045, 4059
Weaver, M., 2609
Weaver, M. J., 3575
Webb, G., 155
Webster, B., 155
Webster, C. R., 3063
Weckhuysen, B. M., 953, 3245
Weinberg, W. H., 3695
Weingärt, H., 1877
Weinhold, J. D., 2457
Weissensteiner, W., 2149
Wells, P. B., 2167
Welsh, H. K., 4009
Wendlandt, K-P., 549
Wennerström, H., 4269
Western, C. M., 773
Widmann, A. H., 2355
Wiering, P. G., 2107
Wilde, P. J., 1991, 4133
Wilhelm, E., 1941
Williams, A. C., 3883
Williams, B. P., 3219
Williams, D. E., 1961, 3307, 4299
Williams, J. O., 3475
Williams, M. A. K., 2871
Williams, P. A., 911, 1483, 3901, 3919
Wilson, C., 793, 3783
Wilson, G., 2087
Wilson, S. H. S., 3327
Wilson, W. R., 2115
Windle, A. H., 2497, 2615
Winfield, J. M., 155
Winkler, H., 1091
Winstanley, A. W., 1689
Woermann, D., 3385, 3889
Wojciechowska, M., 2207
Wolcyrz, M., 507
Wongchanapiboon, T., 2623
Woodruff, D. P., 3555
Wormald, C. J., 269
Wozniak, K., 77, 3925
Wright, A. C., 3475
Wright, G. A., 4403
Wright, M. A. P., 2203
Wright, P. A., 3537
Wright, S. J., 2403
Wu, C-n., 167
Wu, H., 463
Wu, X., 887
Wunderlich, B., 2601
Würz, U., 4269
Wüstneck, R., 1991
Xianbin, W., 2733
Xie, Z-x., 987
Xu, C., 3709
Xu, Q., 2949
Xu, R., 2797
Yabuki, S., 1081
Yacob, A. R., 3799
Yahiro, H., 767
Yahsi, U., 2443
Yajima, S., 4079
Yamada, K., 1601
Yamaguchi, Y., 1663
Yamaji, M., 2751
Yamamoto, H., 4279
Yamamoto, K., 3209
Yamamoto, M., 1967, 4143
Yamamoto, S., 603, 3795
Yamamoto, T., 2559
Yamasaki, M., 3525
Yan, Q. J., 381
Yang, B., 4121
Yang, Y-W., 3461
Yang, Y., 2827, 4121
Yanjun, X., 2733
Yano, H., 3525
Yashima, T., 3275
Yasuda, T., 3379
Yeh, C-T., 949
Yin, Z. R., 381
Yobiko, Y., 4279
Yokoyama, K., 3771
Yokoyama, M., 1237
Yonezawa, S., 3469
Yonezawa, T., 4111
Yoshida, K., 1647
Yoshida, M., 1563
Yoshihisa, H., 895
Yoshikawa, Y., 2287
Young, R. N., 2403
Yoxall, K. R., 3073
Yu, J-S., 3987
Zaitsev, A. I., 703
Zanasi, R., 4031
Zang, L., 917
Zanini, G. P., 1197
Zannoni, C., 3441
Zanoni, R., 2045
Zecchina, A., 3285, 4445
Zemicael, F. W., 3659
Zerbetto, F., 1421
Zhang, B-J., 3255
Zhang, J., 1471
Zhang, Q., 241
Zhang, W-X., 767
Zhang, X. X., 4207
Zhao, Y., 2979
Zhao, Z., 3133
Zheng, L-s., 987
Zhide, H., 2733
Zhmud, B. V., 2965
Zhou, J-L., 3255
Zhou, N. F., 3873
Zhou, W., 2955
Zhu, Q-s., 13, 2975
Zielesny, A., 3889
Zifferer, G., 2551
Zing, C., 4431
Ziyad, M., 3231
Zukal, A., 937
Zundel, G., 3141, 3831

Subject Index 1995

***Ab initio* calculation**
Ab initio MO studies of nuclear spin–spin interactions in CH_3F, SiH_3F and CH_3OH, 23
X-Ray photoelectron spectrum of glassy B_2S_3. Experimental and theoretical study, 93
Catalytic properties of γ-alumina. *Ab initio* molecular orbital studies of clusters of chlorinated γ-alumina, 155
Theoretical and experimental studies on the novel thiazylfluoroformate, FC(O)SN, 231
Model to study delocalization, 241
Derivation of accurate kinetic and potential-energy functions for several simultaneous large-amplitude vibrations: Application to acetaldehyde in the S_0 and T_1 states, 399
Physico-chemical characterisation of oil-soluble overbased phenate detergents, 687
Ab initio perspective on the experimental identification of chloroformic acid by IR spectroscopy, 789
High-level *ab initio* study of the reaction of OCS with OH radicals, 793
Ab initio calculation of the electrical properties of the $X^2\Sigma_g^+$ ground and $A^2\Pi_u$ excited states of N_2^+, 1063
Theoretical calculation of intramolecular reactions in methylperoxyl and ethylperoxyl radicals, 1425
Ab initio studies of the thermal decomposition of azaaromatics: Free radical *versus* intramolecular mechanism, 1587
Ab initio calculations of titanium NMR chemical shifts including the use of effective core potential basis sets, 1735
Thermochemical and theoretical studies of some benzodiazines, 1907
Theoretical potential-energy functions and spectroscopic data for the PH_2^+ ion, 2053
Ab initio and molecular mechanics study of polyaryl ether ketone polymers, 2609
Perturbation theory model of molecular Rydberg orbitals: Application to diatomic molecules, 2699
Ab initio MO study of the molecular structure, vibrational frequencies and bond dissociation energy of bis(2,4-pentanedionato-*O*,*O*′) oxovanadium(IV), 2709
Prototype Si—H insertion reaction of silylene with silane. Absolute rate constants, temperature dependence, RRKM modelling and the potential-energy surface, 2723
Bonding in YXXY dihalides and dihydrides of dioxygen and disulfur, 3357
Modern valence-bond description of the ground state of Li_2^-, 3751
UV-induced isomerization of (*E*)-crotonic acid. Combined matrix-isolated IR and *ab initio* MO study, 3755
Quasiclassical trajectory studies of $N(^2D) + H_2$ reaction on a fitted *ab initio* potential-energy surface, 3771
Theoretical *ab initio* study of the reaction of CH_3SH with OH radical, 3783
Comparison of the water perturbations induced by two small organic solutes: *Ab initio* calculations and molecular dynamics simulation, 3803
Ab initio and experimental study of NMR coupling constants in bicyclo[1.1.1]pentane, 4031
Ab initio calculation of gas-phase ion mobilities of third period atomic ions in helium, 4355

Absorbent
Mixed Co–Zn–Al oxides as absorbents for low-temperature gas desulfurisation, 3219

Absorption
Permeability and the time lag for downstream absorptive permeation with concomitant reaction across a series–parallel path studied by the matrix method, 469
Solubilization of two cyano 3*H*-indole molecular probes in SDS and CTAB micelles: Spectral and photophysical characterization, 2133
Absorption of hydrogen in copper, 3659

Acetic acid dimer
Effect of solvents on adsorption of acetic acid dimer onto activated charcoal, 3949

Acetonitrile
Preferential solvation controlled by clustering conditions of acetonitrile–water mixtures, 4063

Acetonitrile–water
Thermodynamic study of the binding of dibenzo-18-crown-6 with Ag^+, Pb^{2+} and Cd^{2+} in acetonitrile–water solvents, 1607
Corrigendum to IR studies of adhesion promoters. Part 3.—Adsorption and coupling of bifunctional silanes on silica at the solid/liquid interface, 3309
Preferential solvation controlled by clustering conditions of acetonitrile–water mixtures, 4063

Acetylene
(1 + 1) Resonance-enhanced multiphoton ionization spectroscopy of jet-cooled C_2H_2, C_2HD and C_2D_2 in the range 46 400–48 400 cm^{-1}, 3327

Acid–base property
Effect of association of sulfonephthalein dyes with sodium dodecyl sulfate micelles on their acid–base equilibria, 681
Combined DRS–RS–EXAFS–XANES–TPR study of supported chromium catalysts, 3245
Dehydration of 4-methylpentan-2-ol over zirconia catalysts, 3263

Acid catalyst
Acidic and basic properties of titania–alumina mixed oxides: Active sites for propan-2-ol dehydration, 2907

Acid hydrolysis
Effects of ureas on the kinetics of acid hydrolysis of 1-phenylethyl nitrite in water and in aqueous micellar solutions of sodium dodecyl sulfate, 1349

Acidic property
Effect of fluoride ions on the acidic and catalytic properties of beta zeolite, 539

Acidity probe
Reversible interaction of NH_3 with the framework of template-free zeolite-type SAPO-34, 3281

Acid site
IR study of acetonitrile adsorption on hydroxylated zirconium dioxide: Mechanism of acetonitrile hydrolysis, 2913

Acid treatment
Autotransformation and ageing of acid-treated montmorillonite catalysts: A solid-state ^{27}Al NMR study, 1031

Acrylic acid
Rotational isomerism in acrylic acid. A combined matrix-isolated IR, Raman and *ab initio* molecular orbital study, 1571

Activated carbon
Structural and adsorption properties of carbons synthesized within taeniolite matrices, 493
High-resolution ^2H solid-state NMR of ^2H_2O adsorbed onto activated carbon, 1795
Thermal desorption of gallic acid from activated carbon surfaces, 3213
Cobalt catalysts supported on activated carbons: Preparation and behaviour in the hydrogenation of carbon oxides, 3519
Effect of solvents on adsorption of acetic acid dimer onto activated charcoal, 3949

Activity coefficient
Comparison of activity coefficients in the three-component system sodium chloride–sucrose–water from independent isopiestic and EMF measurements at 298.15 K, 1457

Adamantane
EPR spectrum of an acute-angled Na_3 cluster in an adamantane matrix, 3799

Addition gas
Effects of addition gases on the IR multiphon dissociation of haloethanes, 983

Adhesion promoter
IR studies of adhesion promoters. Part 1.—Methoxytrimethylsilane on silica at the solid/liquid interface, 105
IR studies of adhesion promoters. Part 2.—Adsorption of the alkyltrimethoxysilane and alkylamino-trimethoxysilane on silica at the solid/liquid interface, 359
IR studies of adhesion promoters. Part 3.—Adsorption and coupling of bifunctional silanes on silica at the solid/liquid interface, 1253
Corrigendum to IR studies of adhesion promoters. Part 3.—Adsorption and coupling of bifunctional silanes on silica at the solid/liquid interface, 3309

Adsorbed monolayer
Optical second-harmonic generation measurements of molecular adsorption and orientation at the liquid/liquid electrochemical interface, 1411
Corrigendum to Relation between the surface states of oxide films at Rh electrodes and kinetics of the oxygen evolution reaction, 2353

Adsorption
Surface characterisation of yttria-stabilized tetragonal ZrO_2. Part 2.— Adsorption of CO, 113
Surface characterization of yttria-stabilized tetragonal ZrO_2. Part 3.—CO_2 adsorption and the CO_2–CO interaction, 125
FTIR study of the effects of sulfur poisons on NO adsorption on supported copper oxide catalysts, 141
IR spectroscopic study of NO_2 adsorption on chromia, 149
Cadmium-exchanged Y zeolites studied with carbon monoxide and xenon as probes, 163
Resonance Raman spectroscopic study of Methyl Red and Ethyl Red adsorbed on silica, 499
Type III isotherms for the adsorption of ethanol–water mixtures on solid adsorbents, 535
^2H NMR studies of single-component adsorption in silicalite: A comparative study of benzene and *p*-xylene, 559
IR spectroscopic study of butane and propene adsorption on Pt/CeO_2–Al_2O_3 catalysts, 733
Adsorption on MCM-41 mesoporous molecular sieves. Part 2.—Cyclopentane isotherms and their temperature dependence, 937
IR and ^1H NMR studies on the adsorption of gaseous hydrogen chloride on γ-alumina, 941
^2H NMR studies of binary adsorption in silicalite, 963
Adsorbed phase composition in liquid-phase adsorption of organic compounds from aqueous solutions on hydrophobic zeolites, 971
Simultaneous adsorption of thiourea and thiocyanate ions on mercury electrodes. Part 1.—Influence of thiourea on anion adsorption, 1005
Diversity of the kinetics of carbon monoxide oxidation on differently prepared zinc oxides, 1391
Adsorption from associated binary solutions by porous carbon, 1529
Adsorption characteristics and reactions of propyne on microporous crystals, 1707
High-resolution ^2H solid-state NMR of ^2H_2O adsorbed onto activated carbon, 1795
FTIR study of the adsorption and transformation of allylbenzene over oxide catalysts, 1861
Evidence of extraneous surfactant adsorption altering adsorbed layer properties of β-lactoglobulin, 1991
Numerical simulation of surface ionisation and specific adsorption on a two-site model of a carbon surface, 2179
Hydrogen adsorption on silica-supported

platinum studied by ^1H NMR spectroscopy, 2191
^1H NMR of hydrogen chemisorbed on silica-supported platinum particles: An evaluation of different models, 2203
Polyethylene crystallization from dilute solutions: Adsorption isotherm on the growth face, 2581
IR study of acetonitrile adsorption on hydroxylated zirconium dioxide: Mechanism of acetonitrile hydrolysis, 2913
Effects of citrate adsorption on the interactions between zirconia surfaces, 2921
Sorption isotherms of methane, ethane, ethene and carbon dioxide on NaX, NaY and Na-mordenite zeolites, 2935
One-dimensional xenon gas in the pores of mordenite, 2945
Monte Carlo study of adsorption from binary solution on heterogeneous surfaces, 3195
Relationship between carbon black surface chemistry and energy, 3201
Surface composition of Pd–Fe catalysts supported on silica, 3237
Reversible interaction of NH_3 with the framework of template-free zeolite-type SAPO-34, 3281
Quantitative structural study of an Na–O coadsorption phase on Al(111) using X-ray standing waves, 3555
Reflection–absorption IR spectroscopy at cryogenic temperatures, 3563
Photoemission and HREELS study of K adsorption on TiO_2(100), 3569
Adsorption of nitric oxide on Ir{100}: Influence of substrate reconstruction, 3575
CF_3I adsorption on InSb(001), 3603
Interaction of carbon dioxide with oxidised La/Cu(111), 3611
Surface chemistry of methyl groups adsorbed on Pt(111), 3619
Adsorption of O, HCO_2H and $C_6H_5CO_2H$ on Cu(110) studied using reflectance anisotropy. Chemical and structural influences on an optically active surface resonance, 3627
Negative-ion resonances in vibrational excitation and photochemistry of chemisorbed molecules: A critical case study of O_2/Pt(111), 3633
Collision-induced desorption of water from Ru(001), 3655
Cyclohexane adsorption on clean and O-covered Ni{111}: Implications for C—H bond activation, 3703
Surface chemistry of polar oxide surfaces: Formic acid on NiO(111), 3709
Entropy of adsorption of mixed surfactants from solutions onto the air/water interface, 3873
Competitive adsorption of polymers and surfactants at the solid/liquid interface, 3919
Effect of solvents on adsorption of acetic acid dimer onto activated charcoal, 3949
Adsorption and reaction of methanol and carbon dioxide on model ZnO/Ag catalysts, 3963
In situ FTIR studies of high-temperature adsorption of hydrogen on zirconia, 4441
CoO–ZnO solid solution as a model to investigate the CO–cation interaction: An FTIR and HRTEM study, 4445

Adsorption dynamics
Adsorption dynamics for CO and H_2 on an NiAl(110) surface, 3639

Adsorption isotherm
Coadsorption of xenon and carbon monoxide in cadmium-exchanged zeolite Y studied with ^{129}Xe NMR spectroscopy, 555
Nitrogen adsorption and small-angle neutron scattering studies with capped alumina, 1139
Adsorption of carbon dioxide, sulfur dioxide and water vapour by MCM-41, a model mesoporous adsorbent, 2041
Micropore structure of template-derived carbons studied using adsorption of gases with different molecular diameters, 2929

Adsorption site
Site selectivity of methane adsorbed in mordenite as studied by NMR, 2949

Aerosil
Resonance Raman spectroscopic study of Methyl Red and Ethyl Red adsorbed on silica, 499

Ageing
Autotransformation and ageing of acid-treated montmorillonite catalysts: A solid-state ^{27}Al NMR study, 1031

Agglomeration
Theory and experiments for evaluating the number and the dimensions of solid particles dispersed in a liquid medium. Application to the system Si_3N_4/H_2O(l), 323

Aggregation
Thermodynamic study of the aggregation of azo dyes containing two trifluoromethyl groups in aqueous solutions, 1601
EPR study of an associative polymer in solution: Determination of aggregation number and interactions with surfactants, 2863

Ag intercalate
Electrochemical cell for composition-dependent electronic conductivity and chemical diffusion coefficient measurements applied to mixed-conductivity intercalation compounds, 2127

Ag sol
Surface-enhanced resonance Raman spectroscopic studies of the Pb^{II} complex of 1-(2-pyridylazo)-2-naphthol adsorbed on Ag sol, 463

Ag surface
Adsorption and reaction of methanol and carbon dioxide on model ZnO/Ag catalysts, 3963

Air/solvent interface
Surface second harmonic generation at air/solvent and solvent/solvent interfaces, 1763

Air/water interface
Neutron reflectivity of absorbed β-casein and β-lactoglobulin at the air/water interface, 2847
Entropy of adsorption of mixed surfactants from solutions onto the air/water interface, 3873

Alane
Bonding and ligand exchange in pentamethyldialane. An IR, NMR and *ab initio* study, 3015

Aldol condensation
Kinetics by thermometry: An aldol condensation reaction, 991

Aliphatic thiol
In situ quartz-microbalance study of the self-assembly and stability of aliphatic thiols on polarized gold electrodes, 1949

Alkali metal
EPR spectrum of an acute-angled Na_3 cluster in an adamantane matrix, 3799
EPR, ENDOR and TRIPLE resonance characterization of three paramagnetic reduction stages of 5-(9′-fluorenylidene)-5*H*-dibenzo[*a*,*d*] cycloheptene. Radical anions, radical trianions and radical penta-anions, 3821
Density functional theory study of small alkali-metal cluster radicals, 4343

Alkali-metal cation
Specific effect of alkali-metal cations on the kinetics of peroxodisulfate–iodide reactions, 1345

Alkali-metal halide
Partitioning of entropy of solvation: Single-ion entropy of solvation in aqueous and non-aqueous solvents and the correlation of electrostatic entropy of solvation with electrostriction viscosity *B* and NMR *B*′ coefficients, 3373

Alkaline-earth metal
Aggregation of alkaline-earth-metal thiocyanates in aprotic donor solvents, 4395

Alkane
Quantification of the selective activation of C—C bonds in short-chain alkanes. Reactivity of ethane, propane, isobutane, *n*-butane and neopentane on Ir(111), 3695
Elementary radical reactions and autoignition, 4179
Computer simulation of the crystal/melt interface in *n*-alkane with implication for polymer crystallization, 2559

Alkane crystal
Molecular dynamics simulation of the temperature dependence of lattice parameters of alkane crystals during cooling, 2601

Alkanol
Intramolecular charge transfer in rigidly linked naphthalene–trialkylamine compounds, 4047

Alkene
Distinguishing direct and quasi-direct mechanisms for an Eley–Rideal gas/surface reaction. Stereochemistry of H addition to cyclohexene on Cu(100), 3645
Surface science and catalysis of ethylene hydrogenation, 3671
EPR and ENDOR of perfluoroalkyl radical intermediates in the reaction between perfluorohypofluorites and perfluoroalkenes, 3813
Spectroscopic investigation of the molybdenum active sites on Mo^{VI} heterogeneous catalysts for alkene epoxidation, 3969

Alkene oxidation
Alkene oxidation over the Au|yttria-stabilised zirconia|Ag system, 1111
Alkene oxidation over the Mo–Bi mixed oxides/Au|yttria-stabilised zirconia|Ag system, 1117
Alkene oxidation over the (Pb,Bi)MoO_4/Au|yttria-stabilized zirconia|Ag system, 1125

2-Alkoxyethanol–water
Thermochemical properties of electrolyte solutions in 2-alkoxyethanol–water mixtures, 2299

Alkyltrimethylammonium bromide
Denaturation of lysozyme by *n*-alkyltrimethylammonium bromides in alkaline solution, 2805

Allene dication
The allene dication: Calculated and measured singlet-electronic-state energies, 1181

Allylbenzene
FTIR study of the adsorption and transformation of allylbenzene over oxide catalysts, 1861

Alumina
Effect of Pt particle size on H/D exchange of methane over alumina- and zeolite-supported catalysts, 569
IR and ^1H NMR studies on the adsorption of gaseous hydrogen chloride on γ-alumina, 941
Isosteric heat of sorption of dihydrogen on alumina-supported palladium, 949
Magnetic resonance studies on porous alumina doped with iron and chromium, 1519
Acidic and basic properties of titania–alumina mixed oxides: Active sites for propan-2-ol dehydration, 2907
Catalytic properties of γ-alumina. *Ab initio* molecular orbital studies of clusters of chlorinated γ-alumina, 155

Alumina-supported cerium oxide
Behaviour of oxygen species adsorbed on Al_2O_3-supported cerium oxide catalysts for methane oxidation, 4459

Aluminium
EPR spectroscopic study of the reaction of Al and Ga atoms with CO_2 and CS_2 in a rotating cryostat, 799
Influence of the source of silicon and aluminium in the hydrothermal synthesis of sodalite, 1147
Fluorescence spectra of methyl salicylate during the sol–gel–xerogel transitions of mixed silicon–aluminium alkoxides, 4279

Aluminophosphate
Acidity of aluminophosphate structures. Part 1.—Incorporation of silicon into chabazite-like structure 44, 1155
Acidity of aluminophosphate structures. Part 2.—Incorporation of cobalt into CHA and AFI by microwave synthesis, 1163
Synthesis and characterization of VAPSO-44 and VAPSO-5, 1173
Solid-state NMR and powder XRD studies of the structure of SAPO-40 upon hydration–dehydration cycles, 2213
Synthesis, characterisation and catalytic performance of the solid acid DAF-1, 3537
Synthesis and characterization of CAM-1, a novel aluminophosphate molecular sieve precursor, 3995
Surface basicity of a new family of catalysts: Aluminophosphate oxynitride (AlPON), 4477

Aluminosilicate
Atom pair potential for molecular dynamics simulations of structural and dynamical properties of aluminosilicates: Test on

silicalite and anhydrous Na-A and Ca-A zeolites and comparison with experimental data, 525
Effect of structural aluminium on the mesoporous structure of MCM-41, 2955
Amine complex
Proton-exchange mechanisms in phenol–tertiary amine–aprotic solvent systems, 3859
Amino acid
Photocatalytic racemization of amino acids in aqueous polycrystalline cadmium(II) sulfide dispersions, 1103
Aminocarboxylic ligand
Mixed aminocarboxylic ligand complexes, 1619
Ammonia
Redox interaction of ammonia with $(VO)_2P_2O_7$, 725
Trapping of metastable oxygen species at Cu(111) surfaces, 2885
Selective catalytic reduction of nitric oxide with ammonia on MFI-type ferrisilicate, 3275
Theoretical study of cadmium– and mercury–ammonia exciplexes: Comparison with experiment, 3795
Amorphous polymer
Monte Carlo simulations of polymer surfaces in a cubic lattice, two variations of energy parameter and chain-length, 2551
Anionic surfactant
Interaction of the chloropentaamminecobalt(III) cation with mixed micelles of anionic and non-ionic surfactants: A kinetic study, 1075
Determination of thickness and rupture pressure for aqueous foam films. Part 1.—Films stabilized by anionic surfactants, 4251
Anodic process
Surface electrochemistry and kinetics of anodic bromine formation at platinum, 283
Antarctic vortex
Airborne chemistry and dynamics at the edge of the 1994 antarctic vortex, 3063
Anthrahydroquinone
Formation of anthrahydroquinones ($XAQH_2$) *via* excited singlet charge-transfer complexes (or singlet ion pairs) of anthraquinones with 2,5-dimethylhexa-2,4-diene (DMHD), and photochemical reaction of $XAQH_2$ with DMHD, 607
Antimony
Semiconductive properties of some uranium–antimony oxide phases used as catalysts in the mild oxidation of but-1-ene to butadiene, 2343
AOT
Structure and reactivity of aerosol-OT reversed micelles containing α-chymotrypsin, 1081
Aprotic solvent
Protonation of pyridines by phenols, thiophenol, trifluoroacetic acid and methanesulfonic acid in aprotic solvents, 1611
Aqueous–organic solvent
Hydrophobic effects on photochemical and photophysical processes: Evidence for aggregation of perfluorocarbon in aqueous–organic solvents, 2761
Aqueous solution
Complexation of phenylalanine and histidine by β-cyclodextrin, 6^A^-(3-aminopropylamino)-6^A^-deoxy-β-cyclodextrin and its metallocyclodextrins in aqueous solution, 1013
Thermodynamic study of the aggregation of azo dyes containing two trifluoromethyl groups in aqueous solutions, 1601
Mutual-diffusion coefficients and viscosities for the water–2-methylpropan-2-ol system at 15 and 25 °C, 4071
Corrigendum to Complexation of phenylalanine and histidine by β-cyclodextrin, 6^A^-(3-aminopropylamino)-6^A^-deoxy-β-cyclodextrin and its metallocyclodextrins in aqueous solution, 4335
Aqueous suspension
Kinetics and products of the photocatalytic degradation of morpholine (tetrahydro-2*H*-1, 4-oxazine) in TiO_2 aqueous suspensions, 1853
Argon ion
Valence-band and core photoelectron spectroscopic studies of molybdenum aqueous oxidation and the influence of argon-ion etching, 3593
Aromatic hydrocarbon
FTIR studies of the interaction of aromatic hydrocarbons with vanadium oxide layered on ZrO_2 and TiO_2, 3505
Dehydrogenation, hydrogenation, exchange and combustion reactions of aromatic hydrocarbons on Pd(100), 3685
Aromatic interaction
Influence of fluorine on aromatic interactions, 2009
Aromaticity
Aromaticity and superaromaticity in carbon nanotoroids, 1563
Arrhenius parameter
Arrhenius parameters for the reaction of the nitrate radical with 1,1-dichloroethene and (*E*)-1,2-dichloroethene, 1185
AsH radical
IR spectrum of the AsH radical in its $X\,^3\Sigma^-$ state, recorded by laser magnetic resonance, 2999
Associated mixtures
Bulk and surface properties of the highly non-ideal associated mixtures formed by methanol and propanal, 2779
Association
Physicochemical properties of dimethyl sulfoxide–methanol liquid mixtures. Experimental and semiempirical quantum chemical studies, 65
Effect of association of sulfonephthalein dyes with sodium dodecyl sulfate micelles on their acid–base equilibria, 681
Simultaneous description of excess enthalpy and vapour–liquid equilibrium data of associated mixtures by means of a lattice–fluid model, 4381
Asymmetric potential
Selection of Brownian particles, 3163
Atmospheric chemistry
Rates of reaction between the nitrate radical and some aliphatic alcohols, 405
Rate constants for the reactions of C_2H_3, C_2H_3O and $C_2H_3O_2$ radicals with NO_3 at 298 K and 2.2 Torr, 817
Atom
Reactive scattering of atoms and radicals, 575
Atomic force microscopy
Effects of citrate adsorption on the interactions between zirconia surfaces, 2921
Atomic ion
Ab initio calculation of gas-phase ion mobilities of third period atomic ions in helium, 4355
Atomic simulation
Monte Carlo algorithms for the atomistic simulation of condensed polymer phases, 2355
Atomic solid
New model of potential-energy functions for atomic solids, 1567
Atom pair potential
Atom pair potential for molecular dynamics simulations of structural and dynamical properties of aluminosilicates: Test on silicalite and anhydrous Na-A and Ca-A zeolites and comparison with experimental data, 525
Auger electron spectroscopy
Comparison between gas-phase and electrochemical deposition of copper on Pt(100)-(1 × 1) and Pt(100)-hex-*R*0.7°, 3585
CF_3I adsorption on InSb(001), 3603
Autotransformation
Autotransformation and ageing of acid-treated montmorillonite catalysts: A solid-state ^{27}Al NMR study, 1031
1-Azaindolizine
Gas-phase IR spectrum of 1-azaindolizine: Scaled quantum mechanical force field and spectrum assignment, 3741
Azide radical
Mechanism of oxidation of iron(II) complexes by the azide radical, 3133
Azo dye
Thermodynamic study of the aggregation of azo dyes containing two trifluoromethyl groups in aqueous solutions, 1601
Azoisopropane
Thermal reaction of azoisopropane in the presence of $(E)\text{-}CH_3CH{=}CHCH_3$: Reactions of the radical 2-$\dot{C}_3H_7$, 1303
B_2S_3
X-Ray photoelectron spectrum of glassy B_2S_3. Experimental and theoretical study, 93
Bacteriorhodopsin
A model system for the hydrogen-bonded chain with large proton polarizability present in the L_{550} intermediate of bacteriorhodopsin: An FTIR study, 3141
Band structure
Theoretical investigation on the band structures of several Chevrel-phase compounds, 479
Characterisation of bandgap states in V-doped TiO_2 by high-resolution X-ray photoemission spectroscopy, 3495
Barium
Single-crystal EPR study of the compounds $[MCu(edta)(H_2O)_3] \cdot H_2O$ (M = Sr, Ba), 423
Mass-spectrometric study of the production and recombination of $BaOH^+$ ions and free electrons from barium added to flames of $H_2 + O_2 + Ar$, 2257
Base hydrolysis
Corrigendum to Effect of solvent on the reaction of coordination complexes. Part 19.—Base hydrolysis of (αβ*S*)-(*o*-methoxybenzoato)-(tetraethylenepentamine)cobalt(III) in aquo-organic solvent media, 1715
BCl_3-modification
Total characterization of the BCl_3-modified silica surface by means of quantitative surface analysis, 2173
Becke–Wigner
Becke–Wigner: A simple but powerful density functional, 4337
Benzene
Formation of subvalent bismuth cations in molten gallium trichloride and benzene solutions, 4223
Benzene hydrogenation
Effect of chlorine on microstructure and activity of Pd/CeO_2 catalysts, 507
Benzodiazine
Thermochemical and theoretical studies of some benzodiazines, 1907
Benzoic acid
Specific micellar catalytic effects of the protolysis of *o*-benzoic acid derivatives studied by the ultrasonic absorption method, 3525
Beryllium
Steric solvent effect on small and large cations: Calorimetric study of halogeno and thiocyanato complexes of beryllium(II) and cadmium(II) in *N*,*N*-dimethylacetamide, 3851
BET
Relationship between carbon black surface chemistry and energy, 3201
Bicyclo[1.1.1]pentane
Ab initio and experimental study of NMR coupling constants in bicyclo[1.1.1]pentane, 4031
Bifunctional catalyst
Investigations on hydrogen spillover. Part 2.—Hydrocarbon conversion on bifunctional catalysts, 1539
Bilayer
Monte Carlo simulations of a single poly(oxyethylene) $C_{12}E_3$ chain headgroup fixed on a bilayer surface in water, 4261
Phase behaviour and structure in a non-ionic surfactant–oil–water mixture, 4269
Bilirubin
Resonance Raman study of the chromophore-specific vibrational and electronic spectra of bilirubin, 1751
Bimetallic catalyst
Effects of modification of Pd/SiO_2 with Rh on catalytic activity for ethene hydroformylation, 1271
Bimetallic cluster
Mechanistic consideration of formation of polymer-protected nanoscopic bimetallic clusters, 4111
Bimetallic system
Temperature-programmed reduction of alumina-supported Ni–Pt systems, 3481
Bimolecular reaction
Reactive scattering of atoms and radicals, 575
Binary adsorption
Coadsorption of xenon and carbon monoxide in cadmium-exchanged zeolite Y studied with ^{129}Xe NMR spectroscopy, 555

^2H NMR studies of binary adsorption in silicalite, 963

Binary catalyst
Characteristics of Cr_2O_3–CuO/MgF_2 catalysts and a comparison with Cr_2O_3/MgF_2 and CuO/MgF_2 systems, 2207

Binary mixture
Liquid mixtures at high pressures referred to a pseudospinodal curve: Ethanol–methylcyclopentane and carbon disulfide–tetramethylsilane, 59
Physicochemical properties of dimethyl sulfoxide–methanol liquid mixtures. Experimental and semiempirical quantum chemical studies, 65
Solvation of cobalt(II) and perchlorate ions in binary mixtures of donor solvents, 71
Preferential solvation in mixed solvents. Part 7.—Binary mixtures of water and alkanolamines, 427
Type III isotherms for the adsorption of ethanol–water mixtures on solid adsorbents, 535
Rate of decomposition of murexide in mixed solvents: An indicator for proton activity, 637
Adsorbed phase composition in liquid-phase adsorption of organic compounds from aqueous solutions on hydrophobic zeolites, 971
Experimental and predicted excess enthalpies of the 2,2,2-trifluoroethanol–water–tetraethylene glycol dimethyl ether ternary system using binary mixing data, 2071
Volumetric properties of binary mixtures of water with methoxy(ethoxy)$_n$ ethanols, 2291
Corrigendum to Volumetric properties of binary mixtures of water with methoxy(ethoxy)$_n$ ethanols, 3553
Halochromism and solvatochromism of a π^* probe in binary solvent mixtures, 3839
Ultrasonic absorption of nitrobenzene–isooctane mixtures of non-critical composition, 3889

Binary solution
Preferential solvation in mixed binary solvent, 631
Adsorption from associated binary solutions by porous carbon, 1529
Monte Carlo study of adsorption from binary solution on heterogeneous surfaces, 3195

Binary system
Cationic motions and glass transitions of eutectic mixtures in the $(CH_3)_4NHSO_4$–H_2O and $(CH_3)_4NHSO_4$–D_2O binary systems, 4139

Biophysical chemistry
Conformation and dynamics of alkylated bases within DNA: Effect of methyl rotation, 251

Biosensor
Appraisal of the fundamental operation of quartz crystal shear-mode biosensors, 3147

Bismuth
Formation of subvalent bismuth cations in molten gallium trichloride and benzene solutions, 4223

Block copolymer
Solvent-mediated interactions and chain conformations in block copolymer liquids, 2411

Bond activation
Quantification of the selective activation of C—C bonds in short-chain alkanes. Reactivity of ethane, propane, isobutane, *n*-butane and neopentane on Ir(111), 3695

Bond dissociation
Ab initio MO study of the molecular structure, vibrational frequencies and bond dissociation energy of bis(2,4-pentanedionato-*O*,*O*′)-oxovanadium(IV), 2709

Bond-fluctuation model
Structure and swelling of end-linked model networks, 2649

Bonding
Bonding in YXXY dihalides and dihydrides of dioxygen and disulfur, 3357

Bond resonance energy
Kinetic stability of fullerenes with four-membered rings, 4349

Borate glass
Use of ultraviolet excitation spectra of Tl^+ for probing oxidic networks: Alkali-metal borate glasses, 3485

Boron
Vacuum UV fluorescence excitation spectroscopy of BCl_3. Electronic spectroscopy of BCl_2, BCl_2^+, and BCl_3^+, 3073

Bovine serum albumin
NMR studies of $^{23}Na^+$ in frozen bovine serum albumin solution, 1459

Branching
Intermolecular packing of freely jointed branched polyalkene melts: A microscopic approach, 2427

BrCl
Electric polarity $^+BrCl^-$ and rotational *g* factor from analysis of frequencies of pure rotational and vibration–rotational spectra, 3005

Bridging bond
Bonding and ligand exchange in pentamethyldialane. An IR, NMR and *ab initio* study, 3015

Bromide ion
Temperature dependence of EXAFS for bromide ions in solution, 4389

Bromine
Surface electrochemistry and kinetics of anodic bromine formation at platinum, 283
Br_2-sensitised decomposition of ozone: Kinetics of the reaction BrO + O_3 → products, 4189

Brønsted acidity
Catalytic properties of γ-alumina. *Ab initio* molecular orbital studies of clusters of chlorinated γ-alumina, 155
Acidity of aluminophosphate structures. Part 1.—Incorporation of silicon into chabazite-like structure 44, 1155
Acidity of aluminophosphate structures. Part 2.—Incorporation of cobalt into CHA and AFI by microwave synthesis, 1163

Brønsted site
Acidic and basic properties of titania–alumina mixed oxides: Active sites for propan-2-ol dehydration, 2907

Brownian dynamics
Rotational Brownian motion of a two-dimensional rigid rotator: Relaxation and steady-state regimes, 41
Simulated structure of mixed particle gels, 51
Brownian-dynamics simulations of model stabilised colloidal dispersions under shear, 1975

Brownian particle
Selection of Brownian particles, 3163

Bruker lecture
Creation and detection of coherence and polarization in pulsed EPR, 177

Bubble–particle attachment
Bubble–particle attachment, 1997

Butane-1,4-diol dimethacrylate
Raman scattering study of butane-1,4-diol dimethacrylate, 2339

C_2H_4 oxidation
Molecular beam study of C_2H_4 oxidation on platinum: IR chemiluminescence of the CO and CO_2 products, 1801

C_{60}
Solvent effect on photoinduced electron transfer between C_{60} and 3,3′,5,5′-tetramethylbenzidine studied by nanosecond laser photolysis, 2287

Cadmium
Steric solvent effect on small and large cations: Calorimetric study of halogeno and thiocyanato complexes of beryllium(II) and cadmium(II) in *N*,*N*-dimethylacetamide, 3851

Cadmium chalcogenide
Photoelectrochemical behaviour of Q-state $CdS_xSe_{(1-x)}$ particles in arachidic acid Langmuir–Blodgett films, 3399

Cadmium docosanoate
Ion inclusion into Langmuir–Blodgett films studied on a quartz crystal microbalance, 1783

Cadmium sulfide
Photocatalytic racemization of amino acids in aqueous polycrystalline cadmium(II) sulfide dispersions, 1103

Caesium
Equilibrium aspects of the extraction of caesium nitrate by dicyclohexano-21-crown-7, dibenzo-21-crown-7 and bis-[*tert*-alkylbenzo]-21-crown-7 in 1,2-dichloroethane, 4215

Calcification
Effects of silicate ions on the formation and transformation of calcium phosphates in neutral aqueous solutions, 3499

Calcium phosphate
Effects of silicate ions on the formation and transformation of calcium phosphates in neutral aqueous solutions, 3499

Calorimetric technique
Dehydration of 4-methylpentan-2-ol over zirconia catalysts, 3263

Calorimetric titration
Titration calorimetric and spectrophotometric studies of micelle formation by alkyltrimethylammonium bromide in aqueous solution, 1229

Cameron band
Multiconfiguration response calculations on the Cameron bands of the CO molecule, 1729

Camphene
Catalytic transformation of camphene over aluminophosphate-based molecular sieves, 4471

Camphor
Corrigendum to Dielectric studies of orientational disorder in D- and L-systems of camphor and camphoric anhydride, 4009

Capillary method
Simple EPR method for measuring translational diffusion constants, 887

Capped alumina
Nitrogen adsorption and small-angle neutron scattering studies with capped alumina, 1139

Carbenium ions
Propane conversion of dry-air-calcined HZSM-5 zeolite, 1689

Carbohydrate
Structural glass transitions and thermophysical processes in amorphous carbohydrates and their supersaturated solutions, 1511
Interactions between cations and sugars. Part 8.—Gibbs energies, enthalpies and entropies of association of divalent and trivalent metal cations with xylitol and glucitol in water at 298.15 K, 2771

Carbon
Micropore structure of template-derived carbons studied using adsorption of gases with different molecular diameters, 2929
Classification scheme for toroidal molecules, 4037

Carbon black
Relationship between carbon black surface chemistry and energy, 3201
Catalytic activity of platinum after exchange with surface active functional groups of carbon blacks, 4451

Carbon dioxide
Response of fluorescein to carbon dioxide in dimethyl sulfoxide–water mixtures, 881
Interaction of carbon dioxide with oxidised La/Cu(111), 3611

Carbonic acid
A polymorph of carbonic acid and its possible astrophysical relevance, 2823

Carbon monoxide
Multiconfiguration response calculations on the Cameron bands of the CO molecule, 1729

Carbon nanotoroid
Aromaticity and superaromaticity in carbon nanotoroids, 1563

Carbon surface
Numerical simulation of surface ionisation and specific adsorption on a two-site model of a carbon surface, 2179

Carboxylic acid
FTIR investigation of polarizable hydrogen bonds in carboxylic acid–pyridine complexes in the mid- and far-IR region, 3831

Carceplex
Guest dynamics in carceplexes: A ^2H NMR study, 4127

Carotene
Phosphorescence of β-carotene, 4059
ENDOR study of the (7′,7′-dicyano)- and (7′-phenyl)-7′-apo-β-carotene radical cations formed by UV photolysis of carotenoids adsorbed on silica gel, 2881

Carotenoid

ENDOR study of the (7',7'-dicyano)- and (7'-phenyl)-7'-apo-β-carotene radical cations formed by UV photolysis of carotenoids adsorbed on silica gel, 2881

β-Casein
Neutron reflectivity of absorbed β-casein and β-lactoglobulin at the air/water interface, 2847

Catalysis
Catalytic chemistry of furan and thiophene. *Ab initio* calculations, using the spin-coupled valence bond method, of the interaction of furan and thiophene with a positively charged centre, 749
Characterisation and activity of praseodymium oxide catalysts prepared in different gases from praseodymium oxalate hydrate: Microscopic, thermogravimetric and IR spectrosopic studies, 1385
Investigations on hydrogen spillover. Part 2.—Hydrocarbon conversion on bifunctional catalysts, 1539
Characteristics of Cr_2O_3–CuO/MgF_2 catalysts and a comparison with Cr_2O_3/MgF_2 and CuO/MgF_2 systems, 2207
Dehydration of 4-methylpentan-2-ol over zirconia catalysts, 3263
Selective catalytic reduction of nitric oxide with ammonia on MFI-type ferrisilicate, 3275
FTIR studies of the interaction of aromatic hydrocarbons with vanadium oxide layered on ZrO_2 and TiO_2, 3505
Synthesis, characterisation and catalytic performance of the solid acid DAF-1, 3537
Absorption of hydrogen in copper, 3659
CO–NO reaction on Rh(110) studied using molecular beams, 3663
Catalytic effect of vanadium, iron and lead oxides on the oxidation of moderator graphite, 3717
Direct conversion of methane and ethane to the corresponding alcohols using nitrous oxide over iron phosphate catalysts, 3953
Adsorption and reaction of methanol and carbon dioxide on model ZnO/Ag catalysts, 3963
Spectroscopic investigation of the molybdenum active sites on Mo^{VI} heterogeneous catalysts for alkene epoxidation, 3969
In situ Raman studies of the selective oxidation of methanol to formaldehyde and ethene to ethylene oxide on a polycrystalline silver catalyst, 4149
Surface structure change of a [$Pt_4(\mu$-$CH_3COO)_8$]/SiO_2 catalyst active for the decomposition of formic acid, 4161
Catalytic activity of platinum after exchange with surface active functional groups of carbon blacks, 4451
Catalytic transformation of camphene over aluminophosphate-based molecular sieves, 4471

Catalyst characterisation
Effect of chlorine on microstructure and activity of Pd/CeO_2 catalysts, 507
Characterisation and activity of praseodymium oxide catalysts prepared in different gases from praseodymium oxalate hydrate: Microscopic, thermogravimetric and IR spectrosopic studies, 1385

Catalyst properties
IR spectroscopy of hydrotreating catalysts, 517
IR spectroscopic study of butane and propene adsorption on Pt/CeO_2–Al_2O_3 catalysts, 733
Influence of strong metal–support interaction on exchange with deuterium and other reactions of hydrocarbons. Part 1.—Studies with Rh/TiO_2 and Rh/SiO_2, 741
Characterisation of the acidity of well defined Cu-ZSM-5 catalysts using pyridine as a probe molecule, 1841
Surface composition of Pd–Fe catalysts supported on silica, 3237
Intrinsic kinetics of Fischer–Tropsch synthesis over an Fe–Cu–K catalyst, 3255

Catalytic decomposition
Catalytic decomposition reaction of formic acid on an Ar^+-bombarded TiO_2(110) surface: Steady-state kinetics and microscopic surface structure, 1663

Catalytic reduction
IR spectroscopic study of NO_2 adsorption on chromia, 149
Medium-temperature electrolysis of NO and CH_4 under lean-burn conditions using yttria-stabilized zirconia as a solid electrolyte, 1955

Cathodic reduction
Cathodic reduction of oxygen in water and media of low ionic strength, 457

Cation cluster
Time-resolved diffuse reflectance of electron trapping by alkali-metal cation clusters in zeolites and clays following far-UV excitation, 759

Cation location
Cation location and migration in lathanum-exchanged zeolite NaY studied by X-ray powder diffraction and MAS NMR spectroscopy, 1813

Cation migration
Cation location and migration in lathanum-exchanged zeolite NaY studied by X-ray powder diffraction and MAS NMR spectroscopy, 1813

Cation mobility
Cationic mobility in MgX zeolite: An FTIR study, 2961

Cation transfer
Gibbs energies, entropies and enthalpies of transfer for divalent cations to several solvents, 3843

Cd exciplex
Enthalpy changes for the formation of CdA* and CdA_2* exciplexes in the cadmium($5\ ^3P_1$)-photosensitized reaction of some substrates in the gas phase, 603

Cement
Quantification of calcium silicate phases in Portland cements by ^{29}Si MAS NMR spectroscopy, 4423
Quantification of calcium silicate phases in Portland cements by ^{29}Si MAS NMR spectroscopy, 4423

Ceramic powder
Theory and experiments for evaluating the number and the dimensions of solid particles dispersed in a liquid medium. Application to the system Si_3N_4/H_2O(1), 323

Ceria
Transition-metal ion dimers formed in CeO_2: An EPR study, 99
IR spectroscopic study of butane and propene adsorption on Pt/CeO_2–Al_2O_3 catalysts, 733
Spectroscopic study of oxygen adsorption as a method to study surface defects on CeO_2, 1669
NO reaction at surface oxygen vacancies generated in cerium oxide, 1679
Palladium–ceria catalysts: Reversibility of hydrogen chemisorption and redox phenomena, 2185
Thermal stability of doped ceria: Experiment and modelling, 3941
Transformation of cerium(III) hydroxycarbonate into ceria. Part 1.—Nucleation and growth rates of ceria, 4431
Transformation of cerium(III) hydroxycarbonate into ceria. Part 2.—Experimental study of the growth rate, 4437

Cerium hydroxycarbonate
Transformation of cerium(III) hydroxycarbonate into ceria. Part 1.—Nucleation and growth rates of ceria, 4431
Transformation of cerium(III) hydroxycarbonate into ceria. Part 2.—Experimental study of the growth rate, 4437

Chabazite
Acidity of aluminophosphate structures. Part 1.—Incorporation of silicon into chabazite-like structure 44, 1155

Chain folding
Molecular dynamics study of polyethylene chain folding: The effects of chain length and the torsional barrier, 2541

Characteristic polynomial
Linearisation of graphs using walks of unit length, 3095

Charged surface
Interactions between a charge-regulated particle and a charged surface, 4093

Charge regulation
Charge regulation at the surface of porous silica, 2965
Interactions between a charge-regulated particle and a charged surface, 4093

Charge-separation efficiency
Photoinduced electron-transfer quenching of excited singlet states of polycyclic aromatic hydrocarbons by organic acceptors. Solvent effects on the rate constants and the charge-separation efficiency, 1197

Charge transfer
Formation of anthrahydroquinones ($XAQH_2$) *via* excited singlet charge-transfer complexes (or singlet ion pairs) of anthraquinones with 2,5-dimethylhexa-2,4-diene (DMHD), and photochemical reaction of $XAQH_2$ with DMHD, 607
'Charge-transfer' complexes of ammonia with halogens: Nature of the binding in $H_3N\cdots BrCl$ from its rotational spectrum, 781
Solvent-dependent switching between two dipolar excited states in a rigidly extended trichromophoric system, 2107
Intramolecular charge transfer in rigidly linked naphthalene–trialkylamine compounds, 4047
Effect of temperature and viscosity on intramolecular charge-transfer fluorescence of a 4-*p*-dimethylaminostyrylpyridinium salt in protic solvents, 4199

Chemical potential
Determination of the chemical potential by the particle insertion method and by its inverse, 2971

Chemical shift
Ab initio calculations of titanium NMR chemical shifts including the use of effective core potential basis sets, 1735

Chemical vapour deposition
In-situ EXAFS investigation of non-acidic CVD-based Pt/KL catalyst under oxidation–reduction cycles, 2045

Chemi-ionisation
Mass-spectrometric study of the production and recombination of $BaOH^+$ ions and free electrons from barium added to flames of $H_2 + O_2 + Ar$, 2257

Chemiluminescence
Chemiluminescence in 5 μm multiple-photon decomposition of $W(CO)_6$ in the presence of O_2, 597
Molecular beam study of C_2H_4 oxidation on platinum: IR chemiluminescence of the CO and CO_2 products, 1801
Chemiluminescence from the reactions of nitrogen and oxygen atoms with phosphorus vapour, 2989

Chemisorption
Quantification of the selective activation of C—C bonds in short-chain alkanes. Reactivity of ethane, propane, isobutane, *n*-butane and neopentane on Ir(111), 3695
Hydrogen in molybdenum and cobalt sulfide catalysts. A neutron Compton scattering study on the ISIS electronvolt spectrometer, 4467

Chevrel-phase compound
Theoretical investigation on the band structures of several Chevrel-phase compounds, 479

Chloride ion
Effect of oxide contamination on the position of the liquidus curve of the NaCl–$AlCl_3$ system, 3869

Chlorine
Experimental determination of second density virial coefficients of xenon and chlorine at elevated temperatures, 1277
Rate coefficients for quenching of $Cl(^2P_{1/2})$ by various atmospheric gases, 3055

Chlorine complex
The $b\pi.a\sigma$ complex $C_2H_2\cdots Cl_2$ characterised by rotational spectroscopy as an intermediate in a reactive mixture of ethyne and chlorine, 1891
$H_2S\cdots Cl_2$ characterised in a pre-reactive gas mixture of hydrogen sulfide and chlorine through rotational spectroscopy: The nature of the interaction, 2059

Chloroformic acid
Ab initio perspective on the experimental identification of chloroformic acid by IR spectroscopy, 789

Chlorosilane
Hydrodehalogenation of chlorosilanes in the presence of metal silicides: Experimental studies of gas and solid phase composition related to thermodynamic calculations, 3879
Chlorosilylation
Gas-phase chlorosilylation of silica gel: Effectiveness, surface coverage and stoichiometry, 353
Chromia
IR spectroscopic study of NO_2 adsorption on chromia, 149
Chromium
Surface chemistry of silica–titania-supported chromium oxide catalysts, 953
Combined DRS–RS–EXAFS–XANES–TPR study of supported chromium catalysts, 3245
Chromium complex
EPR characterisation of the Cr^{V} intermediates in the $Cr^{VI/V}$ oxidations of organic substrates and of relevance to Cr-induced cancers, 1207
α-Chymotrypsin
Structure and reactivity of aerosol-OT reversed micelles containing α-chymotrypsin, 1081
Cinchona alkaloid
XPS and LEED studies of 10,11-dihydrocinchonidine adsorption at Pt(111). Implications for the role of cinchona alkaloids in enantioselective hydrogenation, 2167
Clay
Time-resolved diffuse reflectance of electron trapping by alkali-metal cation clusters in zeolites and clays following far-UV excitation, 759
Electrochemical control of montmorillonite clay swelling, 1547
Al-pillared saponites. Part 3.—Effect of parent clay layer charge on the intercalation–pillaring mechanism and structural properties, 2229
Cl^- monitoring
Photogenerated chloride ion concentration near the surface of UV-irradiated titanium dioxide in the presence of aqueous 2,4-dichlorophenol probed using an ultramicroelectrode, 3893
^{35}Cl NMR spin-echo
Self-diffusion of the perchlorate ion in aqueous electrolyte solutions measured by ^{35}Cl NMR spin-echo experiments, 1877
Cluster
Catalytic properties of γ-alumina. *Ab initio* molecular orbital studies of clusters of chlorinated γ-alumina, 155
Density functional theory study of small alkali-metal cluster radicals, 4343
^{13}C NMR
Visualization of enantiomers in a polypeptide liquid-crystal solvent through carbon-13 NMR spectroscopy, 1371
Coarse graining polymer chains
New high-coordination lattice model for rotational isomeric state polymer chains, 2435
Cobalt
Acidity of aluminophosphate structures. Part 2.—Incorporation of cobalt into CHA and AFI by microwave synthesis, 1163
Hydrogen in molybdenum and cobalt sulfide catalysts. A neutron Compton scattering study on the ISIS electronvolt spectrometer, 4467
Collision
Theoretical cross-sections for *M*-changing collisions of symmetric-top molecules with rare-gas atoms, 4363
Collision broadening
Collision broadening of CO_2/transitions in the region of 4.3 μm. Effects of broadening gas (He, Ar and N_2), rovibrational states and temperature, 191
Collision-induced desorption
Collision-induced desorption of water from Ru(001), 3655
Collision kinetics
Rate coefficients for quenching of $Cl(^2P_{1/2})$ by various atmospheric gases, 3055
Colloid
Physico-chemical characterisation of oil-soluble overbased phenate detergents, 687
Brownian-dynamics simulations of model stabilised colloidal dispersions under shear, 1975
Effect of the surface chemical modification on the optical properties of polymer-stabilized PbS nanoparticles, 4121
On flocculation and gelation in concentrated particulate systems containing added polymer, 4413
Complex
FTIR investigation of polarizable hydrogen bonds in carboxylic acid–pyridine complexes in the mid- and far-IR region, 3831
Complex formation
Cooperative interactions between ions and water in the chloride ion and water coordination to a square-planar nickel complex ion in concentrated aqueous solutions, 627
Metal extraction in micellar media: A comparison of copper complexation rates and ultrafiltration yields of two isomeric (*E*)-1-(2′-hydroxy-5′-alkylphenyl) 1-alkanone oximes, 657
Solvation and complexation equilibria of nickel(II) thiocyanato complexes in *N*,*N*-dimethylacetamide, 2313
Molecular complexes of nitric acid with N_2, CO and NO studied by matrix isolation IR spectroscopy, 3111
Steric solvent effect on small and large cations: Calorimetric study of halogeno and thiocyanato complexes of beryllium(II) and cadmium(II) in *N*,*N*-dimethylacetamide, 3851
Asymmetrical complexation and simultaneous electrochemical recognition of two different Group 2 metal cations by a 1,1′-ferrocene-bis(methylene aza-18-crown-6) receptor, 4331
Thermodynamics of complexation of sodium, potassium, rubidium, caesium and ammonium ions with 18-crown-6 in acetonitrile and propylene carbonate, 4375
Compressibility
Ultrasonic velocity, conductivity, viscosity and calorimetric studies of copper(I) and sodium perchlorates in cyanobenzene, pyridine and cyanomethane, 2789
Computational chemistry
Thermodynamic properties of transfer RNA: A computational study, 2531
Computer simulation of the crystal/melt interface in *n*-alkane with implication for polymer crystallization, 2559
Computer simulation studies on the role of templating organic molecules in the synthesis of ZSM-5, 4313
Computer simulation
Simulated structure of mixed particle gels, 51
Synthesis of faujasite zeolites with crown-ether templates, 167
MARVIN: A new computer code for studying surfaces and interfaces and its application to calculating the crystal morphologies of corundum and zircon, 925
Brownian-dynamics simulations of model stabilised colloidal dispersions under shear, 1975
Inhibition of crystal growth in methane hydrate, 3449
Concentration-modulated absorption spectroscopy
Temporal and spatial distribution profiles of lithium atoms in low-pressure discharges by concentration-modulated absorption spectroscopy, 1297
Concentration-modulated absorption spectroscopy. Part 5.—Influence of molecular diffusion, 3101
Concentration polarization
Theory of concentration polarization in crossflow filtration, 3389
Condensed phase
Monte Carlo algorithms for the atomistic simulation of condensed polymer phases, 2355
Conducting polymer
Surface composition of surfacant-stabilised polypyrrole colloids, 905
Ion binding by poly[4-(pyrrol-1-ylmethyl)benzoic acid] thin films, 1241
Synthesis, characterization and physical properties of tricarbonylmanganese and pentamethylcyclopentadienylcobalt complexes of poly(9-hexylfluorene), 1477
Application of density functional theory in the synthesis of electroactive polymers, 2331
Molecular dynamics simulations of the structure and ion diffusion in poly(ethylene oxide), 2633
Diffusion behaviour of the BF_4^- anion in polyaniline fibrils. Influence of the physical state of polyaniline, 3469
Conductivity
Precision modelling of conductivity data of monovalent aqueous electrolytes, 303
Interaction of water with 1% Li/MgO: DC conductivity of Li/MgO catalyst for methane selective activation, 1805
Ultrasonic velocity, conductivity, viscosity and calorimetric studies of copper(I) and sodium perchlorates in cyanobenzene, pyridine and cyanomethane, 2789
Electrical conductivity of the systems $NaAlCl_4$ and NaCl(s)/$NaAlCl_4$ in the range 100–200 °C, 3157
Configuration
Configurational and rheological properties of cyclic polymers, 2525
Conformation
Conformation and dynamics of alkylated bases within DNA: Effect of methyl rotation, 251
Probing the conformational properties of guest molecules in solid inclusion compounds *via* EXAFS spectroscopy: Bromine K-edge EXAFS studies of the bromocyclohexane/thiourea and *trans*-1-bromo-2-chlorocyclohexane/thiourea inclusion compounds, 1497
Coordination complex
EPR characterisation of the Cr^{V} intermediates in the $Cr^{VI/V}$ oxidations of organic substrates and of relevance to Cr-induced cancers, 1207
Corrigendum to Effect of solvent on the reaction of coordination complexes. Part 19.—Base hydrolysis of (αβ*S*)-(*o*-methoxybenzoato)-(tetraethylenepentamine)cobalt(III) in aquo-organic solvent media, 1715
Oxidation of a tricoordinated Cu^{I} complex to a tetracoordinated Cu^{II} species. A single-crystal EPR study, 2155
Copolymer
Self-consistent field model of the polymer/diblock copolymer/polymer interface, 2381
Linear rheological behaviour of polyisoprene–polystyrene hetero-star and linear diblock copolymer melts, 2403
Gelation of aqueous solutions of diblock and triblock copolymers of ethylene oxide and 1,2-butylene oxide studied by ^1H nuclear magnetic relaxation, 3461
Copper
Reduction of copper(II) with subsequent disproportionation of copper(I) during the hydrothermal syntheses of microporous silicoaluminium phosphates SAPO-5 and -11, 3529
Mechanism of formation of copper thiocyanate on the copper anode, 4403
Copper(I)
Ultrasonic velocity, conductivity, viscosity and calorimetric studies of copper(I) and sodium perchlorates in cyanobenzene, pyridine and cyanomethane, 2789
Copper(I) oxide
Studies on the pre-edge region of the X-ray absorption spectra of copper(I) oxide and the diamminecopper(I) ion, 3189
Copper(I) salt
^{63}Cu and ^{109}Ag NMR studies of copper(I) and silver(I) salts in mixed solvents containing nitriles, 2307
Copper carbonyl
Use of combination modes and overtones of metal carbonyls for the IR study of cation states in zeolites: Copper(I) carbonyls in reduced CuNaY zeolites, 2035
Copper complex
Metal extraction in micellar media: A comparison of copper complexation rates and ultrafiltration yields of two isomeric (*E*)-1-(2′-hydroxy-5′-alkylphenyl) 1-alkanone

oximes, 657
Oxidation of a tricoordinated Cu^{I} complex to a tetracoordinated Cu^{II} species. A single-crystal EPR study, 2155
Copper dimer
Evolution of the EPR copper(II) dimer spectrum observed in CuCe oxide with the applied microwave frequency: A computer-assisted study, 3299
Copper hydride
Studies of copper hydride. Part 1.—Synthesis and solid-state stability, 713
Studies of copper hydride. Part 2.—Transmission electron microscopy, 719
Copper surface
Trapping of metastable oxygen species at Cu(111) surfaces, 2885
Reflection–absorption IR spectroscopy at cryogenic temperatures, 3563
Adsorption of O, HCO_2H and $C_6H_5CO_2H$ on Cu(110) studied using reflectance anisotropy. Chemical and structural influences on an optically active surface resonance, 3627
Distinguishing direct and quasi-direct mechanisms for an Eley–Rideal gas/surface reaction. Stereochemistry of H addition to cyclohexene on Cu(100), 3645
Coprecipitation
Physico-chemical properties and catalytic activities of the spinel series $Mn_xFe_{3-x}O_4$ towards peroxide decomposition, 3489
Coriolis interaction
High-resolution spectroscopic study of $2\nu_1$, $2\nu_3$ and $\nu_1 + \nu_3$ stretching states: The local-mode effects of H_2Se, 13
Cotransport
Model for chemical interdiffusion of solubilizates and ionic micelles. Aqueous solutions of *n*-alcohols and sodium dodecyl sulfate, 2837
Coumarin dye
Excited-state dipole moments of some Coumarin dyes from a solvatochromic method using the solvent polarity parameter, E_T^N, 2739
Cracking
Propane conversion of dry-air-calcined HZSM-5 zeolite, 1689
Critical micelle concentration
Titration calorimetric and spectrophotometric studies of micelle formation by alkyltrimethylammonium bromide in aqueous solution, 1229
Volumetric study of mixed micelles of hexane-1,2-diol and some alkane-1,2,3-triols, 4105
Crossed-beam experiment
Reactive collisions with excited-state atoms, 389
Crossflow filtration
Theory of concentration polarization in crossflow filtration, 3389
Cross-linking
Structure and swelling of end-linked model networks, 2649
Computer simulation of sulfur vulcanization, 2655
Cross-section
Theoretical cross-sections for *M*-changing collisions of symmetric-top molecules with rare-gas atoms, 4363
Crotonic acid
UV-induced isomerization of (*E*)-crotonic acid. Combined matrix-isolated IR and *ab initio* MO study, 3755
Crowned cholesterol
Ion-conducting behaviour and photoinduced ionic-conductivity switching of composite films containing crowned cholesteric liquid crystals, 1237
Crown ether
Synthesis of faujasite zeolites with crown-ether templates, 167
Thermodynamic study of the binding of dibenzo-18-crown-6 with Ag^+, Pb^{2+} and Cd^{2+} in acetonitrile–water solvents, 1607
Corrigendum to IR studies of adhesion promoters. Part 3.—Adsorption and coupling of bifunctional silanes on silica at the solid/liquid interface, 3309
Stabilities in water of 1:1 lariat 16-crown-5 complexes with metal ions: Transfer activity coefficients from protic to aprotic solvents of 1:1 complexes of lariat and substituted 16-crown-5 derivatives with metal ions, 4079
Thermodynamics of the interaction of 18-crown-6 with K^+, Tl^+, Ba^{2+}, Sr^{2+} and Pb^{2+} from 323.15 to 398.15 K, 4207
Equilibrium aspects of the extraction of caesium nitrate by dicyclohexano-21-crown-7, dibenzo-21-crown-7 and bis-[*tert*-alkylbenzo]-21-crown-7 in 1,2-dichloroethane, 4215
Thermodynamics of complexation of sodium, potassium, rubidium, caesium and ammonium ions with 18-crown-6 in acetonitrile and propylene carbonate, 4375
Cryogenic gas mixture
A polymorph of carbonic acid and its possible astrophysical relevance, 2823
Cryptand 222
Temperature coefficients of Ag/Ag^+ and Ag/Ag^+–cryptand 222 electrode potentials, thermodynamics of Ag^+–cryptand 222 complex formation and molar transfer properties for Ag^+ cations into aprotic media, 1097
Crystal field
Crystal fields in $REOF:Eu^{3+}$ (RE = La, Gd and Y), 1503
Crystal force
Crystal-face specificity of electrical double-layer parameters at metal/solution interfaces, 3311
Crystal growth
MARVIN: A new computer code for studying surfaces and interfaces and its application to calculating the crystal morphologies of corundum and zircon, 925
Simulation of growth and surface roughening of polymer single crystals, 2587
Inhibition of crystal growth in methane hydrate, 3449
Thermal stability of doped ceria: Experiment and modelling, 3941
Crystalline polymer
Neutron scattering from solution-grown polymer crystals: A statistical model, 2593
Crystallization
A simple model for the kinetic evaluation of zeolite crystallization processes, 549
New approach to the mechanism of oligomer crystallization, 2565
Crystal modulus
Crystal modulus of poly(hydroxybutyrate), 2623
Crystal structure
X-Ray, FTIR, ^1H and ^{13}C NMR, PM3 and AM1 studies of $(N{-}H\cdots N)^+$ and $(O{-}H\cdots O)^-$ hydrogen bonds in a complex of 1,8-diaminonaphthalene with maleic acid: Proton cavity and basicity of proton sponges, 87
Oxidation of a tricoordinated Cu^{I} complex to a tetracoordinated Cu^{II} species. A single-crystal EPR study, 2155
Determination of the crystal structure of poly(*p*-phenylene terephthalate) from power diffraction data. A computer modelling approach, 2615
^{63}Cu NMR
^{63}Cu and ^{109}Ag NMR studies of copper(I) and silver(I) salts in mixed solvents containing nitriles, 2307
Curved surface
Curvature effects on electric double-layer forces. Part 1.—Comparisons with parallel plate geometry, 2827
Cyano compound
CN^- abstraction from cyano compounds by positrons, 419
Cyanogen
Molecular rotation and isomerisation in hydrogen isocyanide, 1717
Cyclic oligomer
Volume properties of some linear and ring oligomer solutions, 2797
Cyclic polymer
Configurational and rheological properties of cyclic polymers, 2525
Cyclic voltammetry
Reaction of H^+ with tetraphenylborates: An example of an EC mechanism at liquid/liquid interfaces, 3433
Diffusion behaviour of the BF_4^- anion in polyaniline fibrils. Influence of the physical state of polyaniline, 3469
Comparison between gas-phase and electrochemical deposition of copper on Pt(100)-(1 × 1) and Pt(100)-hex-*R*0.7°, 3585
Direct functionalization of silicon *via* the self-assembly of alcohols, 4001
Cyclodextrin
Complexation of phenylalanine and histidine by β-cyclodextrin, 6^A-(3-aminopropylamino)-6^A-deoxy-β-cyclodextrin and its metallocyclodextrins in aqueous solution, 1013
Corrigendum to Complexation of phenylalanine and histidine by β-cyclodextrin, 6^A-(3-aminopropylamino)-6^A-deoxy-β-cyclodextrin and its metallocyclodextrins in aqueous solution, 4335
Femtosecond to nanosecond solvation dynamics in pure water and inside the γ-cyclodextrin cavity, 867
Cyclohexane
Cyclohexane adsorption on clean and O-covered Ni{111}: Implications for C—H bond activation, 3703
Cyclohexene
Distinguishing direct and quasi-direct mechanisms for an Eley–Rideal gas/surface reaction. Stereochemistry of H addition to cyclohexene on Cu(100), 3645
Cyclopentane
Addition of cyclopentane to slowly reacting mixtures of $H_2 + O_2$ between 673 and 783 K: Reactions of H and OH with cyclopentane and of cyclopentyl radicals, 1431
Cyclopropenium cation
Structural and spectroscopic investigations of aminocyclopropenium cations, $[C_3(Nr_2)_3]^+$ (NR_2 = NMe_2, NEt_2, NC_5H_{10} or NC_4H_8O) and $[C_3(NPr^i_2)_2Cl]^+$, 1523
Cyclotrimerisation
Catalysed cyclotrimerisation of acetylene: A computational study, 3975
Decomposition
Adsorption and reaction of methanol and carbon dioxide on model ZnO/Ag catalysts, 3963
Delocalization
Model to study delocalization, 241
Denaturation
Denaturation of lysozyme by *n*-alkyltrimethylammonium bromides in alkaline solution, 2805
Density
Identification of transitions in lyotropic mesophases in hexaethylene glycol dodecyl ether–water by precision densimetry, 319
Measurement of the temperature of maximum density of aqueous solutions of some salts and acids, 999
Volumetric properties of binary mixtures of water with methoxy(ethoxy)$_n$ ethanols, 2291
Corrigendum to Volumetric properties of binary mixtures of water with methoxy(ethoxy)$_n$ ethanols, 3553
Density functional theory
Theoretical and experimental studies on the novel thiazylfluoroformate, FC(O)SN, 231
Application of density functional theory in the synthesis of electroactive polymers, 2331
Becke–Wigner: A simple but powerful density functional, 4337
Density functional theory study of small alkali-metal cluster radicals, 4343
Dentine
Scanning electrochemical microscopy as a probe of local fluid flow through porous solids: Application to the measurement of convective rates through a single dentinal tubule, 1407
Depletion kinetics
Kinetics and mechanism of the reaction between thymol blue and bromate in acidic medium, 1635
Despretz law
Measurement of the temperature of maximum density of aqueous solutions of some salts and acids, 999
Desulfurisation
Mixed Co–Zn–Al oxides as absorbents for low-temperature gas desulfurisation, 3219
Detergent

Physico-chemical characterisation of oil-soluble overbased phenate detergents, 687
Deuterium solubility
Dissolution of hydrogen and deuterium in titanium, $Ti_{94}Al_6$ and Ti_3Al, 1967
Dewar mechanism
Ab initio studies of the thermal decomposition of azaaromatics: Free radical *versus* intramolecular mechanism, 1587
1,8-Diaminonaphthalene
X-Ray, FTIR, ^1H and ^{13}C NMR, PM3 and AM1 studies of $(N—H\cdots N)^+$ and $(O—H\cdots O)^-$ hydrogen bonds in a complex of 1,8-diaminonaphthalene with maleic acid: Proton cavity and basicity of proton sponges, 87
Diamond surface
Diffuse reflectance infrared Fourier-transform study of the direct thermal fluorination of diamond powder surfaces, 3209
Diatomic
Perturbation theory model of molecular Rydberg orbitals: Application to diatomic molecules, 2699
Diblock copolymer
Self-consistent field model of the polymer/diblock copolymer/polymer interface, 2381
Linear rheological behaviour of polyisoprene–polystyrene hetero-star and linear diblock copolymer melts, 2403
Dichloromethane
Equilibrium aspects of the extraction of caesium nitrate by dicyclohexano-21-crown-7, dibenzo-21-crown-7 and bis-[*tert*-alkylbenzo]-21-crown-7 in 1,2-dichloroethane, 4215
Dielectric layer
Complex permittivity of a conducting, dielectric layer containing arbitrary binary Nernst–Planck electrolytes with applications to polymer films and cellulose acetate membranes, 4235
Dielectric property
Analyses for a dipolar relaxation in the featureless dielectric spectrum, and a comparison between the permittivity, modulus and impedence representations, 329
Corrigendum to Dielectric studies of orientational disorder in D- and L-systems of camphor and camphoric anhydride, 4009
Dielectric relaxation
Rotational Brownian motion of a two-dimensional rigid rotator: Relaxation and steady-state regimes, 41
High-temperature dielectric relaxation in Nylon 12 and the effects of annealing and absorbed water, 337
Temperature- and frequency-dependent dielectric studies of *p*-fluorophenylacetonitrile–methanol mixtures using time-domain reflectometry, 623
Dielectric spectroscopy
Analyses for a dipolar relaxation in the featureless dielectric spectrum, and a comparison between the permittivity, modulus and impedence representations, 329
Molecular kinetics during the growth of the macromolecule poly(di-2-hydroxypropyl ether of bisphenol-A-*n*-hexylamine) studied by dielectric spectroscopy, 343
Differential scanning calorimetry
Differential scanning calorimetric study of the interactions of some stabilizing amino acids and oligopeptides with hen egg white lysozyme, 2101
Differential thermal analysis
Cationic motions and glass transitions of eutectic mixtures in the $(CH_3)_4NHSO_4$–H_2O and $(CH_3)_4NHSO_4$–D_2O binary systems, 4139
Differential thermogravimetry
Thermal desorption of gallic acid from activated carbon surfaces, 3213
Diffuse reflectance spectroscopy
Time-resolved diffuse reflectance of electron trapping by alkali-metal cation clusters in zeolites and clays following far-UV excitation, 759
Diffusion
Simple determination of experimental isotherms using diffusion denuder tubes, 485
Simple EPR method for measuring translational diffusion constants, 887
Intracrystalline diffusion of benzene in silicalite: Effect of structural heterogeneity, 1143
Effect of mass on particle diffusion in liquids studied by electron spin exchange and chemical reaction of muonium with oxygen in aqueous solution, 1935
Analysis of bimodal frequency-response behaviour of *p*-xylene diffusion in silicalite-1, 2027
Concentration-modulated absorption spectroscopy. Part 5.—Influence of molecular diffusion, 3101
Diffusivity in nitrobenzene–isooctane mixtures of non-critical composition approaching the liquid–liquid coexistence curve, 3385
Diffusion behaviour of the BF_4^- anion in polyaniline fibrils. Influence of the physical state of polyaniline, 3469
Mutual-diffusion coefficients and viscosities for the water–2-methylpropan-2-ol system at 15 and 25 °C, 4071
Mutual-diffusion coefficients and viscosities for the water–2-methylpropan-2-ol system at 15 and 25 °C, 4071
Reaction–diffusion effects and systematic design of gas-sensitive resistors based on semiconducting oxides, 4299
Dihalide
Bonding in YXXY dihalides and dihydrides of dioxygen and disulfur, 3357
Dimerization
Partition and dimerization of ion-pair tetraalkylammonium salts in xylene, 643
Dimethyl sulfide
Resonance-enhanced multiphoton ionisation spectroscopy of dimethyl sulfide, 3339
Dimethylzinc
Homogeneous thermal decomposition of dimethylzinc in a metal–organic vapour phase epitaxy reactor. An *ex situ* investigation by FTIR absorption spectroscopy, 3475
Diol
Volumetric study of mixed micelles of hexane-1,2-diol and some alkane-1,2,3-triols, 4105
Dipolar soft-sphere fluid
Influence of static electric field on the vapour–liquid coexistence of dipolar soft-sphere fluids, 889
Dipole moment
Excited-state dipole moments of some Coumarin dyes from a solvatochromic method using the solvent polarity parameter, E_T^N, 2739
Electric polarity $^+BrCl^-$ and rotational *g* factor from analysis of frequencies of pure rotational and vibration–rotational spectra, 3005
Discharge-flow technique
Arrhenius parameters for the reaction of the nitrate radical with 1,1-dichloroethene and (*E*)-1,2-dichloroethene, 1185
Disproportionation
Effect of iodide concentration upon the kinetics of disproportionation of hypoiodous acid in borate buffer, 863
Kinetics of disproportionation of hypoiodous acid in phosphate and borate buffer at pH < 8.5 modelled using iodide feedback, 2269
Reduction of copper(II) with subsequent disproportionation of copper(I) during the hydrothermal syntheses of microporous silicoaluminium phosphates SAPO-5 and -11, 3529
Dissociation
Specific micellar catalytic effects of the protolysis of *o*-benzoic acid derivatives studied by the ultrasonic absorption method, 3525
Aggregation of alkaline-earth-metal thiocyanates in aprotic donor solvents, 4395
Dissociative electron attachment
Molecular dynamics of dissociative electron attachment in water, 2249
Dissolution
Dissolution of hydrogen and deuterium in titanium, $Ti_{94}Al_6$ and Ti_3Al, 1967
Thermochemical properties of electrolyte solutions in 2-alkoxyethanol–water mixtures, 2299
Sonochemical dissolution of MnO_2 colloids, 2843
DMSO–water
Response of fluorescein to carbon dioxide in dimethyl sulfoxide–water mixtures, 881
DNA
Conformation and dynamics of alkylated bases within DNA: Effect of methyl rotation, 251
Photosensitization of DNA bases by 4(5)-nitroimidazole: A steady state and flash photolysis study, 1191
Conformation and dynamics of ethylated DNA, 1465
Conformation and dynamics of ethylated DNA, 1465
Pulse radiolysis studies on the oxidation of $OH^•$ radical-damaged DNA by nitroquinolines in aqueous solution, 2115
Molecular modelling of ligand–DNA intercalation interactions, 2515
Donor–acceptor complex
Donor–acceptor complexes of Lewis bases with bromine monochloride in the gas phase: some generalisations from rotation spectroscopy, 1881
Effect of molecular conformation on the electronic properties of donor–acceptor azobenzenes, 2067
Donor solvent
Solvation of cobalt(II) and perchlorate ions in binary mixtures of donor solvents, 71
Dopant
Thermal stability of doped ceria: Experiment and modelling, 3941
Doppler broadening
CN^- abstraction from cyano compounds by positrons, 419
Double-charge-transfer spectroscopy
The allene dication: Calculated and measured singlet-electronic-state energies, 1181
Combined experimental and computational investigation of the double ionization of $(CH_3)_4M$ molecules (M = Si, Ge, Sn and Pb), 1901
Double harmonic oscillator approximation
Static vibrational polarizability of all-*trans* polyethylene and polysilane, 1641
DPPH
Investigation of the consumption of diphenylpicrylhydrazyl in solution in the absence and presence of ultrasound, 1067
DRIFTS
Diffuse reflectance infrared Fourier-transform study of the direct thermal fluorination of diamond powder surfaces, 3209
Surface basicity of a new family of catalysts: Aluminophosphate oxynitride (AlPON), 4477
Dye
Thermodynamic study of the aggregation of azo dyes containing two trifluoromethyl groups in aqueous solutions, 1601
Dynamic light scattering
Studies of poly(styrene) solutions in an electric field: Viscosity and dynamic light scattering, 1357
Dynamics
Dynamics study of a closed diffusion cell by using a frequency response method: Single resonator, 1695
Dynamic scaling theory
Ultrasonic absorption of nitrobenzene–isooctane mixtures of non-critical composition, 3889
EC mechanism
Reaction of H^+ with tetraphenylborates: An example of an EC mechanism at liquid/liquid interfaces, 3433
EDX analysis
Characterization of precipitates formed from the tetraiodomercurate(II) anion and mercury(I) or silver(I) cations, 1217
EELS
Negative-ion resonances in vibrational excitation and photochemistry of chemisorbed molecules: A critical case study of O_2/Pt(111), 3633
Egg white lysozyme
Vibrational Raman optical activity of lysozyme: Hydrogen–deuterium exchange, unfolding and ligand binding, 2087
Differential scanning calorimetric study of the interactions of some stabilizing amino acids and oligopeptides with hen egg white

lysozyme, 2101
Einstein coefficient
Multiconfiguration response calculations on the Cameron bands of the CO molecule, 1729
Elastic behaviour
Opposite electrorheological effects between urethane-based polymers having different terminal groups, 1051
Prediction of microstructure in liquid-crystalline polymers, 2497
Molecular modelling of the elastic behaviour of polymer chains in networks: Comparison of polymethylene and poly(dimethysiloxane), 2639
Electrical conductivity
Investigations on hydrogen spillover. Part 1.—Electrical conductivity studies on titanium dioxide, 1091
Diversity of the kinetics of carbon monoxide oxidation on differently prepared zinc oxides, 1391
Electrical double layer
Curvature effects on electric double-layer forces. Part 1.—Comparisons with parallel plate geometry, 2827
Crystal-face specificity of electrical double-layer parameters at metal/solution interfaces, 3311
Electrical property
Electrically induced reversible structural change of a highly swollen polymer gel network, 473
Ab initio calculation of the electrical properties of the $X^2\Sigma_g^+$ ground and $A^2\Pi_u$ excited states of N_2^+, 1063
Electric field
Influence of static electric field on the vapour–liquid coexistence of dipolar soft-sphere fluids, 889
Studies of poly(styrene) solutions in an electric field: Viscosity and dynamic light scattering, 1357
Ion-beam spectroscopy of long-range complexes, 3725
Electroactive polymer
Application of density functional theory in the synthesis of electroactive polymers, 2331
Electrochemical catalysis
Alkene oxidation over the Au|yttria-stabilised zirconia|Ag system, 1111
Alkene oxidation over the Mo–Bi mixed oxides/Au|yttria-stabilised zirconia|Ag system, 1117
Alkene oxidation over the (Pb,Bi)MoO_4/Au|yttria-stabilized zirconia|Ag system, 1125
Low-temperature synthesis of perovskite-type oxides of lanthanum and cobalt and their electrocatalytic properties for oxygen evolution in alkaline solutions, 1871
Electrochemical cell
Electrochemical cell for composition-dependent electronic conductivity and chemical diffusion coefficient measurements applied to mixed-conductivity intercalation compounds, 2127
Electrochemical deposition
Comparison between gas-phase and electrochemical deposition of copper on Pt(100)-(1 × 1) and Pt(100)-hex-*R*0.7°, 3585
Electrochemical membrane reactor
Partial oxidation of CH_4 to synthesis gas using an Rh|YSZ|Ag electrochemical membrane reactor, 1655
Electrochemical reduction
Choice of the reaction coordinate in electron-transfer reactions in solution, 1451
Electrochemistry
Surface electrochemistry and kinetics of anodic bromine formation at platinum, 283
Cathodic reduction of oxygen in water and media of low ionic strength, 457
Electrochemical control of montmorillonite clay swelling, 1547
Corrigendum to Relation between the surface states of oxide films at Rh electrodes and kinetics of the oxygen evolution reaction, 2353
Crystal-face specificity of electrical double-layer parameters at metal/solution interfaces, 3311
Kinetics of solvated electrons in reaction with hexamethylphosphoric triamide, 3809
Asymmetrical complexation and simultaneous electrochemical recognition of two different Group 2 metal cations by a 1,1′-ferrocene-bis(methylene aza-18-crown-6) receptor, 4331
Mechanism of formation of copper thiocyanate on the copper anode, 4403
Electrode
Simultaneous adsorption of thiourea and thiocyanate ions on mercury electrodes. Part 1.—Influence of thiourea on anion adsorption, 1005
Mechanism of formation of copper thiocyanate on the copper anode, 4403
Electrode potential
Temperature coefficients of Ag/Ag^+ and Ag/Ag^+–cryptand 222 electrode potentials, thermodynamics of Ag^+–cryptand 222 complex formation and molar transfer properties for Ag^+ cations into aprotic media, 1097
Electrolysis
Medium-temperature electrolysis of NO and CH_4 under lean-burn conditions using yttria-stabilized zirconia as a solid electrolyte, 1955
Electrolyte
Precision modelling of conductivity data of monovalent aqueous electrolytes, 303
Measurement of the temperature of maximum density of aqueous solutions of some salts and acids, 999
Solution to the Poisson–Boltzmann equation for particles covered by an ion-penetrable charged membrane, 1223
Solubility and Pitzer model parameters in thallium(I) chloride systems, TlCl–$MgCl_2$–H_2O and TlCl–$CaCl_2$–H_2O, 1759
Thermochemical properties of electrolyte solutions in 2-alkoxyethanol–water mixtures, 2299
Interactions between a charge-regulated particle and a charged surface, 4093
Electronic energy transfer
Quenching rate constants for NCl($b\,^1\Sigma^+$) and PCl($b\,^1\Sigma^+$) and radiative lifetimes of NCl($b\,^1\Sigma^+$), PCl($b\,^1\Sigma^+$) and PBr($b\,^1\Sigma^+$), 2979
Electronic spectroscopy
Electronic spectroscopy of size-selected ionic complexes, 91
Millimetre-wave electronic spectrum of the D_2^+ ion, 1887
Electronic state
Observation of the SCl radical by resonance-enhanced multiphoton ionisation spectroscopy, 773
Electronic structure
Catalytic chemistry of furan and thiophene. *Ab initio* calculations, using the spin-coupled valence bond method, of the interaction of furan and thiophene with a positively charged centre, 749
Modern valence-bond description of the ground state of Li_2^-, 3751
Aromatic electrophilic substitution. A modern valence bond study, 4011
Becke–Wigner: A simple but powerful density functional, 4337
Electronic transition
Multiconfiguration response calculations on the Cameron bands of the CO molecule, 1729
Combined experimental and computational investigation of the double ionization of $(CH_3)_4M$ molecules (M = Si, Ge, Sn and Pb), 1901
Electron spin exchange
Effect of mass on particle diffusion in liquids studied by electron spin exchange and chemical reaction of muonium with oxygen in aqueous solution, 1935
Electron transfer
Solvent effect on the photoinduced electron-transfer reactions between dicyanobis(polypyridine)ruthenium(II) complexes and tris(β-diketonato) ruthenium(III) complexes, 437
Imaging local mass-transfer rates within an impinging jet and studies of fast heterogeneous electron-transfer kinetics using the microjet electrode, 899
Choice of the reaction coordinate in electron-transfer reactions in solution, 1451
Laser flash photolysis studies and magnetic field effect on a new heteroexcimer between *N*-ethylcarbazole and 1,4-dicyanobenzene in homogeneous and heterogeneous media, 1593
Electrochemical properties of myoglobin embedded in Langmuir–Blodgett and cast films of synthetic lipids, 1775
Solvent effect on photoinduced electron transfer between C_{60} and 3,3′,5,5′-tetramethylbenzidine studied by nanosecond laser photolysis, 2287
Stopped-flow kinetic study of the formation and decay of the 4,4′-(dimethylamino)-diphenylmethane radical cation in aqueous solution, 2743
Kinetics of intra-polymer electron-transfer reactions in macromolecule–metal complexes, 2877
Orbital symmetry effects in photoinduced bimolecular electron-transfer reactions, 3123
Electron trapping
Time-resolved diffuse reflectance of electron trapping by alkali-metal cation clusters in zeolites and clays following far-UV excitation, 759
Electrophilic substitution
Aromatic electrophilic substitution. A modern valence bond study, 4011
Electroreduction of oxygen
Electroreduction of oxygen on Fe_3O_4 electrodes. Part 2.—Rotating ring–disc electrode studies and mechanism, 2323
Electro rheological fluid
Microstructural studies of electro-rheological fluids under shear, 1787
Electrorheology
Opposite electrorheological effects between urethane-based polymers having different terminal groups, 1051
Electrostatic interaction
Influence of fluorine on aromatic interactions, 2009
Electrostriction
Partitioning of entropy of solvation: Single-ion entropy of solvation in aqueous and non-aqueous solvents and the correlation of electrostatic entropy of solvation with electrostriction viscosity *B* and NMR *B*′ coefficients, 3373
Eletrochemical recognition
Voltammetric and NMR studies of a bis(ferrocenecarboxamide)-substituted diaza-18-crown-6 receptor that simultaneously complexes and electrochemically recognises both cations and anions, 295
Eley–Rideal
Distinguishing direct and quasi-direct mechanisms for an Eley–Rideal gas/surface reaction. Stereochemistry of H addition to cyclohexene on Cu(100), 3645
Emf
Comparison of activity coefficients in the three-component system sodium chloride–sucrose–water from independent isopiestic and emf measurements at 298.15 K, 1457
Emission
Hydrophobic effects on photochemical and photophysical processes: Evidence for aggregation of perfluorocarbon in aqueous–organic solvents, 2761
Enantioselective hydrogenation
XPS and LEED studies of 10,11-dihydrocinchonidine adsorption at Pt(111). Implications for the role of cinchona alkaloids in enantioselective hydrogenation, 2167
ENDOR
ENDOR study of the (7′,7′-dicyano)- and (7′-phenyl)-7′-apo-β-carotene radical cations formed by UV photolysis of carotenoids adsorbed on silica gel, 2881
EPR and ENDOR of perfluoroalkyl radical intermediates in the reaction between perfluorohypofluorites and perfluoroalkenes, 3813
EPR, ENDOR and TRIPLE resonance characterization of three paramagnetic

reduction stages of 5-(9′-fluorenylidene)-5*H*-dibenzo[*a*,*d*] cycloheptene. Radical anions, radical trianions and radical penta-anions, 3821
Energy calculation
Influence of fluorine on aromatic interactions, 2009
Energy change
Force–extension relations in macromolecules of variable excluded volume and flexibility: Energy and entropy changes on stretching, 2465
Energy pooling
Kinetic investigation of energy pooling from Sr[5s5p(^3P_J)] studied by time-resolved atomic emission following pulsed dye-laser excitation, 811
Energy transfer
Dominant role of internal rotation in the dissociation of polyatomic ligands from the binding site. The case of opiates, 2811
Enthalpy
Enthalpy changes for the formation of CdA* and CdA_2* exciplexes in the cadmium(5 $^3P_1$)-photosensitized reaction of some substrates in the gas phase, 603
Modelling the influence of monomer properties on hydrogen bond density in oriented, rigid copolymer systems, 2629
Gibbs energies, entropies and enthalpies of transfer for divalent cations to several solvents, 3843
Entropy
Thermodynamic transfer properties for Na^+, Tl^+ and Ag^+ to water–acetonitrile mixtures, 875
Force–extension relations in macromolecules of variable excluded volume and flexibility: Energy and entropy changes on stretching, 2465
Gibbs energies, entropies and enthalpies of transfer for divalent cations to several solvents, 3843
Enzyme
Structure and reactivity of aerosol-OT reversed micelles containing α-chymotrypsin, 1081
Epoxidation
Spectroscopic investigation of the molybdenum active sites on Mo^{VI} heterogeneous catalysts for alkene epoxidation, 3969
EPR spectroscopy
EPR studies of the reactions of high-energy copper species with hydrocarbons using a rotating cryostat, 17
Transition-metal ion dimers formed in CeO_2: An EPR study, 99
Creation and detection of coherence and polarization in pulsed EPR, 177
Single-crystal EPR study of the compounds $[MCu(edta)(H_2O)_3] \cdot H_2O$ (M = Sr, Ba), 423
EPR spectroscopic study of the reaction of Al and Ga atoms with CO_2 and CS_2 in a rotating cryostat, 799
EPR characterisation of the Cr^V intermediates in the $Cr^{VI/V}$ oxidations of organic substrates and of relevance to Cr-induced cancers, 1207
Spectroscopic study of oxygen adsorption as a method to study surface defects on CeO_2, 1669
NO reaction at surface oxygen vacancies generated in cerium oxide, 1679
Oxidation of a tricoordinated Cu^I complex to a tetracoordinated Cu^{II} species. A single-crystal EPR study, 2155
Characteristics of Cr_2O_3–CuO/MgF_2 catalysts and a comparison with Cr_2O_3/MgF_2 and CuO/MgF_2 systems, 2207
Diret EPR measurement of Arrhenius parameters for the reactions of H˙ atoms with H_2O_2 and D˙ atoms with D_2O_2 in aqueous solution, 3127
Evolution of the EPR copper(II) dimer spectrum observed in CuCe oxide with the applied microwave frequency: A computer-assisted study, 3299
EPR spectrum of an acute-angled Na_3 cluster in an adamantane matrix, 3799
EPR and ENDOR of perfluoroalkyl radical intermediates in the reaction between perfluorohypofluorites and perfluoroalkenes, 3813
EPR, ENDOR and TRIPLE resonance characterization of three paramagnetic reduction stages of 5-(9′-fluorenylidene)-5*H*-dibenzo[*a*,*d*] cycloheptene. Radical anions, radical trianions and radical penta-anions, 3821
Spectroscopic investigation of the molybdenum active sites on Mo^{VI} heterogeneous catalysts for alkene epoxidation, 3969
Adsorbate interactions of paramagnetic palladium species in Pd^{II}-exchanged H-rho zeolite characterized by EPR and electron spin echo modulation spectroscopies, 3987
Formation of polypyrrole and polythiophene within Cu^{2+}- and H^+-mordenite hosts studied by EPR and UV–VIS spectroscopy, 4321
Behaviour of oxygen species adsorbed on Al_2O_3-supported cerium oxide catalysts for methane oxidation, 4459
Equation of state
Excess molar enthalpies of (methanol–carbon dioxide)(g) from 448.2 to 548.2 K at pressures up to 15 MPa, 269
Statistical thermodynamics of hydrocarbon fluids: Scaling parameters and their group contributions, 2443
Equilibrium constant
Equilibrium aspects of the extraction of caesium nitrate by dicyclohexano-21-crown-7, dibenzo-21-crown-7 and bis-[*tert*-alkylbenzo]-21-crown-7 in 1,2-dichloroethane, 4215
ESEMS
Adsorbate interactions of paramagnetic palladium species in Pd^{II}-exchanged H-rho zeolite characterized by EPR and electron spin echo modulation spectroscopies, 3987
Etching
Study of silicon etching in HBr solutions using a scanning electrochemical microscope, 1019
Ethane
Direct conversion of methane and ethane to the corresponding alcohols using nitrous oxide over iron phosphate catalysts, 3953
Ethanol–propanal system
Vapour–liquid equilibrium of the ethanol–propanal system, 273
Ethene
Mechanism of the conversion of ethene to ethylidyne on rhodium (111): Evidence for a vinylic intermediate, 3679
In situ Raman studies of the selective oxidation of methanol to formaldehyde and ethene to ethylene oxide on a polycrystalline silver catalyst, 4149
Ethene complex
Microwave spectrum and structure of furan · ethene, 975
Ethene hydroformylation
Effects of modification of Pd/SiO_2 with Rh on catalytic activity for ethene hydroformylation, 1271
Ethylenediaminetetraacetic acid
Effect of surface tension of the matrix on fast-atom bombardment mass spectral determination of ethylenediaminetetraacetic acid, 1203
Ethylene glycol
Molecular dynamics simulations of flexible molecules. Part 1.—Aqueous solution of ethylene glycol, 31
Ethylene oxide
In situ Raman studies of the selective oxidation of methanol to formaldehyde and ethene to ethylene oxide on a polycrystalline silver catalyst, 4149
Ethylperoxyl radical
Theoretical calculation of intramolecular reactions in methylperoxyl and ethylperoxyl radicals, 1425
Ethyl Red
Resonance Raman spectroscopic study of Methyl Red and Ethyl Red adsorbed on silica, 499
Ethyne complex
The bπ.aσ complex $C_2H_2 \cdots Cl_2$ characterised by rotational spectroscopy as an intermediate in a reactive mixture of ethyne and chlorine, 1891
Euler's theorem
Symmetry extensions of Euler's theorem for polyhedral, toroidal and benzenoid molecules, 3089
Europium
Crystal fields in REOF : Eu^{3+} (RE = La, Gd and Y), 1503
Eutectic
Electrical conductivity of the systems $NaAlCl_4$ and NaCl(s)/$NaAlCl_4$ in the range 100–200 °C, 3157
Cationic motions and glass transitions of eutectic mixtures in the $(CH_3)_4NHSO_4$–H_2O and $(CH_3)_4NHSO_4$–D_2O binary systems, 4139
EXAFS
Effect of tetrahedral Ti in titania–silica mixed oxides on epoxidation activity and Lewis acidity, 1261
Probing the conformational properties of guest molecules in solid inclusion compounds *via* EXAFS spectroscopy: Bromine K-edge EXAFS studies of the bromocyclohexane/thiourea and *trans*-1-bromo-2-chlorocyclohexane/thiourea inclusion compounds, 1497
Structure of Fe, Mn-promoted sulfated zirconia catalyst by X-ray and IR absorption spectroscopies, 1825
In-situ EXAFS investigation of non-acidic CVD-based Pt/KL catalyst under oxidation–reduction cycles, 2045
Surface composition, structural and chemisorptive properties of Raney nickel catalysts, 2891
Combined DRS–RS–EXAFS–XANES–TPR study of supported chromium catalysts, 3245
Quantitative structural study of an Na–O coadsorption phase on Al(111) using X-ray standing waves, 3555
Temperature dependence of EXAFS for bromide ions in solution, 4389
Excess enthalpy
Excess molar enthalpies of (methanol–carbon dioxide)(g) from 448.2 to 548.2 K at pressures up to 15 MPa, 269
Experimental and predicted excess enthalpies of the 2,2,2-trifluoroethanol–water–tetraethylene glycol dimethyl ether ternary system using binary mixing data, 2071
Excess property
Volumetric properties of binary mixtures of water with methoxy(ethoxy)$_n$ ethanols, 2291
Bulk and surface properties of the highly non-ideal associated mixtures formed by methanol and propanal, 2779
Corrigendum to Volumetric properties of binary mixtures of water with methoxy(ethoxy)$_n$ ethanols, 3553
Excess volume
Heat capacities and concentration fluctuations in mixtures of 1,2-dibromoethane with alkanes, 1941
Exchange reaction
Exchange reactions of 2,2-dimethylpentane, 2,2-dimethylbutane and 2,2-dimethylpropane over Pt/SiO_2 and Rh/SiO_2, 1131
Dehydrogenation, hydrogenation, exchange and combustion reactions of aromatic hydrocarbons on Pd(100), 3685
Exciplex
Enthalpy changes for the formation of CdA* and CdA_2* exciplexes in the cadmium(5 $^3P_1$)-photosensitized reaction of some substrates in the gas phase, 603
Theoretical study of cadmium– and mercury–ammonia exciplexes: Comparison with experiment, 3795
Excited state
Kinetic investigation of energy pooling from Sr[5s5p(^3P_J)] studied by time-resolved atomic emission following pulsed dye-laser excitation, 811
Photoinduced electron-transfer quenching of excited singlet states of polycyclic aromatic hydrocarbons by organic acceptors. Solvent effects on the rate constants and the charge-separation efficiency, 1197
Excited-state dipole moments of some Coumarin dyes from a solvatochromic method using the solvent polarity parameter, E_T^N, 2739
Vacuum UV fluorescence excitation spectroscopy of BCl_3. Electronic spectroscopy of BCl_2, BCl_2^+, and BCl_3^+, 3073

Concentration-modulated absorption spectroscopy. Part 5.—Influence of molecular diffusion, 3101
Reactive collisions with excited-state atoms, 389
Extended chain
Dependence of the lamellar thickness of an extended-chain single crystal of polyethylene on the degree of supercooling and the pressure, 2573
Extended Hückel theory
Classification scheme for toroidal molecules, 4037
Extraction
Metal extraction in micellar media: A comparison of copper complexation rates and ultrafiltration yields of two isomeric (*E*)-1-(2′-hydroxy-5′-alkylphenyl) 1-alkanone oximes, 657
Equilibrium aspects of the extraction of caesium nitrate by dicyclohexano-21-crown-7, dibenzo-21-crown-7 and bis-[*tert*-alkylbenzo]-21-crown-7 in 1,2-dichloroethane, 4215
Fast-atom bombardment mass spectrometry
Effect of surface tension of the matrix on fast-atom bombardment mass spectral determination of ethylenediaminetetraacetic acid, 1203
Fe_3O_4 electrode
Electroreduction of oxygen on Fe_3O_4 electrodes. Part 2.—Rotating ring–disc electrode studies and mechanism, 2323
Ferrocene
Asymmetrical complexation and simultaneous electrochemical recognition of two different Group 2 metal cations by a 1,1′-ferrocene-bis(methylene aza-18-crown-6) receptor, 4331
Ferrospinel
Physico-chemical properties and catalytic activities of the spinel series $Mn_xFe_{3-x}O_4$ towards peroxide decomposition, 3489
Fibril
Diffusion behaviour of the BF_4^- anion in polyaniline fibrils. Influence of the physical state of polyaniline, 3469
Film
Determination of thickness and rupture pressure for aqueous foam films. Part 1.—Films stabilized by anionic surfactants, 4251
Mechanism of formation of copper thiocyanate on the copper anode, 4403
Fischer–Tropsch
Intrinsic kinetics of Fischer–Tropsch synthesis over an Fe–Cu–K catalyst, 3255
Flame
Ionisation in premixed fuel-lean flames of H_2, O_2 and N_2. Part 1.—Naturally occurring positive ions, 827
Ionisation in premixed fuel-lean flames of H_2, O_2 and N_2. Part 2.—Ions from alkali-metal additives, 835
Flash photolysis
Photosensitization of DNA bases by 4(5)-nitroimidazole: A steady state and flash photolysis study, 1191
Laser flash photolysis studies and magnetic field effect on a new heteroexcimer between *N*-ethylcarbazole and 1,4-dicyanobenzene in homogeneous and heterogeneous media, 1593
A spectroscopic study of Cl_2O_3, 3027
Photophysics of 3- and 4-phenyl pyridyl ketones in submicellar and micellar solutions of ionic and non-ionic surfactants, 3405
Flexible molecule
Molecular dynamics simulations of flexible molecules. Part 1.—Aqueous solution of ethylene glycol, 31
Flexible polymer
Statistical mechanics of semiflexible polymers: Yesterday, today and tomorrow, 2473
Flocculation
Depletion flocculation of polystyrene latices by water-soluble polymers, 1483
On flocculation and gelation in concentrated particulate systems containing added polymer, 4413
Flory–Huggins model
Heat capacities and concentration fluctuations in mixtures of 1,2-dibromoethane with alkanes, 1941
Mixing enthalpy and phase separation in a poly(propylene oxide)–water system, 2081
Flow calorimetry
Excess molar enthalpies of (methanol–carbon dioxide)(g) from 448.2 to 548.2 K at pressures up to 15 MPa, 269
Flow-discharge technique
Rates of reaction between the nitrate radical and some aliphatic alcohols, 405
Fluid flow
Scanning electrochemical microscopy as a probe of local fluid flow through porous solids: Application to the measurement of convective rates through a single dentinal tubule, 1407
Fluorescein dye
Response of fluorescein to carbon dioxide in dimethyl sulfoxide–water mixtures, 881
Fluorescence
Effects of water on the phosphorescence spectra of aromatic carbonyl compounds. Part 3.—Dual- or multiple-component phosphorescence of 1-indanone at 77 K in some protic solvents containing water, 855
Solubilization of two cyano 3*H*-indole molecular probes in SDS and CTAB micelles: Spectral and photophysical characterization, 2133
Characterisation of hydroxide complexes of uranium(VI) by time-resolved fluorescence spectroscopy, 2275
Rate coefficients for quenching of $Cl(^2P_{1/2})$ by various atmospheric gases, 3055
Vacuum UV fluorescence excitation spectroscopy of BCl_3. Electronic spectroscopy of BCl_2, BCl_2^+, and BCl_3^+, 3073
Oligomerization of cationic pyrene derivatives in the presence of sodium dodecyl sulfate: A route to nanoaggregate formation, 3913
Effect of temperature and viscosity on intramolecular charge-transfer fluorescence of a 4-*p*-dimethylaminostyrylpyridinium salt in protic solvents, 4199
Fluorescence spectra of methyl salicylate during the sol–gel–xerogel transitions of mixed silicon–aluminium alkoxides, 4279
Photophysical properties of structurally deformed basket-handle porphyrins, 4369
Fluorescence quenching
Laser flash photolysis studies and magnetic field effect on a new heteroexcimer between *N*-ethylcarbazole and 1,4-dicyanobenzene in homogeneous and heterogeneous media, 1593
Fluorescence spectroscopy
Femtosecond to nanosecond solvation dynamics in pure water and inside the γ-cyclodextrin cavity, 867
Triplet and radical ion properties of (*E*)-1-styrylpyrene and (*E*)-3-styrylchrysene, 3117
Fluoride etching
Direct functionalization of silicon *via* the self-assembly of alcohols, 4001
Fluorination
Diffuse reflectance infrared Fourier-transform study of the direct thermal fluorination of diamond powder surfaces, 3209
Fluorine
Rate constants for the reactions of fluorine atoms with alkanes and hydrofluorocarbons at room temperature, 3041
Foam
Determination of thickness and rupture pressure for aqueous foam films. Part 1.—Films stabilized by anionic surfactants, 4251
Food science
Evidence of extraneous surfactant adsorption altering adsorbed layer properties of β-lactoglobulin, 1991
Formaldehyde
In situ Raman studies of the selective oxidation of methanol to formaldehyde and ethene to ethylene oxide on a polycrystalline silver catalyst, 4149
Formic acid
Catalytic decomposition reaction of formic acid on an Ar^+-bombarded TiO_2(110) surface: Steady-state kinetics and microscopic surface structure, 1663
Oxygen reduction on a rotating Pt disc electrode in formic acid-containing solutions, 2817
Surface chemistry of polar oxide surfaces: Formic acid on NiO(111), 3709
Surface structure change of a $[Pt_4(\mu\text{-}CH_3COO)_8]/SiO_2$ catalyst active for the decomposition of formic acid, 4161
Fourier-transform interferometer
Phosphorescence of β-carotene, 4059
Free radical
Reactive scattering of atoms and radicals, 575
High-level *ab initio* study of the reaction of OCS with OH radicals, 793
Rate constants for the reactions of C_2H_5, C_2H_5O and $C_2H_5O_2$ radicals with NO_3 at 298 K and 2.2 Torr, 817
Investigation of the consumption of diphenylpicrylhydrazyl in solution in the absence and presence of ultrasound, 1067
Thermal reaction of azoisopropane in the presence of (*E*)-$CH_3CH{=}CHCH_3$: Reactions of the radical 2-C_3H_7, 1303
Kinetics and products of the gas-phase reactions of $(CH_3)_4Si$, $(CH_3)_3SiCH_2OH$, $(CH_3)_3SiOSi(CH_3)_3$ and $(CD_3)_3SiOSi(CD_3)_3$ with Cl atoms and OH radicals, 3033
Kinetics and mechanism of the reaction of CH_3 and CH_3O with ClO and OClO at 298 K, 3045
Photophysics of 3- and 4-phenyl pyridyl ketones in submicellar and micellar solutions of ionic and non-ionic surfactants, 3405
Elementary radical reactions and autoignition, 4179
Frequency response
Frequency-response study of micro- and macro-pore diffusion in manufactured zeolite pellets, 1399
Dynamics study of a closed diffusion cell by using a frequency response method: Single resonator, 1695
Analysis of bimodal frequency-response behaviour of *p*-xylene diffusion in silicalite-1, 2027
Freundlich isotherm
Sorption isotherms of methane, ethane, ethene and carbon dioxide on NaX, NaY and Na-mordenite zeolites, 2935
Frontier orbital
Catalysed cyclotrimerisation of acetylene: A computational study, 3975
FTIR-PA spectroscopy
Total characterization of the BCl_3-modified silica surface by means of quantitative surface analysis, 2173
FTIR spectroscopy
Influence of oxidation and reduction conditions upon the morphology of silica-supported polycrystalline silver catalysts, 133
FTIR study of the effects of sulfur poisons on NO adsorption on supported copper oxide catalysts, 141
FTIR studies of adsorption of NO, NO_2 and N_2O on layered V_2O_5/ZrO_2, 1557
Structure of Fe, Mn-promoted sulfated zirconia catalyst by X-ray and IR absorption spectroscopies, 1825
FTIR study of the kinetics of solid-state ion exchange in zeolites using pyridine as a probe, 1845
FTIR study of the adsorption and transformation of allylbenzene over oxide catalysts, 1861
Cationic mobility in MgX zeolite: An FTIR study, 2961
A model system for the hydrogen-bonded chain with large proton polarizability present in the L_{550} intermediate of bacteriorhodopsin: An FTIR study, 3141
Surface composition of Pd–Fe catalysts supported on silica, 3237
Formation of $Cu^I{-}N_2$ adducts at 298 and 77 K in Cu^I-ZSM-5: An FTIR investigation, 3285
FTIR studies of the interaction of aromatic hydrocarbons with vanadium oxide layered on ZrO_2 and TiO_2, 3505
FTIR investigation of polarizable hydrogen bonds in carboxylic acid–pyridine complexes in the mid- and far-IR region, 3831
In situ FTIR studies of high-temperature adsorption of hydrogen on zirconia, 4441
FT-Raman spectroscopy
Novel spectroscopic deconvolution procedure for complex biological systems: Vibrational components in the FT-Raman spectra of

ice-man and contemporary skin, 3883
Fuel cell
Oxygen reduction on a rotating Pt disc electrode in formic acid-containing solutions, 2817
Fullerene
Formation and coalescence of fullerene ions from direct laser vaporization, 987
Energetics and isomerisation pathways of a lower fullerene. The Stone–Wales map for C_{40}, 1421
Isomer counting using point group symmetry, 2241
Kinetic stability of fullerenes with four-membered rings, 4349
Furan complex
Microwave spectrum and structure of furan · ethene, 975
Gallium
EPR spectroscopic study of the reaction of Al and Ga atoms with CO_2 and CS_2 in a rotating cryostat, 799
Gallium fluoride
Vibration–rotational spectra of GaF and molecular properties of diatomic fluorides of elements in Group 13, 3007
Gas-phase kinetics
Rates of reaction between the nitrate radical and some aliphatic alcohols, 405
Kinetics and products of the gas-phase reactions of $(CH_3)_4Si$, $(CH_3)_3SiCH_2OH$, $(CH_3)_3SiOSi(CH_3)_3$ and $(CD_3)_3SiOSi(CD_3)_3$ with Cl atoms and OH radicals, 3033
Kinetics and mechanism of the reaction of CH_3 and CH_3O with ClO and OClO at 298 K, 3045
Br_2-sensitised decomposition of ozone: Kinetics of the reaction $BrO + O_3 \rightarrow$ products, 4189
Gas-phase spectroscopy
Donor–acceptor complexes of Lewis bases with bromine monochloride in the gas phase: some generalisations from rotation spectroscopy, 1881
Gas-sensitive resistor
Theory of self-diagnostic sensor array devices using gas-sensitive resistors, 1961
Gay–Berne model
Computer-simulation studies of anisotropic systems. Part XXIV.—Constant-pressure investigations of the smectic B phase of the Gay–Berne mesogen, 2141
Monte Carlo study of Gay–Berne liquid-crystal droplets, 3441
GeH_4
Arrhenius parameters for the reaction of H atoms with GeH_4, 3367
Gel
Simulated structure of mixed particle gels, 51
Charge regulation at the surface of porous silica, 2965
Gelation of aqueous solutions of diblock and triblock copolymers of ethylene oxide and 1,2-butylene oxide studied by ^1H nuclear magnetic relaxation, 3461
Fluorescence spectra of methyl salicylate during the sol–gel–xerogel transitions of mixed silicon–aluminium alkoxides, 4279
Gelation
Micellization and gelation of a triblock copolymer of oxyethylene and oxypropylene, $E_{93}P_{44}E_{93}$, studied by ^1H nuclear magnetic relaxation, 1491
Computer simulation of sulfur vulcanization, 2655
Thermoreversible gelation of hydrated polymers, 2663
On flocculation and gelation in concentrated particulate systems containing added polymer, 4413
Gibbs energy
Vapour–liquid equilibrium of the ethanol–propanal system, 273
Gibbs energies of transfer of several alkali-metal chlorides from water to sucrose–water mixtures using streaming amalgam electrodes, 451
Thermodynamic transfer properties for Na^+, Tl^+ and Ag^+ to water–acetonitrile mixtures, 875
Gibbs energies, entropies and enthalpies of transfer for divalent cations to several solvents, 3843
Glass
X-Ray photoelectron spectrum of glassy B_2S_3. Experimental and theoretical study, 93
Use of ultraviolet excitation spectra of Tl^+ for probing oxidic networks: Alkali-metal borate glasses, 3485
Glass transition
Structural glass transitions and thermophysical processes in amorphous carbohydrates and their supersaturated solutions, 1511
Neural network prediction of glass-transition temperatures from monomer structure, 2491
Glow-discharge device
Temporal and spatial distribution profiles of lithium atoms in low-pressure discharges by concentration-modulated absorption spectroscopy, 1297
Gold
Mechanistic consideration of formation of polymer-protected nanoscopic bimetallic clusters, 4111
Gold electrode
In situ quartz-microbalance study of the self-assembly and stability of aliphatic thiols on polarized gold electrodes, 1949
Graft-copolymer
Self-organization of graft-copolymers at surfaces, interfaces and in bulk, 2855
Graphite
Catalytic effect of vanadium, iron and lead oxides on the oxidation of moderator graphite, 3717
Graphitic micropore
Molecular dynamics study of the self-diffusion of supercritical methane in slit-shaped graphitic micropores, 1377
Graphitization
Structural and adsorption properties of carbons synthesized within taeniolite matrices, 493
Graph theory
Non-superaromatic reference defined by graph theory for a super-ring molecule, 237
Energetics and isomerisation pathways of a lower fullerene. The Stone–Wales map for C_{40}, 1421
Symmetry extensions of Euler's theorem for polyhedral, toroidal and benzenoid molecules, 3089
Linearisation of graphs using walks of unit length, 3095
Guanine derivative
Thermodynamic investigation of the effect of octanol–water mutual miscibility on the partitioning and solubility of some guanine derivatives, 995
Guest dynamics
Guest dynamics in carceplexes: A ^2H NMR study, 4127
Guest molecule
Probing the conformational properties of guest molecules in solid inclusion compounds *via* EXAFS spectroscopy: Bromine K-edge EXAFS studies of the bromocyclohexane/thiourea and *trans*-1-bromo-2-chlorocyclohexane/thiourea inclusion compounds, 1497
Haemoglobin
STM of folded and unfolded haemoglobin molecules electrochemically deposited on highly oriented pyrolytic graphite, 1471
Organic phosphate-binding groups electrostatically linked to the reactivity of the Cys F9 [93] β sulfhydryl group of haemoglobin, 2095
Halide
Laser-Raman spectroscopic study of the vapour phase of $NbCl_5$ and mixtures of $NbCl_5$ and $SnCl_2$, 1445
Halochromism
Halochromism and solvatochromism of a π^* probe in binary solvent mixtures, 3839
Halogenoethane
Effects of addition gases on the IR multiphoton dissociation of haloethanes, 983
Hard-rod model
One-dimensional xenon gas in the pores of mordenite, 2945
Harmonic force field
Structure, harmonic force field and hyperfine coupling constants of nitrosyl chloride, 3347
H/D exchange
Effect of Pt particle size on H/D exchange of methane over alumina- and zeolite-supported catalysts, 569
Heat capacity
Heat capacities and concentration fluctuations in mixtures of 1,2-dibromoethane with alkanes, 1941
Hessian response equilibria
Unnoticed identities in chemical thermodynamics, 1325
Heteroexcimer
Laser flash photolysis studies and magnetic field effect on a new heteroexcimer between *N*-ethylcarbazole and 1,4-dicyanobenzene in homogeneous and heterogeneous media, 1593
Heterogeneous catalysis
Is the observed hydrogenation of formate the rate-limiting step in methanol synthesis?, 1267
FTIR study of the adsorption and transformation of allylbenzene over oxide catalysts, 1861
Electrical properties of doped vanadium phosphate phases and VPO catalysts used in the partial oxidation of *n*-butane to maleic anhydride, 3231
Cobalt catalysts supported on activated carbons: Preparation and behaviour in the hydrogenation of carbon oxides, 3519
Behaviour of oxygen species adsorbed on Al_2O_3-supported cerium oxide catalysts for methane oxidation, 4459
Surface basicity of a new family of catalysts: Aluminophosphate oxynitride (AlPON), 4477
12-Heteropolyacid
NMR characterization of the supported 12-heteropoly acids, 375
Heteropolyacid catalyst
EPR of vanadium in $Ce_{0.25}H_3PVMo_{11}O_{40}$ catalyst. Formation of vanadyl dimers during the oxidative dehydrogenation of isobutyric acid, 1025
Hexaethylbenzene
Variable-temperature X-ray crystallographic and magic-angle spinning NMR spectral studies on hexaethylbenzene, 2149
Hexapole state selection
Hexapole state selection and focusing *vs.* brute force orientation of beam molecules, 205
High-energy copper species
EPR studies of the reactions of high-energy copper species with hydrocarbons using a rotating cryostat, 17
High-pressure liquid mixture
Liquid mixtures at high pressures referred to a pseudospinodal curve: Ethanol–methylcyclopentane and carbon disulfide–tetramethylsilane, 59
High-resolution spectroscopy
High-resolution spectroscopic study of $2\nu_1$, $2\nu_3$ and $\nu_1 + \nu_3$ stretching states: The local-mode effects of H_2Se, 13
High-resolution study of the 000–000 band of the $\tilde{A}\,^1A''$–$\tilde{X}\,^1A'$ system of HNO in emission from the H + NO reaction, 2975
HNC molecule
Molecular rotation and isomerisation in hydrogen isocyanide, 1717
^1H NMR spectroscopy
Physicochemical properties of dimethyl sulfoxide–methanol liquid mixtures. Experimental and semiempirical quantum chemical studies, 65
HNO
High-resolution study of the 000–000 band of the $\tilde{A}\,^1A''$–$\tilde{X}\,^1A'$ system of HNO in emission from the H + NO reaction, 2975
HNO_3
Molecular complexes of nitric acid with N_2, CO and NO studied by matrix isolation IR spectroscopy, 3111
HOMO
Time-resolved resonance Raman spectroscopy of triplet-state metallated and free-base tetraarylporphyrins, 411
Homogeneous chemical equilibria
Unnoticed identities in chemical thermodynamics, 1325
Honeycomb geometry
Auxetic two-dimensional polymer networks. An

example of tailoring geometry for specific mechanical properties, 2671
HREELS
Is the observed hydrogenation of formate the rate-limiting step in methanol synthesis?, 1267
Photoemission and HREELS study of K adsorption on TiO_2(100), 3569
HRTEM
CoO–ZnO solid solution as a model to investigate the CO–cation interaction: An FTIR and HRTEM study, 4445
Hydrated electron
Transformation reactions of the electron adducts of methyl derivatives of xanthine in aqueous solution by pulse radiolysis, 615
Hydration
Precision modelling of conductivity data of monovalent aqueous electrolytes, 303
Cationic mobility in MgX zeolite: An FTIR study, 2961
Hydrocarbon
Influence of strong metal–support interaction on exchange with deuterium and other reactions of hydrocarbons. Part 1.—Studies with Rh/TiO_2 and Rh/SiO_2, 741
Investigations on hydrogen spillover. Part 2.—Hydrocarbon conversion on bifunctional catalysts, 1539
Statistical thermodynamics of hydrocarbon fluids: Scaling parameters and their group contributions, 2443
Hydrocarbon matrix
EPR studies of the reactions of high-energy copper species with hydrocarbons using a rotating cryostat, 17
Hydrocarbon polymer
Thermodynamic properties of a coarse-grained model of hydrocarbon polymers. Computer simulations on articulated chain structures, 2457
Hydrochlorofluorocarbon
Kinetics of the reactions of the HO_2 radical with peroxyl radicals derived from hydrochlorofluorocarbons and hydrofluorocarbons, 1313
Hydroconversion
Catalytic properties of the silicoaluminophosphates SAPO-5 and SAPO-11 in *n*-octane and isooctane hydroconversion, 4171
Hydrocracking
Pt/SAPO-5 and Pt/SAPO-11 as catalysts for the hydroisomerization and hydrocracking of *n*-octane, 1551
Hydrodehalogenation
Hydrodehalogenation of chlorosilanes in the presence of metal silicides: Experimental studies of gas and solid phase composition related to thermodynamic calculations, 3879
Hydrofluorocarbon
Kinetics of the reactions of the HO_2 radical with peroxyl radicals derived from hydrochlorofluorocarbons and hydrofluorocarbons, 1313
High-resolution IR spectrosopy of jet-cooled CF_3CH_2F, 1723
Rate constants for the reactions of fluorine atoms with alkanes and hydrofluorocarbons at room temperature, 3041
Hydrogel
Measurement of viscoelastic changes at electrodes modified with redox hydrogels with a quartz crystal device, 4083
Hydrogen
Hydrogenation of propyne over palladium catalysts, 3269
In situ FTIR studies of high-temperature adsorption of hydrogen on zirconia, 4441
Hydrogen absorption
Absorption of hydrogen in copper, 3659
Hydrogen abstraction
Laser flash photolysis studies on hydrogen atom abstraction from phenol by triplet naphthoquinones in acetonitrile, 2751
Theoretical *ab initio* study of the reaction of CH_3SH with OH radical, 3783
Hydrogenation
Surface composition of Pd–Fe catalysts supported on silica, 3237
Cobalt catalysts supported on activated carbons: Preparation and behaviour in the hydrogenation of carbon oxides, 3519
Distinguishing direct and quasi-direct mechanisms for an Eley–Rideal gas/surface reaction. Stereochemistry of H addition to cyclohexene on Cu(100), 3645
Surface science and catalysis of ethylene hydrogenation, 3671
Hydrogen bond
Molecular dynamics simulations of flexible molecules. Part 1.—Aqueous solution of ethylene glycol, 31
X-Ray, FTIR, ^1H and ^{13}C NMR, PM3 and AM1 studies of $(N-H\cdots N)^+$ and $(O-H\cdots O)^-$ hydrogen bonds in a complex of 1,8-diaminonaphthalene with maleic acid: Proton cavity and basicity of proton sponges, 87
Effects of water on the phosphorescence spectra of aromatic carbonyl compounds. Part 3.—Dual- or multiple-component phosphorescence of 1-indanone at 77 K in some protic solvents containing water, 855
Differential scanning calorimetric study of the interactions of some stabilizing amino acids and oligopeptides with hen egg white lysozyme, 2101
Modelling the influence of monomer properties on hydrogen bond density in oriented, rigid copolymer systems, 2629
A model system for the hydrogen-bonded chain with large proton polarizability present in the L_{550} intermediate of bacteriorhodopsin: An FTIR study, 3141
Intramolecular hydrogen bonding and molecular conformation. Part 4.—Corrections of thermodynamic properties obtained by IR measurements at different temperatures and pressures, 3379
FTIR investigation of polarizable hydrogen bonds in carboxylic acid–pyridine complexes in the mid- and far-IR region, 3831
Long range H-bond specific interactions between nucleosides, 4329
Simultaneous description of excess enthalpy and vapour–liquid equilibrium data of associated mixtures by means of a lattice–fluid model, 4381
Hydrogen bridge
Protonation of pyridines by phenols, thiophenol, trifluoroacetic acid and methanesulfonic acid in aprotic solvents, 1611
Hydrogen chemisorption
^1H NMR of hydrogen chemisorbed on silica-supported platinum particles: An evaluation of different models, 2203
Surface composition, structural and chemisorptive properties of Raney nickel catalysts, 2891
Hydrogen–deuterium exchange
Vibrational Raman optical activity of lysozyme: Hydrogen–deuterium exchange, unfolding and ligand binding, 2087
Hydrogen peroxide
Direct EPR measurement of Arrhenius parameters for the reactions of H˙ atoms with H_2O_2 and D˙ atoms with D_2O_2 in aqueous solution, 3127
Hydrogen selenide
High-resolution spectroscopic study of $2\nu_1$, $2\nu_3$ and $\nu_1 + \nu_3$ stretching states: The local-mode effects of H_2Se, 13
Hydrogen solubility
Dissolution of hydrogen and deuterium in titanium, $Ti_{9.4}Al_6$ and Ti_3Al, 1967
Hydrogen spillover
Investigations on hydrogen spillover. Part 1.—Electrical conductivity studies on titanium dioxide, 1091
Investigations on hydrogen spillover. Part 2.—Hydrocarbon conversion on bifunctional catalysts, 1539
Palladium–ceria catalysts: Reversibility of hydrogen chemisorption and redox phenomena, 2185
Hydrogen sulfide complex
$H_2S\cdots Cl_2$ characterised in a pre-reactive gas mixture of hydrogen sulfide and chlorine through rotational spectroscopy: The nature of the interaction, 2059
Hydroisomerization
Pt/SAPO-5 and Pt/SAPO-11 as catalysts for the hydroisomerization and hydrocracking of *n*-octane, 1551
Catalytic properties of the silicoaluminophosphates SAPO-5 and SAPO-11 in *n*-octane and isooctane hydroconversion, 4171
Hydrolysis
IR study of acetonitrile adsorption on hydroxylated zirconium dioxide: Mechanism of acetonitrile hydrolysis, 2913
Hydrothermal synthesis
Influence of the source of silicon and aluminium in the hydrothermal synthesis of sodalite, 1147
Hydrotreating catalyst
IR spectroscopy of hydrotreating catalysts, 517
Hydroxyl radical
Temperature dependence of the rate of reaction of OH with some aromatic compounds in aqueous solution, 1631
β-Hydroxyperoxyl radical
Kinetics of reactions of primary, secondary and tertiary β-hydroxy peroxyl radicals. Application to isoprene degradation, 1911
Hypoiodous acid
Effect of iodide concentration upon the kinetics of disproportionation of hypoiodous acid in borate buffer, 863
Kinetics of disproportionation of hypoiodous acid in phosphate and borate buffer at pH < 8.5 modelled using iodide feedback, 2269
Inclusion
Femtosecond to nanosecond solvation dynamics in pure water and inside the γ-cyclodextrin cavity, 867
Probing the conformational properties of guest molecules in solid inclusion compounds *via* EXAFS spectroscopy: Bromine K-edge EXAFS studies of the bromocyclohexane/thiourea and *trans*-1-bromo-2-chlorocyclohexane/thiourea inclusion compounds, 1497
Dynamics of benzene and pyridine guest molecules in their tri-*ortho*-thymotide inclusion compounds. Solid-state ^2H NMR studies, 2017
Stresses in lipid membranes and interactions between inclusions, 3415
1-Indanone
Effects of water on the phosphorescence spectra of aromatic carbonyl compounds. Part 3.—Dual- or multiple-component phosphorescence of 1-indanone at 77 K in some protic solvents containing water, 855
Indicator dye
Effect of association of sulfonephthalein dyes with sodium dodecyl sulfate micelles on their acid–base equilibria, 681
Indicator electrode
Photogenerated chloride ion concentration near the surface of UV-irradiated titanium dioxide in the presence of aqueous 2,4-dichlorophenol probed using an ultramicroelectrode, 3893
InSb
CF_3I adsorption on InSb(001), 3603
Interacting sphere model
Modified interacting-sphere model for self-diffusion and infinite-dilution mutual-diffusivity of *n*-alkanes, 245
Interaction potential
Ab initio calculation of gas-phase ion mobilities of third period atomic ions in helium, 4355
Interatomic potential
New model of potential-energy functions for atomic solids, 1567
Determination of a transferable interatomic potential for alkali-metal perchlorates and its application to morphological modelling, 4133
Intercalation
Electrochemical cell for composition-dependent electronic conductivity and chemical diffusion coefficient measurements applied to mixed-conductivity intercalation compounds, 2127
Al-Pillared saponites. Part 3.—Effect of parent clay layer charge on the intercalation–pillaring mechanism and structural properties, 2229
Molecular modelling of ligand–DNA

intercalation interactions, 2515
Interdiffusion
Model for chemical interdiffusion of solubilizates and ionic micelles. Aqueous solutions of *n*-alcohols and sodium dodecyl sulfate, 2837
Interface
Structural and thermodynamic properties of interfaces between coexisting phases in polymer blends: a Monte Carlo simulation, 2369
Liquid droplets and solid particles at surfactant solution interfaces, 2681
Crystal-face specificity of electrical double-layer parameters at metal/solution interfaces, 3311
Phase behaviour and structure in a non-ionic surfactant–oil–water mixture, 4269
Intermetallic compound
Dissolution of hydrogen and deuterium in titanium, $Ti_{94}Al_6$ and Ti_3Al, 1967
Intermolecular interaction
Influence of fluorine on aromatic interactions, 2009
Intramolecular hydrogen bonding
Intramolecular hydrogen bonding in *N*-salicylideneanilines. X-Ray diffraction and solid-state NMR studies, 77
Intramolecular rearrangement
Theoretical calculation of intramolecular reactions in methylperoxyl and ethylperoxyl radicals, 1425
Ion-beam spectroscopy
Ion-beam spectroscopy of long-range complexes, 3725
Ion binding
Ion binding by poly[4-(pyrrol-1-ylmethyl)benzoic acid] thin films, 1241
Ion exchange
Reversible and irreversible adsorption of nitrogen monoxide on cobalt ion-exchanged ZSM-5 and mordenite zeolites at 273–523 K, 767
Ion binding by poly[4-(pyrrol-1-ylmethyl)benzoic acid] thin films, 1241
Nickel ion-exchanged zeolite-4A: Reduction behaviour of nickel and structure stability, 3983
FTIR study of the kinetics of solid-state ion exchange in zeolites using pyridine as a probe, 1845
Ionic complex
Electronic spectroscopy of size-selected ionic complexes, 91
Ionic-conductivity switching
Ion-conducting behaviour and photoinduced ionic-conductivity switching of composite films containing crowned cholesteric liquid crystals, 1237
Ionic species
Aggregation of alkaline-earth-metal thiocyanates in aprotic donor solvents, 4395
Ion inclusion
Ion inclusion into Langmuir–Blodgett films studied on a quartz crystal microbalance, 1783
Ionisation
Ionisation in premixed fuel-lean flames of H_2, O_2 and N_2. Part 1.—Naturally occurring positive ions, 827
Ionisation in premixed fuel-lean flames of H_2, O_2 and N_2. Part 2.—Ions from alkali-metal additives, 835
Ion mobility
Ab initio calculation of gas-phase ion mobilities of third period atomic ions in helium, 4355
Ion pairing
Partition and dimerization of ion-pair tetraalkylammonium salts in xylene, 643
Iridium surface
Adsorption of nitric oxide on Ir{100}: Influence of substrate reconstruction, 3575
Quantification of the selective activation of C—C bonds in short-chain alkanes. Reactivity of ethane, propane, isobutane, *n*-butane and neopentane on Ir(111), 3695
IR multiphoton dissociation
Effects of addition gases on the IR multiphoton dissociation of haloethanes, 983
Iron
Selective catalytic reduction of nitric oxide with ammonia on MFI-type ferrisilicate, 3275
Iron(II) complex
Mechanism of oxidation of iron(II) complexes by the azide radical, 3133
Iron oxide film
Mixed-valence formation in highly oriented Ti-doped iron oxide film, 2161
Iron–phosphorus alloy
Thermodynamic properties and phase equilibria in the Fe–P system, 703
Iron porphyrin
A force field for molecular mechanics studies of iron porphyrins, 1741
Irreversible adsorption
Reversible and irreversible adsorption of nitrogen monoxide on cobalt ion-exchanged ZSM-5 and mordenite zeolites at 273–523 K, 767
IR spectroscopy
IR studies of adhesion promoters. Part 1.—Methoxytrimethylsilane on silica at the solid/liquid interface, 105
Surface characterisation of yttria-stabilized tetragonal ZrO_2. Part 2.— Adsorption of CO, 113
Surface characterization of yttria-stabilized tetragonal ZrO_2. Part 3.—CO_2 adsorption and the CO_2–CO interaction, 125
IR spectroscopic study of NO_2 adsorption on chromia, 149
Collision broadening of CO_2 transitions in the region of 4.3 μm. Effects of broadening gas (He, Ar and N_2), rovibrational states and temperature, 191
IR studies of adhesion promoters. Part 2.—Adsorption of the alkyltrimethoxysilane and alkylamino-trimethoxysilane on silica at the solid/liquid interface, 359
IR spectroscopic study of acid sites in mordenites fluorinated under mild conditions, 385
IR spectroscopy of hydrotreating catalysts, 517
IR spectroscopic study of butane and propene adsorption on Pt/CeO_2–Al_2O_3 catalysts, 733
IR and ^1H NMR studies on the adsorption of gaseous hydrogen chloride on γ-alumina, 941
IR studies of adhesion promoters. Part 3.—Adsorption and coupling of bifunctional silanes on silica at the solid/liquid interface, 1253
Rotational isomerism in acrylic acid. A combined matrix-isolated IR, Raman and *ab initio* molecular orbital study, 1571
High-resolution IR spectrosopy of jet-cooled CF_3CH_2F, 1723
Molecular beam study of C_2H_4 oxidation on platinum: IR chemiluminescence of the CO and CO_2 products, 1801
In-situ IR monitoring of the acidic and structural variations of mordenite caused by pressure and temperature, 1835
Use of combination modes and overtones of metal carbonyls for the IR study of cation states in zeolites: Copper(I) carbonyls in reduced CuNaY zeolites, 2035
High-resolution spectroscopic study of the oxidation of white phosphorus, 2993
IR spectrum of the AsH radical in its $X\,^3\Sigma^-$ state, recorded by laser magnetic resonance, 2999
Bonding and ligand exchange in pentamethyldialane. An IR, NMR and *ab initio* study, 3015
Molecular complexes of nitric acid with N_2, CO and NO studied by matrix isolation IR spectroscopy, 3111
Corrigendum to IR studies of adhesion promoters. Part 3.—Adsorption and coupling of bifunctional silanes on silica at the solid/liquid interface, 3309
Gas-phase IR spectrum of 1-azaindolizine: Scaled quantum mechanical force field and spectrum assignment, 3741
Isocyanogen
Molecular rotation and isomerisation in hydrogen isocyanide, 1717
Isomer counting
Isomer counting using point group symmetry, 2241
Isomerisation
Energetics and isomerisation pathways of a lower fullerene. The Stone–Wales map for C_{40}, 1421
Molecular rotation and isomerisation in hydrogen isocyanide, 1717
Isooctane
Catalytic properties of the silicoaluminophosphates SAPO-5 and SAPO-11 in *n*-octane and isooctane hydroconversion, 4171
Isopiestic measurement
Comparison of activity coefficients in the three-component system sodium chloride–sucrose–water from independent isopiestic and emf measurements at 298.15 K, 1457
Isotherm
Simple determination of experimental isotherms using diffusion denuder tubes, 485
Sloping plateaux in the pressure–composition isotherms of the titanium–hydrogen and $Ti_{94}Al_6$–hydrogen systems, 4143
Isothermal compressibility
Intermolecular packing of freely jointed branched polyalkene melts: A microscopic approach, 2427
Isotope effect
Isotope effects of rubidium in amalgam/aqueous solution systems, 2319
Kerr function
Rotational Brownian motion of a two-dimensional rigid rotator: Relaxation and steady-state regimes, 41
Kinetic-energy function
Derivation of accurate kinetic and potential-energy functions for several simultaneous large-amplitude vibrations: Application to acetaldehyde in the S_0 and T_1 states, 399
Kinetic model
A simple model for the kinetic evaluation of zeolite crystallization processes, 549
Kinetics
Surface electrochemistry and kinetics of anodic bromine formation at platinum, 283
Metal extraction in micellar media: A comparison of copper complexation rates and ultrafiltration yields of two isomeric (*E*)-1-(2′-hydroxy-5′-alkylphenyl) 1-alkanone oximes, 657
Kinetic investigation of energy pooling from Sr[5s5p(^3P_J)] studied by time-resolved atomic emission following pulsed dye-laser excitation, 811
Ionisation in premixed fuel-lean flames of H_2, O_2 and N_2. Part 1.—Naturally occurring positive ions, 827
Ionisation in premixed fuel-lean flames of H_2, O_2 and N_2. Part 2.—Ions from alkali-metal additives, 835
Effect of iodide concentration upon the kinetics of disproportionation of hypoiodous acid in borate buffer, 863
Kinetics by thermometry: An aldol condensation reaction, 991
Investigation of the consumption of diphenylpicrylhydrazyl in solution in the absence and presence of ultrasound, 1067
Interaction of the chloropentaamminecobalt(III) cation with mixed micelles of anionic and non-ionic surfactants: A kinetic study, 1075
Is the observed hydrogenation of formate the rate-limiting step in methanol synthesis?, 1267
Thermal reaction of azoisopropane in the presence of (*E*)-$CH_3CH{=}CHCH_3$: Reactions of the radical 2-C_3H_7, 1303
Kinetics of the reactions of the HO_2 radical with peroxyl radicals derived from hydrochlorofluorocarbons and hydrofluorocarbons, 1313
Effect of the matrix on the kinetics of dynamic supercritical fluid extraction, 1333
Specific effect of alkali-metal cations on the kinetics of peroxodisulfate–iodide reactions, 1345
Effects of ureas on the kinetics of acid hydrolysis of 1-phenylethyl nitrite in water and in aqueous micellar solutions of sodium dodecyl sulfate, 1349
Diversity of the kinetics of carbon monoxide oxidation on differently prepared zinc oxides, 1391
Addition of cyclopentane to slowly reacting mixtures of $H_2 + O_2$ between 673 and 783 K: Reactions of H and OH with

cyclopentane and of cyclopentyl radicals, 1431
Kinetic study of the formation of cation-excess magnetite, 1533
Kinetics and mechanism of the reaction between thymol blue and bromate in acidic medium, 1635
Catalytic decomposition reaction of formic acid on an Ar^+-bombarded TiO_2(110) surface: Steady-state kinetics and microscopic surface structure, 1663
Kinetics and products of the photocatalytic degradation of morpholine (tetrahydro-2*H*-1, 4-oxazine) in TiO_2 aqueous suspensions, 1853
Kinetics of reactions of primary, secondary and tertiary *β*-hydroxy peroxyl radicals. Application to isoprene degradation, 1911
Determination of absolute rate constants for the reversible hydrogen-atom transfer between thiyl radicals and alcohols or ethers, 1923
Kinetics of disproportionation of hypoiodous acid in phosphate and borate buffer at pH < 8.5 modelled using iodide feedback, 2269
Corrigendum to Relation between the surface states of oxide films at Rh electrodes and kinetics of the oxygen evolution reaction, 2353
Polyethylene crystallization from dilute solutions: Adsorption isotherm on the growth face, 2581
Structure and swelling of end-linked model networks, 2649
Kinetics of intra-polymer electron-transfer reactions in macromolecule–metal complexes, 2877
Kinetic study of the effects of H, O, N, S, NO, NO_2 and O_2 on the surface states of InGaAs and GaAs, 3021
Rate constants for the reactions of fluorine atoms with alkanes and hydrofluorocarbons at room temperature, 3041
Direct EPR measurement of Arrhenius parameters for the reactions of H˙ atoms with H_2O_2 and D˙ atoms with D_2O_2 in aqueous solution, 3127
Intrinsic kinetics of Fischer–Tropsch synthesis over an Fe–Cu–K catalyst, 3255
Kinetics of solvated electrons in reaction with hexamethylphosphoric triamide, 3809
Thermal stability of doped ceria: Experiment and modelling, 3941
Elementary radical reactions and autoignition, 4179
Reaction–diffusion effects and systematic design of gas-sensitive resistors based on semiconducting oxides, 4299
Transformation of cerium(III) hydroxycarbonate into ceria. Part 1.—Nucleation and growth rates of ceria, 4431
Transformation of cerium(III) hydroxycarbonate into ceria. Part 2.—Experimental study of the growth rate, 4437

Kinetic stability
Kinetic stability of fullerenes with four-membered rings, 4349

Kirkwood–Buff integral
Preferential solvation in mixed solvents. Part 7.—Binary mixtures of water and alkanolamines, 427
Kirkwood–Buff integrals and preferential solvation in ternary non-electrolyte mixtures, 431
Corrigendum to Kirkwood–Buff integrals and preferential solvation in ternary non-electrolyte mixtures, 1885

β-Lactoglobulin
Evidence of extraneous surfactant adsorption altering adsorbed layer properties of *β*-lactoglobulin, 1991
Neutron reflectivity of absorbed *β*-casein and *β*-lactoglobulin at the air/water interface, 2847

Lamellar thickness
Dependence of the lamellar thickness of an extended-chain single crystal of polyethylene on the degree of supercooling and the pressure, 2573

Laminar shear
Microstructural studies of electro-rheological fluids under shear, 1787

Langmuir–Blodgett film
Photoelectrochemical properties of 'Q-state' CdS particles in arachidic acid Langmuir–Blodgett films, 665
Electrochemical properties of myoglobin embedded in Langmuir–Blodgett and cast films of synthetic lipids, 1775
Ion inclusion into Langmuir–Blodgett films studied on a quartz crystal microbalance, 1783
Photoelectrochemical behaviour of Q-state $CdS_xSe_{(1-x)}$ particles in arachidic acid Langmuir–Blodgett films, 3399

Langmuir isotherm
Sorption isotherms of methane, ethane, ethene and carbon dioxide on NaX, NaY and Na-mordenite zeolites, 2935

Lanthanum film
Interaction of carbon dioxide with oxidised La/Cu(111), 3611

Lanthanum oxide
Low-temperature synthesis of perovskite-type oxides of lanthanum and cobalt and their electrocatalytic properties for oxygen evolution in alkaline solutions, 1871

Large pore
Synthesis and characterization of CAM-1, a novel aluminophosphate molecular sieve precursor, 3995

Lariat crown ether
Stabilities in water of 1:1 lariat 16-crown-5 complexes with metal ions: Transfer activity coefficients from protic to aprotic solvents of 1:1 complexes of lariat and substituted 16-crown-5 derivatives with metal ions, 4079

Laser
Concentration-modulated absorption spectroscopy. Part 5.—Influence of molecular diffusion, 3101

Laser ablation
EPR studies of the reactions of high-energy copper species with hydrocarbons using a rotating cryostat, 17

Laser flash photolysis
Kinetics of reactions of primary, secondary and tertiary *β*-hydroxy peroxyl radicals. Application to isoprene degradation, 1911
Laser flash photolysis studies on hydrogen atom abstraction from phenol by triplet naphthoquinones in acetonitrile, 2751
Elementary radical reactions and autoignition, 4179

Laser-induced fluorescence
Discovery of two rotational isomers of 4-methoxystyrene by laser-induced fluorescence in a supersonic jet, 197
Rate constants for the reactions of C_2H_5, C_2H_5O and $C_2H_5O_2$ radicals with NO_3 at 298 K and 2.2 Torr, 817
Kinetics and mechanism of the reaction of CH_3 and CH_3O with ClO and OClO at 298 K, 3045

Laser magnetic resonance
IR spectrum of the AsH radical in its $X\,^3\Sigma^-$ state, recorded by laser magnetic resonance, 2999

Laser photodissociation
Electronic spectroscopy of size-selected ionic complexes, 91

Laser photolysis
Solvent effect on photoinduced electron transfer between C_{60} and 3,3',5,5'-tetramethylbenzidine studied by nanosecond laser photolysis, 2287

Laser vaporization
Formation and coalescence of fullerene ions from direct laser vaporization, 987

Lattice-fluid model
Bulk and surface properties of the highly non-ideal associated mixtures formed by methanol and propanal, 2779
Simultaneous description of excess enthalpy and vapour–liquid equilibrium data of associated mixtures by means of a lattice–fluid model, 4381

Lattice parameter
Molecular dynamics simulation of the temperature dependence of lattice parameters of alkane crystals during cooling, 2601

Lattice simulation
New high-coordination lattice model for rotational isomeric state polymer chains, 2435

Layered material
FTIR studies of adsorption of NO, NO_2 and N_2O on layered V_2O_5/ZrO_2, 1557

Lead sulfide
Effect of the surface chemical modification on the optical properties of polymer-stabilized PbS nanoparticles, 4121

Le Chatelier principle
Response reactions: A way to explain the unusual behaviour of multiple equilibrium systems, 259

LEED
XPS and LEED studies of 10,11-dihydrocinchonidine adsorption at Pt(111). Implications for the role of cinchona alkaloids in enantioselective hydrogenation, 2167
Comparison between gas-phase and electrochemical deposition of copper on Pt(100)-(1 × 1) and Pt(100)-hex-*R*0.7°, 3585

Lewis acidity
Catalytic properties of *γ*-alumina. *Ab initio* molecular orbital studies of clusters of chlorinated *γ*-alumina, 155
IR spectroscopic study of acid sites in mordenites fluorinated under mild conditions, 385
Effect of tetrahedral Ti in titania–silica mixed oxides on epoxidation activity and Lewis acidity, 1261

Lewis base
Donor–acceptor complexes of Lewis bases with bromine monochloride in the gas phase: some generalisations from rotation spectroscopy, 1881

Lewis site
Acidic and basic properties of titania–alumina mixed oxides; Active sites for propan-2-ol dehydration, 2907

Ligand exchange
EPR characterisation of the Cr^V intermediates in the $Cr^{VI/V}$ oxidations of organic substrates and of relevance to Cr-induced cancers, 1207
Bonding and ligand exchange in pentamethyldialane. An IR, NMR and *ab initio* study, 3015

Light scattering
Diffusivity in nitrobenzene–isooctane mixtures of non-critical composition approaching the liquid–liquid coexistence curve, 3385

Linear oligomer
Volume properties of some linear and ring oligomer solutions, 2797

Lineshape
Proton CRAMPS of NH_3^+ groups: Line broadening and molecular dynamics, 805

Lipid film
Electrochemical properties of myoglobin embedded in Langmuir–Blodgett and cast films of synthetic lipids, 1775
Stresses in lipid membranes and interactions between inclusions, 3415

Liquid crystal
Near-IR molar absorption coefficient for the OH-stretching mode of *cis*-9-octadecenoic acid and dissociation of the acid dimers in the pure liquid state, 697
Ion-conducting behaviour and photoinduced ionic-conductivity switching of composite films containing crowned cholesteric liquid crystals, 1237
Computer-simulation studies of anisotropic systems. Part XXIV.—Constant-pressure investigations of the smectic B phase of the Gay–Berne mesogen, 2141
Prediction of microstructure in liquid-crystalline polymers, 2497
The search for thermotropic biaxial nematics, 3177
Vesicle–surfactant interactions: Effects of added surfactants on the gel to liquid-crystal transition for two vesicular systems, 4275
Visualization of enantiomers in a polypeptide liquid-crystal solvent through carbon-13 NMR spectroscopy, 1371
Monte Carlo study of Gay–Berne liquid-crystal droplets, 3441

Liquid droplet
Liquid droplets and solid particles at surfactant solution interfaces, 2681

Liquid–liquid coexistence curve

Diffusivity in nitrobenzene–isooctane mixtures of non-critical composition approaching the liquid–liquid coexistence curve, 3385

Liquid/liquid electrochemical interface
Optical second-harmonic generation measurements of molecular adsorption and orientation at the liquid/liquid electrochemical interface, 1411
Corrigendum to Relation between the surface states of oxide films at Rh electrodes and kinetics of the oxygen evolution reaction, 2353

Liquidus curve
Effect of oxide contamination on the position of the liquidus curve of the NaCl–$AlCl_3$ system, 3869

Lithium dimer
Modern valence-bond description of the ground state of Li_2^-, 3751

Long-range complex
Ion-beam spectroscopy of long-range complexes, 3725

Luminescence
Enthalpy changes for the formation of CdA* and CdA_2* exciplexes in the cadmium($5\ ^2P_1$)-photosensitized reaction of some substrates in the gas phase, 603
Effect of the surface chemical modification on the optical properties of polymer-stabilized PbS nanoparticles, 4121

Luminescence spectroscopy
Crystal fields in REOF:Eu^{3+} (RE = La, Gd and Y), 1503

LUMO
Time-resolved resonance Raman spectroscopy of triplet-state metallated and free-base tetraarylporphyrins, 411

Lyman absorption
Arrhenius parameters for the reaction of H atoms with GeH_4, 3367

Lyotropic mesophase
Identification of transitions in lyotropic mesophases in hexaethylene glycol dodecyl ether–water by precision densimetry, 319

Lysozyme unfolding
Denaturation of lysozyme by *n*-alkyltrimethylammonium bromides in alkaline solution, 2805

Macrocyclic compound
Thermodynamics of the interaction of 18-crown-6 with K^+, Tl^+, Ba^{2+}, Sr^{2+} and Pb^{2+} from 323.15 to 398.15 K, 4207

Macromolecule
Molecular kinetics during the growth of the macromolecule poly(di-2-hydroxypropyl ether of bisphenol-A-*n*-hexylamine) studied by dielectric spectroscopy, 343

Macropore diffusion
Frequency-response study of micro- and macro-pore diffusion in manufactured zeolite pellets, 1399
Dynamics study of a closed diffusion cell by using a frequency response method: Single resonator, 1695

Magnetic field effect
Laser flash photolysis studies and magnetic field effect on a new heteroexcimer between *N*-ethylcarbazole and 1,4-dicyanobenzene in homogeneous and heterogeneous media, 1593

Magnetite
Kinetic study of the formation of cation-excess magnetite, 1533

Maleic acid
X-Ray, FTIR, ^1H and ^{13}C NMR, PM3 and AM1 studies of $(N{-}H{\cdots}N)^+$ and $(O{-}H{\cdots}O)^-$ hydrogen bonds in a complex of 1,8-diaminonaphthalene with maleic acid: Proton cavity and basicity of proton sponges, 87

Manganese complex
Synthesis, characterization and physical properties of tricarbonylmanganese and pentamethylcyclopentadienylcobalt complexes of poly(9-hexylfluorene), 1477

Manganese
Physico-chemical properties and catalytic activities of the spinel series $Mn_xFe_{3-x}O_4$ towards peroxide decomposition, 3489

MAS NMR spectroscopy
Autotransformation and ageing of acid-treated montmorillonite catalysts: A solid-state ^{27}Al NMR study, 1031
Synthesis and characterization of the large-pore molecular sieve SAPO-46, 1045
Magnetic resonance studies on porous alumina doped with iron and chromium, 1519
Cation location and migration in lathanum-exchanged zeolite NaY studied by X-ray powder diffraction and MAS NMR spectroscopy, 1813
Variable-temperature X-ray crystallographic and magic-angle spinning NMR spectral studies on hexaethylbenzene, 2149
Reversible interaction of NH_3 with the framework of template-free zeolite-type SAPO-34, 3281
Multinuclear MAS NMR spectroscopic study of the zeolite, MCM-22, 3549
Solid-state ^1H NMR studies of the acidity of mordenites, 3933
^{29}Si MAS NMR study of a highly siliceous EUO-type material, 4309
Quantification of calcium silicate phases in Portland cements by ^{29}Si MAS NMR spectroscopy, 4423
IR and ^1H NMR studies on the adsorption of gaseous hydrogen chloride on γ-alumina, 941
NMR characterization of the supported 12-heteropoly acids, 375

Mass effect
Effect of mass on particle diffusion in liquids studied by electron spin exchange and chemical reaction of muonium with oxygen in aqueous solution, 1935

Mass spectrometry
Ionisation in premixed fuel-lean flames of H_2, O_2 and N_2. Part 1.—Naturally occurring positive ions, 827
Ionisation in premixed fuel-lean flames of H_2, O_2 and N_2. Part 2.—Ions from alkali-metal additives, 835
Mass spectrometry of and deposition-rate measurements from radiofrequency-induced plasmas of methyl isobutyrate, methyl methacrylate and *n*-butyl methacrylate, 1363
Combined experimental and computational investigation of the double ionization of $(CH_3)_4M$ molecules (M = Si, Ge, Sn and Pb), 1901
Corrigendum to Mass spectrometry of and deposition-rate measurements from radiofrequency-induced plasmas of methyl isobutyrate, methyl methacrylate and *n*-butyl methacrylate, 2051
Mass-spectrometric study of the production and recombination of $BaOH^+$ ions and free electrons from barium added to flames of $H_2 + O_2 + Ar$, 2257
Kinetics and products of the gas-phase reactions of $(CH_3)_4Si$, $(CH_3)_3SiCH_2OH$, $(CH_3)_3SiOSi(CH_3)_3$ and $(CD_3)_3SiOSi(CD_3)_3$ with Cl atoms and OH radicals, 3033

Mass transfer
Imaging local mass-transfer rates within an impinging jet and studies of fast heterogeneous electron-transfer kinetics using the microjet electrode, 899

Matrix
Permeability and the time lag for downstream absorptive permeation with concomitant reaction across a series–parallel path studied by the matrix method, 469
Effect of the matrix on the kinetics of dynamic supercritical fluid extraction, 1333

Matrix isolation
EPR studies of the reactions of high-energy copper species with hydrocarbons using a rotating cryostat, 17
Theoretical and experimental studies on the novel thiazylfluoroformate, FC(O)SN, 231
Molecular complexes of nitric acid with N_2, CO and NO studied by matrix isolation IR spectroscopy, 3111
UV-induced isomerization of (*E*)-crotonic acid. Combined matrix-isolated IR and *ab initio* MO study, 3755

MCM-22
Multinuclear MAS NMR spectroscopic study of the zeolite, MCM-22, 3549

MCM-41
Adsorption of carbon dioxide, sulfur dioxide and water vapour by MCM-41, a model mesoporous adsorbent, 2041

Melt
Effect of oxide contamination on the position of the liquidus curve of the NaCl–$AlCl_3$ system, 3869

Melting
Electrical conductivity of the systems $NaAlCl_4$ and NaCl(s)/$NaAlCl_4$ in the range 100–200 °C, 3157

Membrane
Solvent composition dependence of the voltage generation and the electric pulse formation in the water–nitrobenzene–water liquid membrane system, 895
Solution to the Poisson–Boltzmann equation for particles covered by an ion-penetrable charged membrane, 1223

Membrane reactor
Membrane reactor for oxidative coupling of CH_4 with an oxide ion–electron hole mixed conductor, 4419

Mercury electrode
Simultaneous adsorption of thiourea and thiocyanate ions on mercury electrodes. Part 1.—Influence of thiourea on anion adsorption, 1005

Mesopore
Adsorption on MCM-41 mesoporous molecular sieves. Part 2.—Cyclopentane isotherms and their temperature dependence, 937
Effect of structural aluminium on the mesoporous structure of MCM-41, 2955

Mesoporous adsorbent
Adsorption of carbon dioxide, sulfur dioxide and water vapour by MCM-41, a model mesoporous adsorbent, 2041

Metal carbonyl
Time-resolved IR studies of gas-phase photochemistry of $Co(CO)_3NO$, 847

Metal complex
Theoretical study of cadmium– and mercury–ammonia exciplexes: Comparison with experiment, 3795

Metal ion
Thermodynamic study of the binding of dibenzo-18-crown-6 with Ag^+, Pb^{2+} and Cd^{2+} in acetonitrile–water solvents, 1607
Corrigendum to IR studies of adhesion promoters. Part 3.—Adsorption and coupling of bifunctional silanes on silica at the solid/liquid interface, 3309

Metallated porphyrin
Time-resolved resonance Raman spectroscopy of triplet-state metallated and free-base tetraarylporphyrins, 411

Metallocyclodextrin
Complexation of phenylalanine and histidine by β-cyclodextrin, 6^A^-(3-aminopropylamino)-6^A^-deoxy-β-cyclodextrin and its metallocyclodextrins in aqueous solution, 1013
Corrigendum to Complexation of phenylalanine and histidine by β-cyclodextrin, 6^A^-(3-aminopropylamino)-6^A^-deoxy-β-cyclodextrin and its metallocyclodextrins in aqueous solution, 4335

Metal–organic vapour phase epitaxy
Homogeneous thermal decomposition of dimethylzinc in a metal–organic vapour phase epitaxy reactor. An *ex situ* investigation by FTIR absorption spectroscopy, 3475

Metal oxide
Surface chemistry of polar oxide surfaces: Formic acid on NiO(111), 3709

Metal silicide
Hydrodehalogenation of chlorosilanes in the presence of metal silicides: Experimental studies of gas and solid phase composition related to thermodynamic calculations, 3879

Metal/solution interface
Crystal-face specificity of electrical double-layer parameters at metal/solution interfaces, 3311

Metal substrate
Optical effects in the IR reflection–absorption spectra of thin water-ice films on metal substrates, 4005

Metathesis catalysis
Mössbauer and solid-state NMR spectroscopic

studies of tin-modified rhenium-based metathesis catalysts, 3511
Methane
Site selectivity of methane adsorbed in mordenite as studied by NMR, 2949
Reflection–absorption IR spectroscopy at cryogenic temperatures, 3563
Tunnel effects in oxidative addition reaction of methane to bare Pd atom, 3779
Direct conversion of methane and ethane to the corresponding alcohols using nitrous oxide over iron phosphate catalysts, 3953
Methane activation
Interaction of water with 1% Li/MgO: DC conductivity of Li/MgO catalyst for methane selective activation, 1805
Methane oxidation
Partial oxidation of CH_4 to synthesis gas using an Rh | YSZ | Ag electrochemical membrane reactor, 1655
Methane oxidative coupling
Secondary ion mass spectroscopy and X-ray photoelectron spectroscopy of Na_2MoO_4/SiO_2 catalysts for methane oxidative coupling, 381
Methanethiol
Resonance-enhanced multiphoton ionisation spectroscopy of methanethiol, 2715
Theoretical *ab initio* study of the reaction of CH_3SH with OH radical, 3783
Methanol
Adsorption and reaction of methanol and carbon dioxide on model ZnO/Ag catalysts, 3963
In situ Raman studies of the selective oxidation of methanol to formaldehyde and ethene to ethylene oxide on a polycrystalline silver catalyst, 4149
Methanol–carbon dioxide mixture
Excess molar enthalpies of (methanol–carbon dioxide)(g) from 448.2 to 548.2 K at pressures up to 15 MPa, 269
Methanol synthesis
Is the observed hydrogenation of formate the rate-limiting step in methanol synthesis?, 1267
4-Methoxystyrene
Discovery of two rotational isomers of 4-methoxystyrene by laser-induced fluorescence in a supersonic jet, 197
Methyllithium
Modern valence-bond description of $(CH_3)_4Li_4$, 3363
Methylperoxyl radical
Theoretical calculation of intramolecular reactions in methylperoxyl and ethylperoxyl radicals, 1425
***N*-Methylpyrrolidone**
Analysis of velocity cross-correlation and preferential solvation for the system *N*-methylpyrrolidone–water at 20 °C, 1339
Methyl Red
Resonance Raman spectroscopic study of Methyl Red and Ethyl Red adsorbed on silica, 499
Methyl rotation
Conformation and dynamics of alkylated bases within DNA: Effect of methyl rotation, 251
Methyl salicylate
Fluorescence spectra of methyl salicylate during the sol–gel–xerogel transitions of mixed silicon–aluminium alkoxides, 4279
Micelle
Identification of transitions in lyotropic mesophases in hexaethylene glycol dodecyl ether–water by precision densimetry, 319
Metal extraction in micellar media: A comparison of copper complexation rates and ultrafiltration yields of two isomeric (*E*)-1-(2′-hydroxy-5′-alkylphenyl) 1-alkanone oximes, 657
Interaction of the chloropentaamminecobalt(III) cation with mixed micelles of anionic and non-ionic surfactants: A kinetic study, 1075
Titration calorimetric and spectrophotometric studies of micelle formation by alkyltrimethylammonium bromide in aqueous solution, 1229
Effects of ureas on the kinetics of acid hydrolysis of 1-phenylethyl nitrite in water and in aqueous micellar solutions of sodium dodecyl sulfate, 1349
Micellization and gelation of a triblock copolymer of oxyethylene and oxypropylene, $E_{93}P_{44}E_{93}$, studied by ^1H nuclear magnetic relaxation, 1491
Solubilization of two cyano 3*H*-indole molecular probes in SDS and CTAB micelles: Spectral and photophysical characterization, 2133
Model for chemical interdiffusion of solubilizates and ionic micelles. Aqueous solutions of *n*-alcohols and sodium dodecyl sulfate, 2837
Photophysics of 3- and 4-phenyl pyridyl ketones in submicellar and micellar solutions of ionic and non-ionic surfactants, 3405
Specific micellar catalytic effects of the protolysis of *o*-benzoic acid derivatives studied by the ultrasonic absorption method, 3525
Oligomerization of cationic pyrene derivatives in the presence of sodium dodecyl sulfate: A route to nanoaggregate formation, 3913
Photochromism and thermochromism of spiro[indolinoxazines] in normal and reversed micelles, 4099
Volumetric study of mixed micelles of hexane-1,2-diol and some alkane-1,2,3-triols, 4105
Vesicle–surfactant interactions: Effects of added surfactants on the gel to liquid-crystal transition for two vesicular systems, 4275
Microcalorimetry
Surface characterisation of yttria-stabilized tetragonal ZrO_2. Part 2.— Adsorption of CO, 113
Interactions between cations and sugars. Part 8.—Gibbs energies, enthalpies and entropies of association of divalent and trivalent metal cations with xylitol and glucitol in water at 298.15 K, 2771
Microdisc electrode
Cathodic reduction of oxygen in water and media of low ionic strength, 457
Microjet electrode
Imaging local mass-transfer rates within an impinging jet and studies of fast heterogeneous electron-transfer kinetics using the microjet electrode, 899
Micropore
Micropore structure of template-derived carbons studied using adsorption of gases with different molecular diameters, 2929
Reduction of copper(II) with subsequent disproportionation of copper(I) during the hydrothermal syntheses of microporous silicoaluminium phosphates SAPO-5 and -11, 3529
Micropore diffusion
Frequency-response study of micro- and macro-pore diffusion in manufactured zeolite pellets, 1399
Dynamics study of a closed diffusion cell by using a frequency response method: Single resonator, 1695
Microporous crystal
Adsorption characteristics and reactions of propyne on microporous crystals, 1707
Microscopy
Ultra-thin particulate films prepared from capped and uncapped reverse-micelle-entrapped silver particles, 673
Microstructural study
Microstructural studies of electro-rheological fluids under shear, 1787
Microwave
Microwave effects on the oxidative coupling of methane over proton conductive catalysts, 1179
Evolution of the EPR copper(II) dimer spectrum observed in CuCe oxide with the applied microwave frequency: A computer-assisted study, 3299
Microwave attenuation
Experimental determination of molecular radii using a microwave attenuation method, 2733
Microwave crystallization
Synthesis and characterization of VAPSO-44 and VAPSO-5, 1173
Microwave spectroscopy
Microwave spectrum and structure of furan·ethene, 975
Microwave synthesis
Acidity of aluminophosphate structures. Part 2.—Incorporation of cobalt into CHA and AFI by microwave synthesis, 1163
Millimetre-wave spectroscopy
Millimetre-wave electronic spectrum of the D_2^+ ion, 1887
Mixed oxide
FTIR studies of adsorption of NO, NO_2 and N_2O on layered V_2O_5/ZrO_2, 1557
Mixed Co–Zn–Al oxides as absorbents for low-temperature gas desulfurisation, 3219
Mixed oxide catalyst
Alkene oxidation over the Mo–Bi mixed oxides/Au | yttria-stabilised zirconia | Ag system, 1117
Mixed solvent
^{63}Cu and ^{109}Ag NMR studies of copper(I) and silver(I) salts in mixed solvents containing nitriles, 2307
MM2 force field
A force field for molecular mechanics studies of iron porphyrins, 1741
MnO_2 colloid
Sonochemical dissolution of MnO_2 colloids, 2843
Modal correlation
Coupling between different modes in local chain dynamics: A modal correlation analysis, 2483
Modelling
Intermolecular packing of freely jointed branched polyalkene melts: A microscopic approach, 2427
Prediction of microstructure in liquid-crystalline polymers, 2497
Simulation of growth and surface roughening of polymer single crystals, 2587
Modelling the influence of monomer properties on hydrogen bond density in oriented, rigid copolymer systems, 2629
Dominant role of internal rotation in the dissociation of polyatomic ligands from the binding site. The case of opiates, 2811
Stresses in lipid membranes and interactions between inclusions, 3415
Molar volume
Liquid mixtures at high pressures referred to a pseudospinodal curve: Ethanol–methylcyclopentane and carbon disulfide–tetramethylsilane, 59
Physicochemical properties of dimethyl sulfoxide–methanol liquid mixtures. Experimental and semiempirical quantum chemical studies, 65
Molecular beam
Hexapole state selection and focusing *vs.* brute force orientation of beam molecules, 205
Molecular beam study of C_2H_4 oxidation on platinum: IR chemiluminescence of the CO and CO_2 products, 1801
CO–NO reaction on Rh(110) studied using molecular beams, 3663
Molecular chain
A model system for the hydrogen-bonded chain with large proton polarizability present in the L_{550} intermediate of bacteriorhodopsin: An FTIR study, 3141
Molecular collisions
Modified interacting-sphere model for self-diffusion and infinite-dilution mutual-diffusivity of *n*-alkanes, 245
Molecular conformation
Effect of molecular conformation on the electronic properties of donor–acceptor azobenzenes, 2067
Intramolecular hydrogen bonding and molecular conformation. Part 4.—Corrections of thermodynamic properties obtained by IR measurements at different temperatures and pressures, 3379
Molecular dynamics
Molecular dynamics simulations of flexible molecules. Part 1.—Aqueous solution of ethylene glycol, 31
Hexapole state selection and focusing *vs.* brute force orientation of beam molecules, 205
Molecular dynamics simulation of nuclear spin relaxation of $^7Li^+$ in water, 215
Modified interacting-sphere model for self-diffusion and infinite-dilution mutual-diffusivity of *n*-alkanes, 245
Conformation and dynamics of alkylated bases within DNA: Effect of methyl rotation, 251
Reactive collisions with excited-state atoms, 389

Atom pair potential for molecular dynamics simulations of structural and dynamical properties of aluminosilicates: Test on silicalite and anhydrous Na-A and Ca-A zeolites and comparison with experimental data, 525
Physico-chemical characterisation of oil-soluble overbased phenate detergents, 687
Proton CRAMPS of NH_3^+ groups: Line broadening and molecular dynamics, 805
Femtosecond to nanosecond solvation dynamics in pure water and inside the γ-cyclodextrin cavity, 867
Molecular dynamics study of the self-diffusion of supercritical methane in slit-shaped graphitic micropores, 1377
Conformation and dynamics of ethylated DNA, 1465
Computer-simulation studies of anisotropic systems. Part XXIV.—Constant-pressure investigations of the smectic B phase of the Gay–Berne mesogen, 2141
Molecular dynamics of dissociative electron attachment in water, 2249
Thermodynamic properties of a coarse-grained model of hydrocarbon polymers. Computer simulations on articulated chain structures, 2457
Coupling between different modes in local chain dynamics: A modal correlation analysis, 2483
Molecular dynamics study of polyethylene chain folding: The effects of chain length and the torsional barrier, 2541
Molecular dynamics simulation of the temperature dependence of lattice parameters of alkane crystals during cooling, 2601
Molecular dynamics simulations of the structure and ion diffusion in poly(ethylene oxide), 2633
Zero-point energy problem in molecular dynamics caculations, and an improved method for sampling trajectories, 3747
Comparison of the water perturbations induced by two small organic solutes: *Ab initio* calculations and molecular dynamics simulation, 3803

Molecular fluid
Bulk and surface properties of the highly non-ideal associated mixtures formed by methanol and propanal, 2779

Molecular kinetics
Molecular kinetics during the growth of the macromolecule poly(di-2-hydroxypropyl ether of bisphenol-A-*n*-hexylamine) studied by dielectric spectroscopy, 343

Molecular mechanics
A force field for molecular mechanics studies of iron porphyrins, 1741
Ab initio and molecular mechanics study of polyaryl ether ketone polymers, 2609

Molecular modelling
Molecular modelling of ligand–DNA intercalation interactions, 2515
Determination of the crystal structure of poly(*p*-phenylene terephthalate) from power diffraction data. A computer modelling approach, 2615
Crystal modulus of poly(hydroxybutyrate), 2623
Catalysed cyclotrimerisation of acetylene: A computational study, 3975

Molecular modulation
Kinetics of reactions of primary, secondary and tertiary β-hydroxy peroxyl radicals. Application to isoprene degradation, 1911

Molecular motion
Molecular motions in a rigid backbone polymer: Poly(*n*-hexyl isocyanate). A study by thermally stimulated currents, 2003

Molecular orbital
Ab initio MO studies of nuclear spin–spin interactions in CH_3F, SiH_3F and CH_3OH, 23
Effect of molecular conformation on the electronic properties of donor–acceptor azobenzenes, 2067
Orbital symmetry effects in photoinduced bimolecular electron-transfer reactions, 3123

Molecular orientation
Hexapole state selection and focusing *vs.* brute force orientation of beam molecules, 205

Molecular probe
Solubilization of two cyano 3*H*-indole molecular probes in SDS and CTAB micelles: Spectral and photophysical characterization, 2133

Molecular radius
Experimental determination of molecular radii using a microwave attenuation method, 2733

Molecular receptor
Voltammetric and NMR studies of a bis(ferrocenecarboxamide)-substituted diaza-18-crown-6 receptor that simultaneously complexes and electrochemically recognises both cations and anions, 295

Molecular recognition
Long range H-bond specific interactions between nucleosides, 4329

Molecular rotation
Molecular rotation and isomerisation in hydrogen isocyanide, 1717
Dominant role of internal rotation in the dissociation of polyatomic ligands from the binding site. The case of opiates, 2811

Molecular sieve
Adsorption on MCM-41 mesoporous molecular sieves. Part 2.—Cyclopentane isotherms and their temperature dependence, 937
Synthesis and characterization of the large-pore molecular sieve SAPO-46, 1045
V-Ti and V-Al silicate molecular sieves of MFI topology: Synthesis and characteristics, 2217
Effect of structural aluminium on the mesoporous structure of MCM-41, 2955
Synthesis and characterization of CAM-1, a novel aluminophosphate molecular sieve precursor, 3995
Catalytic transformation of camphene over aluminophosphate-based molecular sieves, 4471

Molecular simulation
Determination of the chemical potential by the particle insertion method and by its inverse, 2971

Molten gallium trichloride
Formation of subvalent bismuth cations in molten gallium trichloride and benzene solutions, 4223

Molybdenum
Insertion of vanadium or molybdenum as oxides in LaNaY zeolite: Comparison with NaY, 1037
Spectroscopic investigation of the molybdenum active sites on Mo^{VI} heterogeneous catalysts for alkene epoxidation, 3969
Hydrogen in molybdenum and cobalt sulfide catalysts. A neutron Compton scattering study on the ISIS electronvolt spectrometer, 4467

Molybdenum oxide
Selective photooxidation of light alkanes to oxygenates using supported molybdenum oxide catalysts, 1647
Valence-band and core photoelectron spectroscopic studies of molybdenum aqueous oxidation and the influence of argon-ion etching, 3593

Monte Carlo
Spin effects on spur kinetics. Re-encounters and the independent pairs approximation, 223
Choice of the reaction coordinate in electron-transfer reactions in solution, 1451
Monte Carlo simulation of radiation trapping and quenching of photofragment fluorescence after 193 nm photolysis of NaCl, 1931
Computer-simulation studies of anisotropic systems. Part XXIV.—Constant-pressure investigation of the smectic B phase of the Gay–Berne mesogen, 2141
Monte Carlo algorithms for the atomistic simulation of condensed polymer phases, 2355
Structural and thermodynamic properties of interfaces between coexisting phases in polymer blends: A Monte Carlo simulation, 2369
Thermodynamic properties of a coarse-grained model of hydrocarbon polymers. Computer simulations on articulated chain structures, 2457
Force–extension relations in macromolecules of variable excluded volume and flexibility: Energy and entropy changes on stretching, 2465
Monte Carlo simulations of polymer surfaces in a cubic lattice, two variations of energy parameter and chain-length, 2551
Molecular modelling of the elastic behaviour of polymer chains in networks: Comparison of polymethylene and poly(dimethysiloxane), 2639
Monte Carlo study of adsorption from binary solution on heterogeneous surfaces, 3195
Monte Carlo study of Gay–Berne liquid-crystal droplets, 3441
Inhibition of crystal growth in methane hydrate, 3449
Monte Carlo simulations of a single poly(oxyethylene) $C_{12}E_3$ chain headgroup fixed on a bilayer surface in water, 4261

Montmorillonite
Autotransformation and ageing of acid-treated montmorillonite catalysts: A solid-state ^{27}Al NMR study, 1031
Electrochemical control of montmorillonite clay swelling, 1547

Mordenite
In-situ IR monitoring of the acidic and structural variations of mordenite caused by pressure and temperature, 1835
One-dimensional xenon gas in the pores of mordenite, 2945
Site selectivity of methane adsorbed in mordenite as studied by NMR, 2949
Solid-state ^1H NMR studies of the acidity of mordenites, 3933
Formation of polypyrrole and polythiophene within Cu^{2+}- and H^+-mordenite hosts studied by EPR and UV–VIS spectroscopy, 4321

Morpholine
Kinetics and products of the photocatalytic degradation of morpholine (tetrahydro-2*H*-1,4-oxazine) in TiO_2 aqueous suspensions, 1853

Morphology
Influence of oxidation and reduction conditions upon the morphology of silica-supported polycrystalline silver catalysts, 133
Self-organization of graft copolymers at surfaces, interfaces and in bulk, 2855
CO–NO reaction on Rh(110) studied using molecular beams, 3663
Determination of a transferable interatomic potential for alkali-metal perchlorates and its application to morphological modelling, 4133

Mössbauer spectroscopy
Electroreduction of oxygen on Fe_3O_4 electrodes. Part 2.—Rotating ring–disc electrode studies and mechanism, 2323
Mössbauer and solid-state NMR spectroscopic studies of tin-modified rhenium-based metathesis catalysts, 3511

MOVPE
Homogeneous thermal decomposition of dimethylzinc in a metal–organic vapour phase epitaxy reactor. An *ex situ* investigation by FTIR absorption spectroscopy, 3475

Multiconfiguration response calculation
Multiconfiguration response calculations on the Cameron bands of the CO molecule, 1729

Multiple equilibria
Response reactions: A way to explain the unusual behaviour of multiple equilibrium systems, 259

Multiple-photon decomposition
Chemiluminescence in 5 μm multiple-photon decomposition of $W(CO)_6$ in the presence of O_2, 597

Multipole moment
Ab initio calculation of the electrical properties of the $X^2\Sigma_g^+$ ground and $A^2\Pi_u$ excited states of N_2^+, 1063

Muonium
Effect of mass on particle diffusion in liquids studied by electron spin exchange and chemical reaction of muonium with oxygen in aqueous solution, 1935

Murexide
Rate of decomposition of murexide in mixed solvents: An indicator for proton activity,

637
Myoglobin
Electrochemical properties of myoglobin embedded in Langmuir–Blodgett and cast films of synthetic lipids, 1775
NaCl
Monte Carlo simulation of radiation trapping and quenching of photofragment fluorescence after 193 nm photolysis of NaCl, 1931
Electrical conductivity of the systems $NaAlCl_4$ and NaCl(s)/$NaAlCl_4$ in the range 100–200 °C, 3157
NaCl–$AlCl_3$
Effect of oxide contamination on the position of the liquidus curve of the NaCl–$AlCl_3$ system, 3869
^{23}Na NMR
NMR studies of $^{23}Na^+$ in frozen bovine serum albumin solution, 1459
Nanoaggregate
Oligomerization of cationic pyrene derivatives in the presence of sodium dodecyl sulfate: A route to nanoaggregate formation, 3913
Nanoparticle
Effect of the surface chemical modification on the optical properties of polymer-stabilized PbS nanoparticles, 4121
Nanotoroids
Aromaticity and superaromaticity in carbon nanotoroids, 1563
Naphthalene–trialkylamine
Intramolecular charge transfer in rigidly linked naphthalene–trialkylamine compounds, 4047
Naphthoquinone
Laser flash photolysis studies on hydrogen atom abstraction from phenol by triplet naphthoquinones in acetonitrile, 2751
$NbCl_5$
Laser-Raman spectroscopic study of the vapour phase of $NbCl_5$ and mixtures of $NbCl_5$ and $SnCl_2$, 1445
Near-IR spectroscopy
Near-IR molar absorption coefficient for the OH-stretching mode of *cis*-9-octadecenoic acid and dissociation of the acid dimers in the pure liquid state, 697
High-resolution study of the 000–000 band of the $\tilde{A}\,^1A''$–$\tilde{X}\,^1A'$ system of HNO in emission from the H + NO reaction, 2975
Nematic
The search for thermotropic biaxial nematics, 3177
Nernst–Planck
Model for chemical interdiffusion of solubilizates and ionic micelles. Aqueous solutions of *n*-alcohols and sodium dodecyl sulfate, 2837
Nernst–Planck electrolyte
Complex permittivity of a conducting, dielectric layer containing arbitrary binary Nernst–Planck electrolytes with applications to polymer films and cellulose acetate membranes, 4235
Network
Simulated structure of mixed particle gels, 51
Neural network
Neural network prediction of glass-transition temperatures from monomer structure, 2491
Neutron Compton scattering
Hydrogen in molybdenum and cobalt sulfide catalysts. A neutron Compton scattering study on the ISIS electronvolt spectrometer, 4467
Neutron reflectance
Neutron reflectivity of absorbed β-casein and β-lactoglobulin at the air/water interface, 2847
Neutron scattering
Neutron scattering from solution-grown polymer crystals: A statistical model, 2593
Ni–Al surface
Adsorption dynamics for CO and H_2 on an NiAl(110) surface, 3639
Nickel
Nickel ion-exchanged zeolite-4A: Reduction behaviour of nickel and structure stability, 3983
Nickel complex
Cooperative interactions between ions and water in the chloride ion and water coordination to a square-planar nickel complex ion in concentrated aqueous solutions, 627
Solvation and complexation equilibria of nickel(II) thiocyanato complexes in *N*,*N*-dimethylacetamide, 2313
Nitrate radical
Rates of reaction between the nitrate radical and some aliphatic alcohols, 405
Arrhenius parameters for the reaction of the nitrate radical with 1,1-dichloroethene and (*E*)-1,2-dichloroethene, 1185
Nitric oxide
Adsorption of nitric oxide on Ir{100}: Influence of substrate reconstruction, 3575
Nitrobenzene–isooctane
Ultrasonic absorption of nitrobenzene–isooctane mixtures of non-critical composition, 3889
Nitroimidazole
Photosensitization of DNA bases by 4(5)-nitroimidazole: A steady state and flash photolysis study, 1191
Nitronium ion
Raman spectroscopic study of nitronium ion formation in mixtures of nitric acid, sulfuric acid and water, 1439
Nitroquinoline
Pulse radiolysis studies on the oxidation of $OH^•$ radical-damaged DNA by nitroquinolines in aqueous solution, 2115
Nitrosyl chloride
Structure, harmonic force field and hyperfine coupling constants of nitrosyl chloride, 3347
NIXSW
Quantitative structural study of an Na–O coadsorption phase on Al(111) using X-ray standing waves, 3555
NMR spectroscopy
Cadmium-exchanged Y zeolites studied with carbon monoxide and xenon as probes, 163
Coadsorption of xenon and carbon monoxide in cadmium-exchanged zeolite Y studied with ^{129}Xe NMR spectroscopy, 555
^{2}H NMR studies of single-component adsorption in silicalite: A comparative study of benzene and *p*-xylene, 559
^{2}H NMR studies of binary adsorption in silicalite, 963
Ab initio calculations of titanium NMR chemical shifts including the use of effective core potential basis sets, 1735
Hydrogen adsorption on silica-supported platinum studied by ^{1}H NMR spectroscopy, 2191
^{63}Cu and ^{109}Ag NMR studies of copper(I) and silver(I) salts in mixed solvents containing nitriles, 2307
Nuclear magnetic relaxation study of poly(ethylene oxide) complexed with lithium trifluoromethanesulfonate, 2871
Site selectivity of methane adsorbed in mordenite as studied by NMR, 2949
Second-order quadrupolar effects for directly bonded and remote ^{13}C–$^{79/81}Br$ spin pairs in high-resolution ^{13}C NMR spectra of solids, 3167
Ab initio and experimental study of NMR coupling constants in bicyclo[1.1.1]pentane, 4031
Guest dynamics in carceplexes: A ^{2}H NMR study, 4127
NO adsorption
NO reaction at surface oxygen vacancies generated in cerium oxide, 1679
Non-electrolyte solution
Kirkwood–Buff integrals and preferential solvation in ternary non-electrolyte mixtures, 431
Corrigendum to Kirkwood–Buff integrals and preferential solvation in ternary non-electrolyte mixtures, 1885
Non-freezing water
NMR studies of $^{23}Na^+$ in frozen bovine serum albumin solution, 1459
Non-ionic surfactant
Interaction of the chloropentaamminecobalt(III) cation with mixed micelles of anionic and non-ionic surfactants: A kinetic study, 1075
Non-linear optics
Sum-frequency vibrational spectroscopy of the solid/liquid interface, 1281
Non-linear polarizability
Optical second-harmonic generation measurements of molecular adsorption and orientation at the liquid/liquid electrochemical interface, 1411
Corrigendum to Relation between the surface states of oxide films at Rh electrodes and kinetics of the oxygen evolution reaction, 2353
NO reduction
Medium-temperature electrolysis of NO and CH_4 under lean-burn conditions using yttria-stabilized zirconia as a solid electrolyte, 1955
NQR
Low-temperature single-crystal X-ray diffraction, ^{1}H and ^{13}C solid-state NMR and ^{14}N NQR studies of 1,8-bis(dimethylamino)-naphthalene, 3925
***N*-Salicylideneaniline**
Intramolecular hydrogen bonding in *N*-salicylideneanilines. X-Ray diffraction and solid-state NMR studies, 77
Nuclear magnetic relaxation
Nuclear magnetic relaxation study of poly(ethylene oxide) complexed with lithium trifluoromethanesulfonate, 2871
Gelation of aqueous solutions of diblock and triblock copolymers of ethylene oxide and 1,2-butylene oxide studied by ^{1}H nuclear magnetic relaxation, 3461
Nuclear Overhauser effect
Gelation of aqueous solutions of diblock and triblock copolymers of ethylene oxide and 1,2-butylene oxide studied by ^{1}H nuclear magnetic relaxation, 3461
Nuclear spin relaxation
Molecular dynamics simulation of nuclear spin relaxation of $^7Li^+$ in water, 215
Nuclear spin–spin interaction
Ab initio MO studies of nuclear spin–spin interactions in CH_3F, SiH_3F and CH_3OH, 23
Nucleation
Transformation of cerium(III) hydroxycarbonate into ceria. Part 1.—Nucleation and growth rates of ceria, 4431
Transformation of cerium(III) hydroxycarbonate into ceria. Part 2.—Experimental study of the growth rate, 4437
Nucleoside
Long range H-bond specific interactions between nucleosides, 4329
Numerical simulation
Numerical simulation of surface ionisation and specific adsorption on a two-site model of a carbon surface, 2179
Nylon 12
Analyses for a dipolar relaxation in the featureless dielectric spectrum, and a comparison between the permittivity, modulus and impedence representations, 329
High-temperature dielectric relaxation in Nylon 12 and the effects of annealing and absorbed water, 337
Octadecanethiol
In situ quartz-microbalance study of the self-assembly and stability of aliphatic thiols on polarized gold electrodes, 1949
OH-adduct
Direct evidence for H^+-catalysed dehydration of fluorohydroxycyclohexadienyl radical: A pulse radiolysis study, 2121
Oligomer crystallization
New approach to the mechanism of oligomer crystallization, 2565
Oligomerization
Oligomerization of cationic pyrene derivatives in the presence of sodium dodecyl sulfate: A route to nanoaggregate formation, 3913
Novel routes to designer silicas: Studies of the decomposition of $(M^+)_2[Si(C_6H_4O_2)_3 \cdot xH_2O$. Importance of M^+ identity of the kinetics of oligomerisation and the structural characteristics of the silicas produced, 4287
Optical absorption
Optical absorption and X-ray photoelectron spectroscopic studies of thorium tetrabromide, 2767

Organic template
Computer simulation studies on the role of templating organic molecules in the synthesis of ZSM-5, 4313
Organosilicon
Kinetics and products of the gas-phase reactions of $(CH_3)_4Si$, $(CH_3)_3SiCH_2OH$, $(CH_3)_3SiOSi(CH_3)_3$ and $(CD_3)_3SiOSi(CD_3)_3$ with Cl atoms and OH radicals, 3033
Orientational disorder
Corrigendum to Dielectric studies of orientational disorder in D- and L-systems of camphor and camphoric anhydride, 4009
Oscillating reaction
Oscillations in homogeneous oxidative dehydrogenation of ethane to ethene, 843
Outer-sphere charge transfer
Temperature, pressure and solvent isotope effects on the precursor formation constant and reorganization dynamics in outer-sphere charge transfer between free mobile $[Fe(CN)_6]^{3-}$ and $[Fe(CN)_6]^{4-}$ ions, 1625
Oxidation
Stopped-flow kinetic study of the formation and decay of the 4,4′-(dimethylamino)-diphenylmethane radical cation in aqueous solution, 2743
Selective catalytic reduction of nitric oxide with ammonia on MFI-type ferrisilicate, 3275
Catalytic activity of platinum after exchange with surface active functional groups of carbon blacks, 4451
Oxidative addition
Tunnel effects in oxidative addition reaction of methane to bare Pd atom, 3779
Oxidative coupling
Microwave effects on the oxidative coupling of methane over proton conductive catalysts, 1179
Membrane reactor for oxidative coupling of CH_4 with an oxide ion–electron hole mixed conductor, 4419
Oxidative dehydrogenation
Oscillations in homogeneous oxidative dehydrogenation of ethane to ethene, 843
EPR of vanadium in $Ce_{0.25}H_3PVMo_{11}O_{40}$ catalyst. Formation of vanadyl dimers during the oxidative dehydrogenation of isobutyric acid, 1025
Oxide
Catalytic effect of vanadium, iron and lead oxides on the oxidation of moderator graphite, 3717
Reaction–diffusion effects and systematic design of gas-sensitive resistors based on semiconducting oxides, 4299
Oxide catalyst
Surface chemistry of silica–titania-supported chromium oxide catalysts, 953
FTIR study of the adsorption and transformation of allylbenzene over oxide catalysts, 1861
Oxide film
Corrigendum to Relation between the surface states of oxide films at Rh electrodes and kinetics of the oxygen evolution reaction, 2353
Oxide ion
Effect of oxide contamination on the position of the liquidus curve of the NaCl–$AlCl_3$ system, 3869
Oxydehydrogenation
Semiconductive properties of some uranium–antimony oxide phases used as catalysts in the mild oxidation of but-1-ene to butadiene, 2345
Oxydehydrogenation of propane on V_2O_5/TiO_2 catalyst: Kinetic and mechanistic aspects, 2899
Oxyethylene
Micellization and gelation of a triblock copolymer of oxyethylene and oxypropylene, $E_{93}P_{44}E_{93}$, studied by ^1H nuclear magnetic relaxation, 1491
Oxygen
Negative-ion resonances in vibrational excitation and photochemistry of chemisorbed molecules: A critical case study of O_2/Pt(111), 3633
Oxygen adsorption
Spectroscopic study of oxygen adsorption as a method to study surface defects on CeO_2, 1669
Oxygen reduction
Cathodic reduction of oxygen in water and media of low ionic strength, 457
Oxygen storage capacity
Behaviour of oxygen species adsorbed on Al_2O_3-supported cerium oxide catalysts for methane oxidation, 4459
Oxypropylene
Micellization and gelation of a triblock copolymer of oxyethylene and oxypropylene, $E_{93}P_{44}E_{93}$, studied by ^1H nuclear magnetic relaxation, 1491
Ozone
Airborne chemistry and dynamics at the edge of the 1994 antarctic vortex, 3063
Br_2-sensitised decomposition of ozone: Kinetics of the reaction $BrO + O_3 \rightarrow$ products, 4189
Palladium
Isosteric heat of sorption of dihydrogen on alumina-supported palladium, 949
Effects of modification of Pd/SiO_2 with Rh on catalytic activity for ethene hydroformylation, 1271
Hydrogenation of propyne over palladium catalysts, 3269
Comparison of $Pd(NH_3)_4^{2+}$ decomposition and Pd^{2+} reduction in zeolites NaY, NaX and CsX, 3291
Tunnel effects in oxidative addition reaction of methane to bare Pd atom, 3779
Adsorbate interactions of paramagnetic palladium species in Pd^{II}-exchanged H-rho zeolite characterized by EPR and electron spin echo modulation spectroscopies, 3987
Mechanistic consideration of formation of polymer-protected nanoscopic bimetallic clusters, 4111
Paramagnetic reduction
EPR, ENDOR and TRIPLE resonance characterization of three paramagnetic reduction stages of 5-(9′-fluorenylidene)-5*H*-dibenzo[*a*,*d*] cycloheptene. Radical anions, radical trianions and radical penta-anions, 3821
Partial oxidation
Direct conversion of methane and ethane to the corresponding alcohols using nitrous oxide over iron phosphate catalysts, 3953
Particle insertion method
Determination of the chemical potential by the particle insertion method and by its inverse, 2971
Partition
Partition and dimerization of ion-pair tetraalkylammonium salts in xylene, 643
Thermodynamic study of the partitioning of organic compounds between water and octan-1-ol. Effects of water as cosolvent in the organic phase, 649
Pb complex
Surface-enhanced resonance Raman spectroscopic studies of the Pb^{II} complex of 1-(2-pyridylazo)-2-naphthol adsorbed on Ag sol, 463
Pd–Fe
Surface composition of Pd–Fe catalysts supported on silica, 3237
Perchlorate
Determination of a transferable interatomic potential for alkali-metal perchlorates and its application to morphological modelling, 4133
Perchlorate ion
Self-diffusion of the perchlorate ion in aqueous electrolyte solutions measured by ^{35}Cl NMR spin-echo experiments, 1877
Perdeuteriated benzene
Dynamics of benzene and pyridine guest molecules in their tri-*ortho*-thymotide inclusion compounds. Solid-state ^2H NMR studies, 2017
Perfluoroalkyl radical
EPR and ENDOR of perfluoroalkyl radical intermediates in the reaction between perfluorohypofluorites and perfluoroalkenes, 3813
Perfluorocarbon
Hydrophobic effects on photochemical and photophysical processes: Evidence for aggregation of perfluorocarbon in aqueous–organic solvents, 2761
Permeability
Permeability and the time lag for downstream absorptive permeation with concomitant reaction across a series–parallel path studied by the matrix method, 469
Permittivity spectroscopy
Temperature- and frequency-dependent dielectric studies of *p*-fluorophenylacetonitrile–methanol mixtures using time-domain reflectometry, 623
Perovskite
Low-temperature synthesis of perovskite-type oxides of lanthanum and cobalt and their electrocatalytic properties for oxygen evolution in alkaline solutions, 1871
Peroxodisulfate–iodide reaction
Specific effect of alkali-metal cations on the kinetics of peroxodisulfate–iodide reactions, 1345
Peroxyl radical
Kinetics of the reactions of the HO_2 radical with peroxyl radicals derived from hydrochlorofluorocarbons and hydrofluorocarbons, 1313
Perturbation theory
Influence of static electric field on the vapour–liquid coexistence of dipolar soft-sphere fluids, 889
Perturbation theory model of molecular Rydberg orbitals: Application to diatomic molecules, 2699
Theoretical cross-sections for *M*-changing collisions of symmetric-top molecules with rare-gas atoms, 4363
Pervaporation
Contribution of sorption to global mass transfer during pervaporation of ethyl *tert*-butyl ether–ethanol mixtures through a polyurethaneimide film, 1247
PH_2^+
Theoretical potential-energy functions and spectroscopic data for the PH_2^+ ion, 2053
Phase behaviour
Thermodynamic properties and phase equilibria in the Fe–P system, 703
Mixing enthalpy and phase separation in a poly(propylene oxide)–water system, 2081
Phase separation in concentrated mixtures of polymers and surfactants, 3901
Phase behaviour and structure in a non-ionic surfactant–oil–water mixture, 4269
Phase diagram
Thermoreversible gelation of hydrated polymers, 2663
Phase transition
Identification of transitions in lyotropic mesophases in hexaethylene glycol dodecyl ether–water by precision densimetry, 319
The search for thermotropic biaxial nematics, 3177
Vesicle–surfactant interactions: Effects of added surfactants on the gel to liquid-crystal transition for two vesicular systems, 4275
Phenol
Preferential solvation controlled by clustering conditions of acetonitrile–water mixtures, 4063
Phenol complex
Proton-exchange mechanisms in phenol–tertiary amine–aprotic solvent systems, 3859
Phosphate binding
Organic phosphate-binding groups electrostatically linked to the reactivity of the Cys F9 [93] β sulfhydryl group of haemoglobin, 2095
Phosphorescence
Effects of water on the phosphorescence spectra of aromatic carbonyl compounds. Part 3.—Dual- or multiple-component phosphorescence of 1-indanone at 77 K in some protic solvents containing water, 855
Phosphorescence of β-carotene, 4059
Phosphorus
Chemiluminescence from the reactions of nitrogen and oxygen atoms with phosphorus vapour, 2989
High-resolution spectroscopic study of the oxidation of white phosphorus, 2993
Photocatalysis
Photocatalytic racemization of amino acids in aqueous polycrystalline cadmium(II) sulfide dispersions, 1103

Photochemistry
Formation of anthrahydroquinones ($XAQH_2$) *via* excited singlet charge-transfer complexes (or singlet ion pairs) of anthraquinones with 2,5-dimethylhexa-2,4-diene (DMHD), and photochemical reaction of $XAQH_2$ with DMHD, 607
Time-resolved IR studies of gas-phase photochemistry of $Co(CO)_3NO$, 847
Triplet and radical ion properties of (*E*)-1-styrylpyrene and (*E*)-3-styrylchrysene, 3117
Photochromism
Photochromism and thermochromism of spiro[indolinoxazines] in normal and reversed micelles, 4099
Photodegradation
Photochemistry of semiconductor particles. Part 4.—Effects of surface conditions on the photodegradation of 2,4-dichlorophenol catalysed by TiO_2 suspensions, 917
Photodissociation
Kinetics and products of the photocatalytic degradation of morpholine (tetrahydro-2*H*-1,4-oxazine) in TiO_2 aqueous suspensions, 1853
Temperature-dependent studies of the reaction of W(a ^5D_J, a $^7S_3$) with O_2, 3787
Photoelectrochemistry
Photoelectrochemical properties of 'Q-state' CdS particles in arachidic acid Langmuir–Blodgett films, 665
Photoelectrochemical behaviour of Q-state $CdS_xSe_{(1-x)}$ particles in arachidic acid Langmuir–Blodgett films, 3399
Photoemission
Photoemission and HREELS study of K adsorption on TiO_2(100), 3569
Photoexcitation
Solvent-dependent switching between two dipolar excited states in a rigidly extended trichromophoric system, 2107
Orbital symmetry effects in photoinduced bimolecular electron-transfer reactions, 3123
Photoinduced electron transfer
Solvent effect on the photoinduced electron-transfer reactions between dicyanobis(polypyridine)ruthenium(II) complexes and tris(β-diketonato) ruthenium(III) complexes, 437
Photoinduced electron-transfer quenching of excited singlet states of polycyclic aromatic hydrocarbons by organic acceptors. Solvent effects on the rate constants and the charge-separation efficiency, 1197
Photoirradiation
Hydrophobic effects on photochemical and photophysical processes: Evidence for aggregation of perfluorocarbon in aqueous–organic solvents, 2761
Photoluminescence
Kinetic study of the effects of H, O, N, S, NO, NO_2 and O_2 on the surface states of InGaAs and GaAs, 3021
Photolysis
Monte Carlo simulation of radiation trapping and quenching of photofragment fluorescence after 193 nm photolysis of NaCl, 1931
ENDOR study of the (7′,7′-dicyano)- and (7′-phenyl)-7′-apo-β-carotene radical cations formed by UV photolysis of carotenoids adsorbed on silica gel, 2881
Molecular complexes of nitric acid with N_2, CO and NO studied by matrix isolation IR spectroscopy, 3111
Photomineralization
Photogenerated chloride ion concentration near the surface of UV-irradiated titanium dioxide in the presence of aqueous 2,4-dichlorophenol probed using an ultramicroelectrode, 3893
Photooxidation
Selective photooxidation of light alkanes to oxygenates using supported molybdenum oxide catalysts, 1647
Photophysics
Photophysics of 3- and 4-phenyl pyridyl ketones in submicellar and micellar solutions of ionic and non-ionic surfactants, 3405
Intramolecular charge transfer in rigidly linked naphthalene–trialkylamine compounds, 4047
Photophysical properties of structurally deformed basket-handle porphyrins, 4369
Photosensitivity
Photosensitization of DNA bases by 4(5)-nitroimidazole: A steady state and flash photolysis study, 1191
Photosensitization
Enthalpy changes for the formation of CdA* and CdA_2* exciplexes in the cadmium(5 $^3P_1$)-photosensitized reaction of some substrates in the gas phase, 603
Picric acid
Solvent composition dependence of the voltage generation and the electric pulse formation in the water–nitrobenzene–water liquid membrane system, 895
Pillaring
Al-Pillared saponites. Part 3.—Effect of parent clay layer charge on the intercalation–pillaring mechanism and structural properties, 2229
Pitzer model
Solubility and Pitzer model parameters in thallium(I) chloride systems, TlCl–$MgCl_2$–H_2O and TlCl–$CaCl_2$–H_2O, 1759
Plasma polymerization
Mass spectrometry of and deposition-rate measurements from radiofrequency-induced plasmas of methyl isobutyrate, methyl methacrylate and *n*-butyl methacrylate, 1363
Corrigendum to Mass spectrometry of and deposition-rate measurements from radiofrequency-induced plasmas of methyl isobutyrate, methyl methacrylate and *n*-butyl methacrylate, 2051
Radiofrequency-induced plasma polymerisation of propenoic acid and propanoic acid, 3907
Plastic-crystalline transition
Detection of the plastic-crystalline transition of trioxane by positron annihilation lifetime spectroscopy, 3185
Plateau
Sloping plateaux in the pressure–composition isotherms of the titanium–hydrogen and $Ti_{94}Al_6$–hydrogen systems, 4143
Platinum
IR spectroscopic study of butane and propene adsorption on Pt/CeO_2–Al_2O_3 catalysts, 733
Mechanistic consideration of formation of polymer-protected nanoscopic bimetallic clusters, 4111
Catalytic activity of platinum after exchange with surface active functional groups of carbon blacks, 4451
Platinum catalyst
In-situ EXAFS investigation of non-acidic CVD-based Pt/KL catalyst under oxidation–reduction cycles, 2045
Hydrogen adsorption on silica-supported platinum studied by ^1H NMR spectroscopy, 2191
Platinum surface
XPS and LEED studies of 10,11-dihydrocinchonidine adsorption at Pt(111). Implications for the role of cinchona alkaloids in enantioselective hydrogenation, 2167
Negative-ion resonances in vibrational excitation and photochemistry of chemisorbed molecules: A critical case study of O_2/Pt(111), 3633
Point group
Isomer counting using point group symmetry, 2241
Poisson–Boltzmann equation
Solution to the Poisson–Boltzmann equation for particles covered by an ion-penetrable charged membrane, 1223
Poisson's ratio
Auxetic two-dimensional polymer networks. An example of tailoring geometry for specific mechanical properties, 2671
Polarizability
Ab initio calculation of the electrical properties of the $X^2\Sigma_g^+$ ground and $A^2\Pi_u$ excited states of N_2^+, 1063
Polarization
Creation and detection of coherence and polarization in pulsed EPR, 177
Polar liquid
Temperature- and frequency-dependent dielectric studies of *p*-fluorophenylacetonitrile–methanol mixtures using time-domain reflectometry, 623
Polar stratosphere
Sticking of HCl and HBr on a type-II polar stratospheric cloud mimic, 2349
Airborne chemistry and dynamics at the edge of the 1994 antarctic vortex, 3063
Poly(aryl–ether–ketone)
Ab initio and molecular mechanics study of poly(aryl–ether–ketone)polymers, 2609
Poly(ethylene oxide)
New approach to the mechanism of oligomer crystallization, 2565
Molecular dynamics simulations of the structure and ion diffusion in poly(ethylene oxide), 2633
Nuclear magnetic relaxation study of poly(ethylene oxide) complexed with lithium trifluoromethanesulfonate, 2871
Poly(hydroxybutyrate)
Crystal modulus of poly(hydroxybutyrate), 2623
Poly(*n*-hexyl isocyanate)
Molecular motions in a rigid backbone polymer: Poly(*n*-hexyl isocyanate). A study by thermally stimulated currents, 2003
Poly(oxyethylene)
Monte Carlo simulations of a single poly(oxyethylene) $C_{12}E_3$ chain headgroup fixed on a bilayer surface in water, 4261
Poly(*p*-phenylene terephthalate)
Determination of the crystal structure of poly(*p*-phenylene terephthalate) from power diffraction data. A computer modelling approach., 2615
Poly(propylene oxide)
Mixing enthalpy and phase separation in a poly(propylene oxide)–water system, 2081
Poly(styrene) solution
Studies of poly(styrene) solutions in an electric field: Viscosity and dynamic light scattering, 1357
Polyalkene
Intermolecular packing of freely jointed branched polyalkene melts: A microscopic approach, 2427
Polyaniline
Diffusion behaviour of the BF_4^- anion in polyaniline fibrils. Influence of the physical state of polyaniline, 3469
Polychromate
Combined DRS–RS–EXAFS–XANES–TPR study of supported chromium catalysts, 3245
Polyelectrolyte
Shear and extensional viscosity characteristics of a series of hydrophobically associating polyelectrolytes, 911
Statistical mechanics of semiflexible polymers: Yesterday, today and tomorrow, 2473
Polyethylene
Static vibrational polarizability of all-*trans* polyethylene and polysilane, 1641
Molecular dynamics study of polyethylene chain folding: The effects of chain length and the torsional barrier, 2541
Dependence of the lamellar thickness of an extended-chain single crystal of polyethylene on the degree of supercooling and the pressure, 2573
Polyethylene crystallization from dilute solutions: Adsorption isotherm on the growth face, 2581
Polyhedral molecule
Symmetry extensions of Euler's theorem for polyhedral, toroidal and benzenoid molecules, 3089
Polyisoprene
Linear rheological behaviour of polyisoprene–polystyrene hetero-star and linear diblock copolymer melts, 2403
Polymer
Molecular kinetics during the growth of the macromolecule poly(di-2-hydroxypropyl ether of bisphenol-A-*n*-hexylamine) studied by dielectric spectroscopy, 343
Monte Carlo algorithms for the atomistic simulation of condensed polymer phases, 2355

Linear rheological behaviour of polyisoprene–polystyrene hetero-star and linear diblock copolymer melts, 2403
Intermolecular packing of freely jointed branched polyalkene melts: A microscopic approach, 2427
Coupling between different modes in local chain dynamics: A modal correlation analysis, 2483
Prediction of microstructure in liquid-crystalline polymers, 2497
Configurational and rheological properties of cyclic polymers, 2525
Dependence of the lamellar thickness of an extended-chain single crystal of polyethylene on the degree of supercooling and the pressure, 2573
Simulation of growth and surface roughening of polymer single crystals, 2587
Determination of the crystal structure of poly(*p*-phenylene terephthalate) from power diffraction data. A computer modelling approach, 2615
Modelling the influence of monomer properties on hydrogen bond density in oriented, rigid copolymer systems, 2629
Structure and swelling of end-linked model networks, 2649
Thermoreversible gelation of hydrated polymers, 2663
EPR study of an associative polymer in solution: Determination of aggregation number and interactions with surfactants, 2863
Phase separation in concentrated mixtures of polymers and surfactants, 3901
Competitive adsorption of polymers and surfactants at the solid/liquid interface, 3919
On flocculation and gelation in concentrated particulate systems containing added polymer, 4413

Polymer aggregation
Depletion flocculation of polystyrene latices by water-soluble polymers, 1483

Polymer alloy
Solvent-mediated interactions and chain conformations in block copolymer liquids, 2411

Polymer blend
Structural and thermodynamic properties of interfaces between coexisting phases in polymer blends: a Monte Carlo simulation, 2369

Polymer chain
Force–extension relations in macromolecules of variable excluded volume and flexibility: Energy and entropy changes on stretching, 2465
Coupling between different modes in local chain dynamics: A modal correlation analysis, 2483
Molecular modelling of the elastic behaviour of polymer chains in networks: Comparison of polymethylene and poly(dimethysiloxane), 2639
Kinetics of intra-polymer electron-transfer reactions in macromolecule–metal complexes, 2877

Polymer crystallization
Computer simulation of the crystal/melt interface in *n*-alkane with implication for polymer crystallization, 2559

Polymer electrolyte
Molecular dynamics simulations of the structure and ion diffusion in poly(ethylene oxide), 2633

Polymer film
Complex permittivity of a conducting, dielectric layer containing arbitrary binary Nernst–Planck electrolytes with applications to polymer films and cellulose acetate membranes, 4235

Polymer gel
Electrically induced reversible structural change of a highly swollen polymer gel network, 473

Polymerization
Mass spectrometry of and deposition-rate measurements from radiofrequency-induced plasmas of methyl isobutyrate, methyl methacrylate and *n*-butyl methacrylate, 1363
Corrigendum to Mass spectrometry of and deposition-rate measurements from radiofrequency-induced plasmas of methyl isobutyrate, methyl methacrylate and *n*-butyl methacrylate, 2051

Polymer lattice model
New high-coordination lattice model for rotational isomeric state polymer chains, 2435

Polymer network
Computer simulation of sulfur vulcanization, 2655
Auxetic two-dimensional polymer networks. An example of tailoring geometry for specific mechanical properties, 2671

Polymer properties
Neural network prediction of glass-transition temperatures from monomer structure, 2491

Polymer solution
Shear and extensional viscosity characteristics of a series of hydrophobically associating polyelectrolytes, 911
Configurational and rheological properties of cyclic polymers, 2525
EPR study of an associative polymer in solution: Determination of aggregation number and interactions with surfactants, 2863
Effect of temperature on poly(ethylene oxide) chains in aqueous solution. A viscometric, ^{1}H NMR and Raman spectroscopic study, 3897

Polymer surface
Monte Carlo simulations of polymer surfaces in a cubic lattice, two variations of energy parameter and chain-length, 2551

Polypeptide
Visualization of enantiomers in a polypeptide liquid-crystal solvent through carbon-13 NMR spectroscopy, 1371

Polypyrrole
Surface composition of surfacant-stabilised polypyrrole colloids, 905
Ion binding by poly[4-(pyrrol-1-ylmethyl)benzoic acid] thin films, 1241
Formation of polypyrrole and polythiophene within Cu^{2+}- and H^+-mordenite hosts studied by EPR and UV–VIS spectroscopy, 4321

Polysilane
Static vibrational polarizability of all-*trans* polyethylene and polysilane, 1641

Polystyrene
Depletion flocculation of polystyrene latices by water-soluble polymers, 1483
Linear rheological behaviour of polyisoprene–polystyrene hetero-star and linear diblock copolymer melts, 2403

Polythiophene
Formation of polypyrrole and polythiophene within Cu^{2+}- and H^+-mordenite hosts studied by EPR and UV–VIS spectroscopy, 4321

Polyurethane elastomer
Reinforcement of polyurethane elastomers with microfibres having varying aspect ratios, 2507

Polyurethaneimide film
Contribution of sorption to global mass transfer during pervaporation of ethyl *tert*-butyl ether–ethanol mixtures through a polyurethaneimide film, 1247

Polyvinyl pyrrolidone
Inhibition of crystal growth in methane hydrate, 3449

Porod analysis
Nitrogen adsorption and small-angle neutron scattering studies with capped alumina, 1139

Porous material
Scanning electrochemical microscopy as a probe of local fluid flow through porous solids: Application to the measurement of convective rates through a single dentinal tubule, 1407
Magnetic resonance studies on porous alumina doped with iron and chromium, 1519
Adsorption from associated binary solutions by porous carbon, 1529
Charge regulation at the surface of porous silica, 2965

Porphyrin
Time-resolved resonance Raman spectroscopy of triplet-state metallated and free-base tetraarylporphyrins, 411
Photophysical properties of structurally deformed basket-handle porphyrins, 4369

Positron
CN^- abstraction from cyano compounds by positrons, 419

Positron annihilation
CN^- abstraction from cyano compounds by positrons, 419

Positron annihilation lifetime spectroscopy
Detection of the plastic-crystalline transition of trioxane by positron annihilation lifetime spectroscopy, 3185

Potential-energy function
Derivation of accurate kinetic and potential-energy functions for several simultaneous large-amplitude vibrations: Application to acetaldehyde in the S_0 and T_1 states, 399
New model of potential-energy functions for atomic solids, 1567
Theoretical potential-energy functions and spectroscopic data for the PH_2^+ ion, 2053

Potential-energy surface
Molecular dynamics of dissociative electron attachment in water, 2249
Quasiclassical trajectory studies of $N(^2D) + H_2$ reaction on a fitted *ab initio* potential-energy surface, 3771

Potentiometry
Thermodynamic transfer properties for Na^+, Tl^+ and Ag^+ to water–acetonitrile mixtures, 875
Mixed aminocarboxylic ligand complexes, 1619

Powder diffraction
Determination of the crystal structure of poly(*p*-phenylene terephthalate) from power diffraction data. A computer modelling approach, 2615

Praseodymium oxide
Characterisation and activity of praseodymium oxide catalysts prepared in different gases from praseodymium oxalate hydrate: Microscopic, thermogravimetric and IR spectrosopic studies, 1385

Precipitate
Characterization of precipitates formed from the tetraiodomercurate(II) anion and mercury(I) or silver (I) cations, 1217

Predissociation
High-resolution study of the 000–000 band of the $\tilde{A}\,^1A''$–$\tilde{X}\,^1A'$ system of HNO in emission from the H + NO reaction, 2975

Preferential solvation
Preferential solvation in mixed solvents. Part 7.—Binary mixtures of water and alkanolamines, 427
Kirkwood–Buff integrals and preferential solvation in ternary non-electrolyte mixtures, 431
Preferential solvation in mixed binary solvent, 631
Analysis of velocity cross-correlation and preferential solvation for the system *N*-methylpyrrolidone–water at 20 °C, 1339
Corrigendum to Kirkwood–Buff integrals and preferential solvation in ternary non-electrolyte mixtures, 1885

PRISM theory
Solvent-mediated interactions and chain conformations in block copolymer liquids, 2411

π* Probe
Halochromism and solvatochromism of a π* probe in binary solvent mixtures, 3839

Promoted catalyst
Electrical properties of doped vanadium phosphate phases and VPO catalysts used in the partial oxidation of *n*-butane to maleic anhydride, 3231

Propane conversion
Propane conversion of dry-air-calcined HZSM-5 zeolite, 1689

Propanoic acid
Radiofrequency-induced plasma polymerisation of propenoic acid and propanoic acid, 3907

Propenoic acid
Radiofrequency-induced plasma polymerisation of propenoic acid and propanoic acid, 3907

Propyne

Adsorption characteristics and reactions of propyne on microporous crystals, 1707

Protein
Neutron reflectivity of absorbed β-casein and β-lactoglobulin at the air/water interface, 2847
Stresses in lipid membranes and interactions between inclusions, 3415

Protein gel
Simulated structure of mixed particle gels, 51

Proton activity
Rate of decomposition of murexide in mixed solvents: An indicator for proton activity, 637

Protonation
Protonation of pyridines by phenols, thiophenol, trifluoroacetic acid and methanesulfonic acid in aprotic solvents, 1611
Mixed aminocarboxylic ligand complexes, 1619

Proton CRAMPS
Proton CRAMPS of NH_3^+ groups: Line broadening and molecular dynamics, 805

Proton exchange
Proton-exchange mechanisms in phenol–tertiary amine–aprotic solvent systems, 3859

Proton irradiation
A polymorph of carbonic acid and its possible astrophysical relevance, 2823

Proton sponge
X-Ray, FTIR, ^1H and ^{13}C NMR, PM3 and AM1 studies of $(N-H\cdots N)^+$ and $(O-H\cdots O)^-$ hydrogen bonds in a complex of 1,8-diaminonaphthalene with maleic acid: Proton cavity and basicity of proton sponges, 87

Proton transfer
Protonation of pyridines by phenols, thiophenol, trifluoroacetic acid and methanesulfonic acid in aprotic solvents, 1611

Pseudo-phase separation
Volumetric study of mixed micelles of hexane-1,2-diol and some alkane-1,2,3-triols, 4105

Pulsed field gradient NMR
Self-diffusion of the perchlorate ion in aqueous electrolyte solutions measured by ^{35}Cl NMR spin-echo experiments, 1877

Pulsed photolysis
Arrhenius parameters for the reaction of H atoms with GeH_4, 3367

Pulse radiolysis
Re-evaluation of the thiocyanate dosimeter for pulse radiolysis, 279
Transformation reactions of the electron adducts of methyl derivatives of xanthine in aqueous solution by pulse radiolysis, 615
Temperature dependence of the rate of reaction of OH with some aromatic compounds in aqueous solution, 1631
Pulse radiolysis studies on the oxidation of $OH^•$ radical-damaged DNA by nitroquinolines in aqueous solution, 2115
Direct evidence for H^+-catalysed dehydration of fluorohydroxycyclohexadienyl radical: A pulse radiolysis study, 2121
Direct EPR measurement of Arrhenius parameters for the reactions of $H^•$ atoms with H_2O_2 and $D^•$ atoms with D_2O_2 in aqueous solution, 3127
Mechanism of oxidation of iron(II) complexes by the azide radical, 3133
Evaluation of the stability constant of $Cl_2^{•-}$ in neutral aqueous solution, 3303

Pyridine
FTIR study of the kinetics of solid-state ion exchange in zeolites using pyridine as a probe, 1845
FTIR investigation of polarizable hydrogen bonds in carboxylic acid–pyridine complexes in the mid- and far-IR region, 3831

Pyridinium
Effect of temperature and viscosity on intramolecular charge-transfer fluorescence of a 4-*p*-dimethylaminostyrylpyridinium salt in protic solvents, 4199

Pyrolysis
Surface chemistry of methyl groups adsorbed on Pt(111), 3619

Pyrolytic graphite
STM of folded and unfolded haemoglobin molecules electrochemically deposited on highly oriented pyrolytic graphite, 1471

Q-State particle
Photoelectrochemical behaviour of Q-state $CdS_xSe_{(1-x)}$ particles in arachidic acid Langmuir–Blodgett films, 3399

Quadrupolar nucleus
Second-order quadrupolar effects for directly bonded and remote ^{13}C–$^{79/81}Br$ spin pairs in high-resolution ^{13}C NMR spectra of solids, 3167

Quantum chemical calculation
Theoretical study of cadmium– and mercury–ammonia exciplexes: Comparison with experiment, 3795

Quantum mechanical force field
Gas-phase IR spectrum of 1-azaindolizine: Scaled quantum mechanical force field and spectrum assignment, 3741

Quartz
Appraisal of the fundamental operation of quartz crystal shear-mode biosensors, 3147

Quartz crystal microbalance
Ion inclusion into Langmuir–Blodgett films studied on a quartz crystal microbalance, 1783
In situ quartz-microbalance study of the self-assembly and stability of aliphatic thiols on polarized gold electrodes, 1949
Measurement of viscoelastic changes at electrodes modified with redox hydrogels with a quartz crystal device, 4083

Quartz particle
Bubble–particle attachment, 1997

Quenched dynamics technique
A force field for molecular mechanics studies of iron porphyrins, 1741

Quenching
Monte Carlo simulation of radiation trapping and quenching of photofragment fluorescence after 193 nm photolysis of NaCl, 1931
Quenching rate constants for $NCl(b\,^1\Sigma^+)$ and $PCl(b\,^1\Sigma^+)$ and radiative lifetimes of $NCl(b\,^1\Sigma^+)$, $PCl(b\,^1\Sigma^+)$ and $PBr(b\,^1\Sigma^+)$, 2979
Rate coefficients for quenching of $Cl(^2P_{1/2})$ by various atmospheric gases, 3055
Temperature-dependent studies of the reaction of W(a ^5D_J, a $^7S_3$) with O_2, 3787

Racemization
Photocatalytic racemization of amino acids in aqueous polycrystalline cadmium(II) sulfide dispersions, 1103

Radiation biology
Determination of absolute rate constants for the reversible hydrogen-atom transfer between thiyl radicals and alcohols or ethers, 1923

Radiation chemistry
Spin effects on spur kinetics. Re-encounters and the independent pairs approximation, 223

Radiative lifetime
Quenching rate constants for $NCl(b\,^1\Sigma^+)$ and $PCl(b\,^1\Sigma^+)$ and radiative lifetimes of $NCl(b\,^1\Sigma^+)$, $PCl(b\,^1\Sigma^+)$ and $PBr(b\,^1\Sigma^+)$, 2979

Radical ion
Direct evidence for H^+-catalysed dehydration of fluorohydroxycyclohexadienyl radical: A pulse radiolysis study, 2121
Stopped-flow kinetic study of the formation and decay of the 4,4′-(dimethylamino) diphenylmethane radical cation in aqueous solution, 2743
Triplet and radical ion properties of (*E*)-1-styrylpyrene and (*E*)-3-styrylchrysene, 3117
EPR, ENDOR and TRIPLE resonance characterization of three paramagnetic reduction stages of 5-(9′-fluorenylidene)-5*H*-dibenzo[*a*,*d*] cycloheptene. Radical anions, radical trianions and radical penta-anions, 3821

Radical reaction
Addition of cyclopentane to slowly reacting mixtures of $H_2 + O_2$ between 673 and 783 K: Reactions of H and OH with cyclopentane and of cyclopentyl radicals, 1431

Radiofrequency-induced plasma
Mass spectrometry of and deposition-rate measurements from radiofrequency-induced plasmas of methyl isobutyrate, methyl methacrylate and *n*-butyl methacrylate, 1363
Corrigendum to Mass spectrometry of and deposition-rate measurements from radiofrequency-induced plasmas of methyl isobutyrate, methyl methacrylate and *n*-butyl methacrylate, 2051

RAIRS
Surface chemistry of methyl groups adsorbed on Pt(111), 3619
Cyclohexane adsorption on clean and O-covered Ni{111}: Implications for C—H bond activation, 3703
Optical effects in the IR reflection–absorption spectra of thin water-ice films on metal substrates, 4005

Raman scattering
Raman scattering study of butane-1,4-diol dimethacrylate, 2339
Effect of temperature on poly(ethylene oxide) chains in aqueous solution. A viscometric, ^1H NMR and Raman spectroscopic study, 3897

Raman spectroscopy
Time-resolved resonance Raman spectroscopy of triplet-state metallated and free-base tetraarylporphyrins, 411
Raman spectroscopic study of nitronium ion formation in mixtures of nitric acid, sulfuric acid and water, 1439
Laser-Raman spectroscopic study of the vapour phase of $NbCl_5$ and mixtures of $NbCl_5$ and $SnCl_2$, 1445
Structural and spectroscopic investigations of aminocyclopropenium cations, $[C_3(Nr_2)_3]^+$ (NR_2 = NMe_2, NEt_2, NC_5H_{10} or NC_4H_8O) and $[C_3(NPr^i_2)_2Cl]^+$, 1523
Rotational isomerism in acrylic acid. A combined matrix-isolated IR, Raman and *ab initio* molecular orbital study, 1571
In situ Raman studies of the selective oxidation of methanol to formaldehyde and ethene to ethylene oxide on a polycrystalline silver catalyst, 4149
Mechanism of formation of copper thiocyanate on the copper anode, 4403

Raney nickel catalyst
Surface composition, structural and chemisorptive properties of Raney nickel catalysts, 2891

Rare-earth-metal oxyfluoride
Crystal fields in REOF: Eu^{3+} (RE = La, Gd and Y), 1503

Rare gas
Theoretical cross-sections for *M*-changing collisions of symmetric-top molecules with rare-gas atoms, 4363

Rate constant
Rate constants for the reactions of C_2H_5, C_2H_5O and $C_2H_5O_2$ radicals with NO_3 at 298 K and 2.2 Torr, 817
Photoinduced electron-transfer quenching of excited singlet states of polycyclic aromatic hydrocarbons by organic acceptors. Solvent effects on the rate constants and the charge-separation efficiency, 1197
Prototype Si—H insertion reaction of silylene with silane. Absolute rate constants, temperature dependence, RRKM modelling and the potential-energy surface, 2723
Arrhenius parameters for the reaction of H atoms with GeH_4, 3367

Reaction kinetics
Spin effects on spur kinetics. Re-encounters and the independent pairs approximation, 223

Reaction mechanism
Gas-phase chlorosilylation of silica gel: Effectiveness, surface coverage and stoichiometry, 353

Reaction rate
Temperature dependence of the rate of reaction of OH with some aromatic compounds in aqueous solution, 1631

Reactive collision
Reactive collisions with excited-state atoms, 389

Reactive scattering
Reactive scattering of atoms and radicals, 575

Recognition
Voltammetric and NMR studies of a bis(ferrocenecarboxamide)-substituted diaza-18-crown-6 receptor that simultaneously complexes and electrochemically recognises both cations and anions, 295

Redox

Measurement of viscoelastic changes at electrodes modified with redox hydrogels with a quartz crystal device, 4083

Redox catalysis
Phases in vanadium pentoxide–tungsten trioxide catalysts, 145

Redox interaction
Redox interaction of ammonia with $(VO)_2P_2O_7$, 725

Reduction
Oxygen reduction on a rotating Pt disc electrode in formic acid-containing solutions, 2817
Selective catalytic reduction of nitric oxide with ammonia on MFI-type ferrisilicate, 3275

Reflectance anisotropy
Adsorption of O, HCO_2H and $C_6H_5CO_2H$ on Cu(110) studied using reflectance anisotropy. Chemical and structural influences on an optically active surface resonance, 3627

Reflection–absorption IR spectroscopy
Reflection–absorption IR spectroscopy at cryogenic temperatures, 3563

Refractive index
Experimental determination of second density virial coefficients of xenon and chlorine at elevated temperatures, 1277

Reinforced polyurethane cellulose fibres
Reinforcement of polyurethane elastomers with microfibres having varying aspect ratios, 2507

Relative permittivity
Rate of decomposition of murexide in mixed solvents: An indicator for proton activity, 637

Relaxation mechanisms
Molecular motions in a rigid backbone polymer: Poly(*n*-hexyl isocyanate). A study by thermally stimulated currents, 2003

REMPI
Observation of the SCl radical by resonance-enhanced multiphoton ionisation spectroscopy, 773
Resonance-enhanced multiphoton ionisation spectroscopy of methanethiol, 2715
Multiphoton ionisation spectroscopy of ethyl iodide and deuteriated ethyl iodide in the region of the 6*s* Rydberg transitions. Evidence of molecular field splitting of spin–orbit degenerate states, 3083
(1 + 1) Resonance-enhanced multiphoton ionization spectroscopy of jet-cooled C_2H_2, C_2HD and C_2D_2 in the range 46 400–48 400 cm^{-1}, 3327
Resonance-enhanced multiphoton ionisation spectroscopy of dimethyl sulfide, 3339

Reorganization dynamics
Temperature, pressure and solvent isotope effects on the precursor formation constant and reorganization dynamics in outer-sphere charge transfer between free mobile $[Fe(CN)_6]^{3-}$ and $[Fe(CN)_6]^{4-}$ ions, 1625

Resonance frequency
Appraisal of the fundamental operation of quartz crystal shear-mode biosensors, 3147

Resonance Raman spectroscopy
Time-resolved resonance Raman spectroscopy of triplet-state metallated and free-base tetraarylporphyrins, 411
Surface-enhanced resonance Raman spectroscopic studies of the Pb^{II} complex of 1-(2-pyridylazo)-2-naphthol adsorbed on Ag sol, 463
Resonance Raman spectroscopic study of Methyl Red and Ethyl Red adsorbed on silica, 499
Resonance Raman study of the chromophore-specific vibrational and electronic spectra of bilirubin, 1751

Response reaction
Response reactions: A way to explain the unusual behaviour of multiple equilibrium systems, 259

Reversed-flow gas chromatography
Simple determination of experimental isotherms using diffusion denuder tubes, 485

Reverse micelle
Ultra-thin particulate films prepared from capped and uncapped reverse-micelle-entrapped silver particles, 673
Structure and reactivity of aerosol-OT reversed micelles containing α-chymotrypsin, 1081
Photochromism and thermochromism of spiro[indolinoxazines] in normal and reversed micelles, 4099

Reversible adsorption
Reversible and irreversible adsorption of nitrogen monoxide on cobalt ion-exchanged ZSM-5 and mordenite zeolites at 273–523 K, 767

Reversible hydrogen transfer
Determination of absolute rate constants for the reversible hydrogen-atom transfer between thiyl radicals and alcohols or ethers, 1923

Rh electrode
Corrigendum to Relation between the surface states of oxide films at Rh electrodes and kinetics of the oxygen evolution reaction, 2353

Rheology
Theory and experiments for evaluating the number and the dimensions of solid particles dispersed in a liquid medium. Application to the system $Si_3N_4/H_2O(l)$, 323
Shear and extensional viscosity characteristics of a series of hydrophobically associating polyelectrolytes, 911
Evidence of extraneous surfactant adsorption altering adsorbed layer properties of β-lactoglobulin, 1991
Configurational and rheological properties of cyclic polymers, 2525

Rhodium
Effects of modification of Pd/SiO_2 with Rh on catalytic activity for ethene hydroformylation, 1271
Mechanism of the conversion of ethene to ethylidyne on rhodium (111): Evidence for a vinylic intermediate, 3679

Rigid copolymer
Modelling the influence of monomer properties on hydrogen bond density in oriented, rigid copolymer systems, 2629

RNA
Thermodynamic properties of transfer RNA: A computational study, 2531

Rotating cryostat
EPR spectroscopic study of the reaction of Al and Ga atoms with CO_2 and CS_2 in a rotating cryostat, 799

Rotating Pt disc electrode
Oxygen reduction on a rotating Pt disc electrode in formic acid-containing solutions, 2817

Rotating ring–disc electrode
Electroreduction of oxygen on Fe_3O_4 electrodes. Part 2.—Rotating ring–disc electrode studies and mechanism, 2323

Rotational *g* factor
Electric polarity $^+BrCl^-$ and rotational *g* factor from analysis of frequencies of pure rotational and vibration–rotational spectra, 3005

Rotational isomerism
Discovery of two rotational isomers of 4-methoxystyrene by laser-induced fluorescence in a supersonic jet, 197
Ultrasonic investigation of the viscosity dependence of the rate constants of rotational isomerism of dibromoethane and dibromopropane in solution, 445
Rotational isomerism in acrylic acid. A combined matrix-isolated IR, Raman and *ab initio* molecular orbital study, 1571

Rotational motion
Coupling between different modes in local chain dynamics: A modal correlation analysis, 2483

Rotational spectroscopy
'Charge-transfer' complexes of ammonia with halogens: Nature of the binding in $H_3N\cdots BrCl$ from its rotational spectrum, 781
Microwave spectrum and structure of furan·ethene, 975
Donor–acceptor complexes of Lewis bases with bromine monochloride in the gas phase: some generalisations from rotation spectroscopy, 1881
The bπ.aσ complex $C_2H_2\cdots Cl_2$ characterised by rotational spectroscopy as an intermediate in a reactive mixture of ethyne and chlorine, 1891
$H_2S\cdots Cl_2$ characterised in a pre-reactive gas mixture of hydrogen sulfide and chlorine through rotational spectroscopy: The nature of the interaction, 2059
Structure, harmonic force field and hyperfine coupling constants of nitrosyl chloride, 3347

Rotational structure
High-resolution IR spectrosopy of jet-cooled CF_3CH_2F, 1723

Rovibrational state
Collision broadening of CO_2/transitions in the region of 4.3 μm. Effects of broadening gas (He, Ar and N_2), rovibrational states and temperature, 191

Rovibronic energy level
Theoretical potential-energy functions and spectroscopic data for the PH_2^+ ion, 2053

RRKM modelling
Prototype Si—H insertion reaction of silylene with silane. Absolute rate constants, temperature dependence, RRKM modelling and the potential-energy surface, 2723

Rubidium
Isotope effects of rubidium in amalgam/aqueous solution systems, 2319

Rupture
Determination of thickness and rupture pressure for aqueous foam films. Part 1.—Films stabilized by anionic surfactants, 4251

Ruthenium complex
Solvent effect on the photoinduced electron-transfer reactions between dicyanobis(polypyridine)ruthenium(II) complexes and tris(β-diketonato) ruthenium(III) complexes, 437

Rydberg orbital
Perturbation theory model of molecular Rydberg orbitals: Application to diatomic molecules, 2699

Rydberg series
Resonance-enhanced multiphoton ionisation spectroscopy of methanethiol, 2715
Resonance-enhanced multiphoton ionisation spectroscopy of dimethyl sulfide, 3339

Rydberg transition
Multiphoton ionisation spectroscopy of ethyl iodide and deuteriated ethyl iodide in the region of the 6*s* Rydberg transitions. Evidence of molecular field splitting of spin–orbit degenerate states, 3083

SANS
Self-organization of graft copolymers at surfaces, interfaces and in bulk, 2855

SAPO
Acidity of aluminophosphate structures. Part 1.—Incorporation of silicon into chabazite-like structure 44, 1155
Pt/SAPO-5 and Pt/SAPO-11 as catalysts for the hydroisomerization and hydrocracking of *n*-octane, 1551
Reversible interaction of NH_3 with the framework of template-free zeolite-type SAPO-34, 3281
Catalytic properties of the silicoaluminophosphates SAPO-5 and SAPO-11 in *n*-octane and isooctane hydroconversion, 4171

Saponite
Al-Pillared saponites. Part 3.—Effect of parent clay layer charge on the intercalation–pillaring mechanism and structural properties, 2229

Scaling parameter
Statistical thermodynamics of hydrocarbon fluids: Scaling parameters and their group contributions, 2443

Scanning electrochemical microscopy
Study of silicon etching in HBr solutions using a scanning electrochemical microscope, 1019
Scanning electrochemical microscopy as a probe of local fluid flow through porous solids: Application to the measurement of convective rates through a single dentinal tubule, 1407

Scanning electron microscopy
Characterization of precipitates formed from the tetraiodomercurate(II) anion and mercury(I) or silver (I) cations, 1217
Diversity of the kinetics of carbon monoxide oxidation on differently prepared zinc oxides, 1391

Scanning tunnelling microscopy
STM of folded and unfolded haemoglobin molecules electrochemically deposited on highly oriented pyrolytic graphite, 1471

SCl radical

Observation of the SCl radical by resonance-enhanced multiphoton ionisation spectroscopy, 773

Second harmonic generation
Surface second harmonic generation at air/solvent and solvent/solvent interfaces, 1763
Optical second-harmonic generation measurements of molecular adsorption and orientation at the liquid/liquid electrochemical interface, 1411
Effect of urea and surfactant on *p*-nitrophenol at the water surface: a surface second-harmonic generation study, 1769
Corrigendum to Relation between the surface states of oxide films at Rh electrodes and kinetics of the oxygen evolution reaction, 2353

Self-assembled film
Direct functionalization of silicon *via* the self-assembly of alcohols, 4001

Self-consistent field model
Self-consistent field model of the polymer/diblock copolymer/polymer interface, 2381

Self-diagnostic gas sensor
Detection of sensor poisoning using self-diagnostic gas sensors, 3307

Self-diagnostic sensor array
Theory of self-diagnostic sensor array devices using gas-sensitive resistors, 1961

Self-diffusion
Modified interacting-sphere model for self-diffusion and infinite-dilution mutual-diffusivity of *n*-alkanes, 245
Molecular dynamics study of the self-diffusion of supercritical methane in slit-shaped graphitic micropores, 1377
Self-diffusion of the perchlorate ion in aqueous electrolyte solutions measured by ^{35}Cl NMR spin-echo experiments, 1877

Self-organization
Self-organization of graft copolymers at surfaces, interfaces and in bulk, 2855

Semiconducting metal oxide
Detection of sensor poisoning using self-diagnostic gas sensors, 3307

Semiconductor
Photoelectrochemical properties of 'Q-state' CdS particles in arachidic acid Langmuir–Blodgett films, 665
Photochemistry of semiconductor particles. Part 4.—Effects of surface conditions on the photodegradation of 2,4-dichlorophenol catalysed by TiO_2 suspensions, 917
Kinetic study of the effects of H, O, N, S, NO, NO_2 and O_2 on the surface states of InGaAs and GaAs, 3021
Reaction–diffusion effects and systematic design of gas-sensitive resistors based on semiconducting oxides, 4299

Semiconductor catalyst
Semiconductive properties of some uranium–antimony oxide phases used as catalysts in the mild oxidation of but-1-ene to butadiene, 2343

Semiempirical calculation
Energetics and isomerisation pathways of a lower fullerene. The Stone–Wales map for C_{40}, 1421

Semiempirical quantum chemical calculation
Physicochemical properties of dimethyl sulfoxide–methanol liquid mixtures. Experimental and semiempirical quantum chemical studies, 65

Semiflexible polymer
Statistical mechanics of semiflexible polymers: Yesterday, today and tomorrow, 2473

Sensitivity coefficient
Response reactions: A way to explain the unusual behaviour of multiple equilibrium systems, 259

Sensor
Theory of self-diagnostic sensor array devices using gas-sensitive resistors, 1961
Detection of sensor poisoning using self-diagnostic gas sensors, 3307

Separation process
Theory of concentration polarization in crossflow filtration, 3389

Series–parallel path
Permeability and the time lag for downstream absorptive permeation with concomitant reaction across a series–parallel path studied by the matrix method, 469

SERRS
Surface-enhanced resonance Raman spectroscopic studies of the Pb^{II} complex of 1-(2-pyridylazo)-2-naphthol adsorbed on Ag sol, 463

Shear flow
Brownian-dynamics simulations of model stabilised colloidal dispersions under shear, 1975

Shear-wave
Appraisal of the fundamental operation of quartz crystal shear-mode biosensors, 3147

Silane
IR studies of adhesion promoters. Part 3.—Adsorption and coupling of bifunctional silanes on silica at the solid/liquid interface, 1253
Prototype Si—H insertion reaction of silylene with silane. Absolute rate constants, temperature dependence, RRKM modelling and the potential-energy surface, 2723
Corrigendum to IR studies of adhesion promoters. Part 3.—Adsorption and coupling of bifunctional silanes on silica at the solid/liquid interface, 3309

Silane coupling agent
IR studies of adhesion promoters. Part 1.—Methoxytrimethylsilane on silica at the solid/liquid interface, 105
IR studies of adhesion promoters. Part 2.—Adsorption of the alkyltrimethoxysilane and alkylamino-trimethoxysilane on silica at the solid/liquid interface, 359

Silica
IR studies of adhesion promoters. Part 1.—Methoxytrimethylsilane on silica at the solid/liquid interface, 105
Surface chemistry of silica–titania-supported chromium oxide catalysts, 953
Exchange reactions of 2,2-dimethylpentane, 2,2-dimethylbutane and 2,2-dimethylpropane over Pt/SiO_2 and Rh/SiO_2, 1131
IR studies of adhesion promoters. Part 3.—Adsorption and coupling of bifunctional silanes on silica at the solid/liquid interface, 1253
Corrigendum to IR studies of adhesion promoters. Part 3.—Adsorption and coupling of bifunctional silanes on silica at the solid/liquid interface, 3309
Effects of silicate ions on the formation and transformation of calcium phosphates in neutral aqueous solutions, 3499
Competitive adsorption of polymers and surfactants at the solid/liquid interface, 3919
Novel routes to designer silicas: Studies of the decomposition of $(M^+)_2[Si(C_6H_4O_2)_3 \cdot xH_2O]$. Importance of M^+ identity of the kinetics of oligomerisation and the structural characteristics of the silicas produced, 4287

Silica gel
Gas-phase chlorosilylation of silica gel: Effectiveness, surface coverage and stoichiometry, 353

Silicalite
Atom pair potential for molecular dynamics simulations of structural and dynamical properties of aluminosilicates: Test on silicalite and anhydrous Na-A and Ca-A zeolites and comparison with experimental data, 525
^2H NMR studies of binary adsorption in silicalite, 963
Intracrystalline diffusion of benzene in silicalite: Effect of structural heterogeneity, 1143
V–Ti and V–Al silicate molecular sieves of MFI topology: Synthesis and characteristics, 2217

Silica sphere
Selection of Brownian particles, 3163

Silica surface
Total characterization of the BCl_3-modified silica surface by means of quantitative surface analysis, 2173

Silica-supported catalyst
Hydrogen adsorption on silica-supported platinum studied by ^1H NMR spectroscopy, 2191
Influence of oxidation and reduction conditions upon the morphology of silica-supported polycrystalline silver catalysts, 133
FTIR study of the effects of sulfur poisons on NO adsorption on supported copper oxide catalysts, 141
NMR characterization of the supported 12-heteropoly acids, 375
Surface chemistry of silica–titania-supported chromium oxide catalysts, 953
FTIR studies of adsorption of NO, NO_2 and N_2O on layered V_2O_5/ZrO_2, 1557
Selective photooxidation of light alkanes to oxygenates using supported molybdenum oxide catalysts, 1647
Characterisation of the acidity of well defined Cu-ZSM-5 catalysts using pyridine as a probe molecule, 1841
^1H NMR of hydrogen chemisorbed on silica-supported platinum particles: An evaluation of different models, 2203
Combined DRS–RS–EXAFS–XANES–TPR study of supported chromium catalysts, 3245
Hydrogenation of propyne over palladium catalysts, 3269
Comparison of $Pd(NH_3)_4^{2+}$ decomposition and Pd^{2+} reduction in zeolites NaY, NaX and CsX, 3291
Temperature-programmed reduction of alumina-supported Ni–Pt systems, 3481
Behaviour of oxygen species adsorbed on Al_2O_3-supported cerium oxide catalysts for methane oxidation, 4459

Silicate
Effects of silicate ions on the formation and transformation of calcium phosphates in neutral aqueous solutions, 3499

Silicoaluminium phosphate
Reduction of copper(II) with subsequent disproportionation of copper(I) during the hydrothermal syntheses of microporous silicoaluminium phosphates SAPO-5 and -11, 3529

Silicon
Study of silicon etching in HBr solutions using a scanning electrochemical microscope, 1019
Influence of the source of silicon and aluminium in the hydrothermal synthesis of sodalite, 1147
Direct functionalization of silicon *via* the self-assembly of alcohols, 4001
Fluorescence spectra of methyl salicylate during the sol–gel–xerogel transitions of mixed silicon–aluminium alkoxides, 4279
^{29}Si MAS NMR study of a highly siliceous EUO-type material, 4309

Silver
In situ Raman studies of the selective oxidation of methanol to formaldehyde and ethene to ethylene oxide on a polycrystalline silver catalyst, 4149

Silver(I) salt
^{63}Cu and ^{109}Ag NMR studies of copper(I) and silver(I) salts in mixed solvents containing nitriles, 2307

Silver catalyst
Influence of oxidation and reduction conditions upon the morphology of silica-supported polycrystalline silver catalysts, 133

Silver complex
Temperature coefficients of Ag/Ag^+ and Ag/Ag^+–cryptand 222 electrode potentials, thermodynamics of Ag^+–cryptand 222 complex formation and molar transfer properties for Ag^+ cations into aprotic media, 1097

Silver particle
Ultra-thin particulate films prepared from capped and uncapped reverse-micelle-entrapped silver particles, 673

Silylene
Prototype Si—H insertion reaction of silylene with silane. Absolute rate constants, temperature dependence, RRKM modelling and the potential-energy surface, 2723

^{29}Si MAS NMR
Solid-state NMR and powder XRD studies of the structure of SAPO-40 upon hydration–dehydration cycles, 2213

Simha–Somcynsky hole theory
Statistical thermodynamics of hydrocarbon fluids: Scaling parameters and their group

contributions, 2443
SIMS
Secondary ion mass spectroscopy and X-ray photoelectron spectroscopy of Na_2MoO_4/SiO_2 catalysts for methane oxidative coupling, 381
Simulation
Molecular dynamics simulation of nuclear spin relaxation of $^7Li^+$ in water, 215
Single crystal
Simulation of growth and surface roughening of polymer single crystals, 2587
Single-crystal EPR
Single-crystal EPR study of the compounds $[MCu(edta)(H_2O)_3] \cdot H_2O$ (M = Sr, Ba), 423
Single-ion transfer
Thermodynamic transfer properties for Na^+, Tl^+ and Ag^+ to water–acetonitrile mixtures, 875
Single resonator
Dynamics study of a closed diffusion cell by using a frequency response method: Single resonator, 1695
Skeletal isomerization
Skeletal isomerization of *n*-butane over caesium hydrogen salts of 12-tungstophosphoric acid, 367
Skin
Novel spectroscopic deconvolution procedure for complex biological systems: Vibrational components in the FT-Raman spectra of ice-man and contemporary skin, 3883
Slag
Use of ultraviolet excitation spectra of Tl^+ for probing oxidic networks: Alkali-metal borate glasses, 3485
Small-angle neutron scattering
Nitrogen adsorption and small-angle neutron scattering studies with capped alumina, 1139
Small-angle X-ray scattering
Electrically induced reversible structural change of a highly swollen polymer gel network, 473
Structure and reactivity of aerosol-OT reversed micelles containing α-chymotrypsin, 1081
Smectic B phase
Computer-simulation studies of anisotropic systems. Part XXIV.—Constant-pressure investigations of the smectic B phase of the Gay–Berne mesogen, 2141
SMSI
Influence of strong metal–support interaction on exchange with deuterium and other reactions of hydrocarbons. Part 1.—Studies with Rh/TiO_2 and Rh/SiO_2, 741
$SnCl_2$
Laser-Raman spectroscopic study of the vapour phase of $NbCl_5$ and mixtures of $NbCl_5$ and $SnCl_2$, 1445
Sodalite
Influence of the source of silicon and aluminium in the hydrothermal synthesis of sodalite, 1147
Sodium dodecyl sulfate
Oligomerization of cationic pyrene derivatives in the presence of sodium dodecyl sulfate: A route to nanoaggregate formation, 3913
Sol–gel
Thermoreversible gelation of hydrated polymers, 2663
Solid/liquid interface
IR studies of adhesion promoters. Part 2.—Adsorption of the alkyltrimethoxysilane and alkylamino-trimethoxysilane on silica at the solid/liquid interface, 359
Sum-frequency vibrational spectroscopy of the solid/liquid interface, 1281
Solid solution
CoO–ZnO solid solution as a model to investigate the CO–cation interaction: An FTIR and HRTEM study, 4445
Solid-state NMR spectroscopy
Intramolecular hydrogen bonding in *N*-salicylideneanilines. X-Ray diffraction and solid-state NMR studies, 77
High-resolution ^2H solid-state NMR of ^2H_2O adsorbed onto activated carbon, 1795
Dynamics of benzene and pyridine guest molecules in their tri-*ortho*-thymotide inclusion compounds. Solid-state ^2H NMR studies, 2017
Variable-temperature X-ray crystallographic and magic-angle spinning NMR spectral studies on hexaethylbenzene, 2149
Solid-state NMR and powder XRD studies of the structure of SAPO-40 upon hydration–dehydration cycles, 2213
Effect of structural aluminium on the mesoporous structure of MCM-41, 2955
Second-order quadrupolar effects for directly bonded and remote ^{13}C–$^{79/81}Br$ spin pairs in high-resolution ^{13}C NMR spectra of solids, 3167
Mössbauer and solid-state NMR spectroscopic studies of tin-modified rhenium-based metathesis catalysts, 3511
Low-temperature single-crystal X-ray diffraction, ^1H and ^{13}C solid-state NMR and ^{14}N NQR studies of 1,8-bis(dimethylamino)-naphthalene, 3925
Solid-state ^1H NMR studies of the acidity of mordenites, 3933
Solubility
Thermodynamic investigation of the effect of octanol–water mutual miscibility on the partitioning and solubility of some guanine derivatives, 995
Solubility and Pitzer model parameters in thallium(I) chloride systems, TlCl–$MgCl_2$–H_2O and TlCl–$CaCl_2$–H_2O, 1759
Solubility and Pitzer model parameters in thallium(I) chloride systems, TlCl–$MgCl_2$–H_2O and TlCl–$CaCl_2$–H_2O, 1759
Solubilization
Solubilization of two cyano 3*H*-indole molecular probes in SDS and CTAB micelles: Spectral and photophysical characterization, 2133
Solution interface
Liquid droplets and solid particles at surfactant solution interfaces, 2681
Solution property
Choice of the reaction coordinate in electron-transfer reactions in solution, 1451
Temperature dependence of the rate of reaction of OH with some aromatic compounds in aqueous solution, 1631
Heat capacities and concentration fluctuations in mixtures of 1,2-dibromoethane with alkanes, 1941
Evaluation of the stability constant of $Cl_2^{\bullet-}$ in neutral aqueous solution, 3303
Steric solvent effect on small and large cations: Calorimetric study of halogeno and thiocyanato complexes of beryllium(II) and cadmium(II) in *N*,*N*-dimethylacetamide, 3851
Temperature dependence of EXAFS for bromide ions in solution, 4389
Solvated electron
Kinetics of solvated electrons in reaction with hexamethylphosphoric triamide, 3809
Solvation
Solvation of cobalt(II) and perchlorate ions in binary mixtures of donor solvents, 71
Preferential solvation in mixed solvents. Part 7.—Binary mixtures of water and alkanolamines, 427
Preferential solvation in mixed binary solvent, 631
Thermodynamic study of the partitioning of organic compounds between water and octan-1-ol. Effects of water as cosolvent in the organic phase, 649
^{63}Cu and ^{109}Ag NMR studies of copper(I) and silver(I) salts in mixed solvents containing nitriles, 2307
Solvation and complexation equilibria of nickel(II) thiocyanato complexes in *N*,*N*-dimethylacetamide, 2313
Partitioning of entropy of solvation: Single-ion entropy of solvation in aqueous and non-aqueous solvents and the correlation of electrostatic entropy of solvation with electrostriction viscosity *B* and NMR *B'* coefficients, 3373
Intramolecular hydrogen bonding and molecular conformation. Part 4.—Corrections of thermodynamic properties obtained by IR measurements at different temperatures and pressures, 3379
Preferential solvation controlled by clustering conditions of acetonitrile–water mixtures, 4063
Solvation dynamics
Femtosecond to nanosecond solvation dynamics in pure water and inside the γ-cyclodextrin cavity, 867
Solvatochromism
Excited-state dipole moments of some Coumarin dyes from a solvatochromic method using the solvent polarity parameter, E_T^N, 2739
Halochromism and solvatochromism of a π^* probe in binary solvent mixtures, 3839
Solvent dependence
Solvent-dependent switching between two dipolar excited states in a rigidly extended trichromophoric system, 2107
Solvent effect
Solvent effect on the photoinduced electron-transfer reactions between dicyanobis(polypyridine)ruthenium(II) complexes and tris(β-diketonato)-ruthenium(III) complexes, 437
Photoinduced electron-transfer quenching of excited singlet states of polycyclic aromatic hydrocarbons by organic acceptors. Solvent effects on the rate constants and the charge-separation efficiency, 1197
Corrigendum to Effect of solvent on the reaction of coordination complexes. Part 19.—Base hydrolysis of (α*βS*)-(*o*-methoxybenzoato)-(tetraethylenepentamine)cobalt(III) in aquo-organic solvent media, 1715
Solvent effect on photoinduced electron transfer between C_{60} and 3,3',5,5'-tetramethylbenzidine studied by nanosecond laser photolysis, 2287
Solvent isotope effect
Temperature, pressure and solvent isotope effects on the precursor formation constant and reorganization dynamics in outer-sphere charge transfer between free mobile $[Fe(CN)_6]^{3-}$ and $[Fe(CN)_6]^{4-}$ ions, 1625
Solvent mixture
Simultaneous description of excess enthalpy and vapour–liquid equilibrium data of associated mixtures by means of a lattice–fluid model, 4381
Solvent/solvent interface
Surface second harmonic generation at air/solvent and solvent/solvent interfaces, 1763
Sonochemical dissolution
Sonochemical dissolution of MnO_2 colloids, 2843
Sorption
Isosteric heat of sorption of dihydrogen on alumina-supported palladium, 949
Contribution of sorption to global mass transfer during pervaporation of ethyl *tert*-butyl ether–ethanol mixtures through a polyurethaneimide film, 1247
Sorption isotherm
Sorption isotherms of methane, ethane, ethene and carbon dioxide on NaX, NaY and Na-mordenite zeolites, 2935
Sorption kinetics
Intracrystalline diffusion of benzene in silicalite: Effect of structural heterogeneity, 1143
Spectral deconvolution
Characterisation of hydroxide complexes of uranium(VI) by time-resolved fluorescence spectroscopy, 2275
Spectrophotometric titration
Titration calorimetric and spectrophotometric studies of micelle formation by alkyltrimethylammonium bromide in aqueous solution, 1229
Spectrophotometry
Cooperative interactions between ions and water in the chloride ion and water coordination to a square-planar nickel complex ion in concentrated aqueous solutions, 627
Spin-coupled valence bond method
Catalytic chemistry of furan and thiophene. *Ab initio* calculations, using the spin-coupled valence bond method, of the interaction of furan and thiophene with a positively charged centre, 749
Spinel
Physico-chemical properties and catalytic activities of the spinel series $Mn_xFe_{3-x}O_4$ towards peroxide decomposition, 3489

Spin–lattice relaxation
Nuclear magnetic relaxation study of poly(ethylene oxide) complexed with lithium trifluoromethanesulfonate, 2871
Effect of temperature on poly(ethylene oxide) chains in aqueous solution. A viscometric, ^{1}H NMR and Raman spectroscopic study, 3897
Spin–orbit state
Multiphoton ionisation spectroscopy of ethyl iodide and deuteriated ethyl iodide in the region of the 6s Rydberg transitions. Evidence of molecular field splitting of spin–orbit degenerate states, 3083
Spin–spin coupling
Ab initio and experimental study of NMR coupling constants in bicyclo[1.1.1]pentane, 4031
Spur kinetics
Spin effects on spur kinetics. Re-encounters and the independent pairs approximation, 223
Sputtered lithium
Temporal and spatial distribution profiles of lithium atoms in low-pressure discharges by concentration-modulated absorption spectroscopy, 1297
SSHG
Effect of urea and surfactant on *p*-nitrophenol at the water surface: A surface second-harmonic generation study, 1769
Stability constant
Temperature coefficients of Ag/Ag^+ and Ag/Ag^+–cryptand 222 electrode potentials, thermodynamics of Ag^+–cryptand 222 complex formation and molar transfer properties for Ag^+ cations into aprotic media, 1097
Evaluation of the stability constant of $Cl_2^{\bullet-}$ in neutral aqueous solution, 3303
Stabilities in water of 1:1 lariat 16-crown-5 complexes with metal ions: Transfer activity coefficients from protic to aprotic solvents of 1:1 complexes of lariat and substituted 16-crown-5 derivatives with metal ions, 4079
Static vibrational polarizability
Static vibrational polarizability of all-*trans* polyethylene and polysilane, 1641
Statistical mechanics
Statistical mechanics of semiflexible polymers: Yesterday, today and tomorrow, 2473
Statistical model
Neutron scattering from solution-grown polymer crystals: A statistical model, 2593
Statistical thermodynamics
Statistical thermodynamics of hydrocarbon fluids: Scaling parameters and their group contributions, 2443
Step-addition
Molecular kinetics during the growth of the macromolecule poly(di-2-hydroxypropyl ether of bisphenol-A-*n*-hexylamine) studied by dielectric spectroscopy, 343
Sticking coefficient
Adsorption dynamics for CO and H_2 on an NiAl(110) surface, 3639
Sticking profile
Sticking of HCl and HBr on a type-II polar stratospheric cloud mimic, 2349
Stokesian dynamics
Microstructural studies of electro-rheological fluids under shear, 1787
Stratosphere
Sticking of HCl and HBr on a type-II polar stratospheric cloud mimic, 2349
Airborne chemistry and dynamics at the edge of the 1994 antarctic vortex, 3063
Streaming amalgam electrode
Gibbs energies of transfer of several alkali-metal chlorides from water to sucrose–water mixtures using streaming amalgam electrodes, 451
Strontium
Single-crystal EPR study of the compounds $[MCu(edta)(H_2O)_3] \cdot H_2O$ (M = Sr, Ba), 423
Kinetic investigation of energy pooling from $Sr[5s5p(^3P_J)]$ studied by time-resolved atomic emission following pulsed dye-laser excitation, 811
Sucrose–water
Gibbs energies of transfer of several alkali-metal chlorides from water to sucrose–water mixtures using streaming amalgam electrodes, 451
Sulfur
Hydrogen in molybdenum and cobalt sulfide catalysts. A neutron Compton scattering study on the ISIS electronvolt spectrometer, 4467
Sulfur poison
FTIR study of the effects of sulfur poisons on NO adsorption on supported copper oxide catalysts, 141
Sum-frequency spectroscopy
Sum-frequency vibrational spectroscopy of the solid/liquid interface, 1281
Superaromaticity
Non-superaromatic reference defined by graph theory for a super-ring molecule, 237
Aromaticity and superaromaticity in carbon nanotoroids, 1563
Superconductivity
Theoretical investigation on the band structures of several Chevrel-phase compounds, 479
Supercooling
Electrical conductivity of the systems $NaAlCl_4$ and NaCl(s)/$NaAlCl_4$ in the range 100–200 °C, 3157
Supercritical fluid extraction
Effect of the matrix on the kinetics of dynamic supercritical fluid extraction, 1333
Super-ring molecule
Non-superaromatic reference defined by graph theory for a super-ring molecule, 237
Supersaturated solution
Structural glass transitions and thermophysical processes in amorphous carbohydrates and their supersaturated solutions, 1511
Supersonic jet
Discovery of two rotational isomers of 4-methoxystyrene by laser-induced fluorescence in a supersonic jet, 197
Supersonic jet expansion
High-resolution IR spectrosopy of jet-cooled CF_3CH_2F, 1723
Supported metal catalyst
Effect of chlorine on microstructure and activity of Pd/CeO_2 catalysts, 507
Effect of Pt particle size on H/D exchange of methane over alumina- and zeolite-supported catalysts, 569
Exchange reactions of 2,2-dimethylpentane, 2,2-dimethylbutane and 2,2-dimethylpropane over Pt/SiO_2 and Rh/SiO_2, 1131
Microwave effects on the oxidative coupling of methane over proton conductive catalysts, 1179
Pt/SAPO-5 and Pt/SAPO-11 as catalysts for the hydroisomerization and hydrocracking of *n*-octane, 1551
Interaction of water with 1% Li/MgO:DC conductivity of Li/MgO catalyst for methane selective activation, 1805
Palladium–ceria catalysts: Reversibility of hydrogen chemisorption and redox phenomena, 2185
Surface studies
Charge regulation at the surface of porous silica, 2965
Surface basicity
Surface basicity of a new family of catalysts: Aluminophosphate oxynitride (AlPON), 4477
Surface composition
Surface composition of surfacant-stabilised polypyrrole colloids, 905
Surface coverage
^{1}H NMR of hydrogen chemisorbed on silica-supported platinum particles: An evaluation of different models, 2203
Surface defect
Spectroscopic study of oxygen adsorption as a method to study surface defects on CeO_2, 1669
Surface electrochemistry
Surface electrochemistry and kinetics of anodic bromine formation at platinum, 283
Surface interaction
Effects of citrate adsorption on the interactions between zirconia surfaces, 2921
Surface ionisation
Numerical simulation of surface ionisation and specific adsorption on a two-site model of a carbon surface, 2179
Surface oxygen vacancy
NO reaction at surface oxygen vacancies generated in cerium oxide, 1679
Surface potential
Curvature effects on electric double-layer forces. Part 1.—Comparisons with parallel plate geometry, 2827
Surface reconstruction
Adsorption of nitric oxide on Ir{100}: Influence of substrate reconstruction, 3575
Surface resonance
Adsorption of O, HCO_2H and $C_6H_5CO_2H$ on Cu(110) studied using reflectance anisotropy. Chemical and structural influences on an optically active surface resonance, 3627
Surface science
Kinetic study of the effects of H, O, N, S, NO, NO_2 and O_2 on the surface states of InGaAs and GaAs, 3021
Relationship between carbon black surface chemistry and energy, 3201
Quantitative structural study of an Na–O coadsorption phase on Al(111) using X-ray standing waves, 3555
Reflection–absorption IR spectroscopy at cryogenic temperatures, 3563
Valence-band and core photoelectron spectroscopic studies of molybdenum aqueous oxidation and the influence of argon-ion etching, 3593
Surface second harmonic generation
Surface second harmonic generation at air/solvent and solvent/solvent interfaces, 1763
Surface structure
Catalytic decomposition reaction of formic acid on an Ar^+-bombarded TiO_2(110) surface: Steady-state kinetics and microscopic surface structure, 1663
Surface structure change of a $[Pt_4(\mu\text{-}CH_3COO)_8]/SiO_2$ catalyst active for the decomposition of formic acid, 4161
Surface tension
Effect of surface tension of the matrix on fast-atom bombardment mass spectral determination of ethylenediaminetetraacetic acid, 1203
Surfactant
Effect of association of sulfonephthalein dyes with sodium dodecyl sulfate micelles on their acid–base equilibria, 681
Liquid droplets and solid particles at surfactant solution interfaces, 2681
EPR study of an associative polymer in solution: Determination of aggregation number and interactions with surfactants, 2863
Photophysics of 3- and 4-phenyl pyridyl ketones in submicellar and micellar solutions of ionic and non-ionic surfactants, 3405
Entropy of adsorption of mixed surfactants from solutions onto the air/water interface, 3873
Phase separation in concentrated mixtures of polymers and surfactants, 3901
Competitive adsorption of polymers and surfactants at the solid/liquid interface, 3919
Phase behaviour and structure in a non-ionic surfactant–oil–water mixture, 4269
Vesicle–surfactant interactions: Effects of added surfactants on the gel to liquid-crystal transition for two vesicular systems, 4275
Swelling ratio
Structure and swelling of end-linked model networks, 2549
Symmetric top
Theoretical cross-sections for *M*-changing collisions of symmetric-top molecules with rare-gas atoms, 4363
Symmetry
^{29}Si MAS NMR study of a highly siliceous EUO-type material, 4309
Synthesis
Low-temperature synthesis of perovskite-type oxides of lanthanum and cobalt and their electrocatalytic properties for oxygen evolution in alkaline solutions, 1871
Synthesis gas
Partial oxidation of CH_4 to synthesis gas using an Rh|YSZ|Ag electrochemical membrane reactor, 1655
Taeniolite matrix
Structural and adsorption properties of carbons

synthesized within taeniolite matrices, 493
Temperature dependence
Total characterization of the BCl_3-modified silica surface by means of quantitative surface analysis, 2173
Temperature-programmed desorption
Synthesis and characterization of the large-pore molecular sieve SAPO-46, 1045
Temperature-programmed method
Redox interaction of ammonia with $(VO)_2P_2O_7$, 725
Temperature-programmed reduction
Temperature-programmed reduction of alumina-supported Ni–Pt systems, 3481
Template
Synthesis, characterisation and catalytic performance of the solid acid DAF-1, 3537
Ternary mixture
Kirkwood–Buff integrals and preferential solvation in ternary non-electrolyte mixtures, 431
Raman spectroscopic study of nitronium ion formation in mixtures of nitric acid, sulfuric acid and water, 1439
Corrigendum to Kirkwood–Buff integrals and preferential solvation in ternary non-electrolyte mixtures, 1885
Experimental and predicted excess enthalpies of the 2,2,2-trifluoroethanol–water–tetraethylene glycol dimethyl ether ternary system using binary mixing data, 2071
Tetraalkylammonium salt
Partition and dimerization of ion-pair tetraalkylammonium salts in xylene, 643
Tetramer
Modern valence-bond description of $(CH_3)_4Li_4$, 3363
Tetraphenylborate
Reaction of H^+ with tetraphenylborates: An example of an EC mechanism at liquid/liquid interfaces, 3433
Thallium
Use of ultraviolet excitation spectra of Tl^+ for probing oxidic networks: Alkali-metal borate glasses, 3485
Thallium(I) chloride
Solubility and Pitzer model parameters in thallium(I) chloride systems, TlCl–$MgCl_2$–H_2O and TlCl–$CaCl_2$–H_2O, 1759
Thallium(IV) halide
Optical absorption and X-ray photoelectron spectroscopic studies of thorium tetrabromide, 2767
Thermal analysis
Synthesis and characterization of the large-pore molecular sieve SAPO-46, 1045
Thermal decomposition
Homogeneous thermal decomposition of dimethylzinc in a metal–organic vapour phase epitaxy reactor. An *ex situ* investigation by FTIR absorption spectroscopy, 3475
Thermal denaturation
Differential scanning calorimetric study of the interactions of some stabilizing amino acids and oligopeptides with hen egg white lysozyme, 2101
Thermally stimulated current
Molecular motions in a rigid backbone polymer: Poly(*n*-hexyl isocyanate). A study by thermally stimulated currents, 2003
Thermal reaction
Thermal reaction of azoisopropane in the presence of (*E*)-$CH_3CH{=}CHCH_3$: Reactions of the radical 2-$\dot{C}_3H_7$, 1303
Thermal regeneration
Thermal desorption of gallic acid from activated carbon surfaces, 3213
Thermochemical data
Thermochemical and theoretical studies of some benzodiazines, 1907
Thermochromism
Photochromism and thermochromism of spiro[indolinoxazines] in normal and reversed micelles, 4099
Thermodynamics
Vapour–liquid equilibrium of the ethanol–propanal system, 273
Thermodynamic study of the partitioning of organic compounds between water and octan-1-ol. Effects of water as cosolvent in the organic phase, 649
Thermodynamic properties and phase equilibria in the Fe–P system, 703
Thermodynamic transfer properties for Na^+, Tl^+ and Ag^+ to water–acetonitrile mixtures, 875
Thermodynamic investigation of the effect of octanol–water mutual miscibility on the partitioning and solubility of some guanine derivatives, 995
Unnoticed identities in chemical thermodynamics, 1325
Thermodynamic study of the aggregation of azo dyes containing two trifluoromethyl groups in aqueous solutions, 1601
Thermodynamic study of the binding of dibenzo-18-crown-6 with Ag^+, Pb^{2+} and Cd^{2+} in acetonitrile–water solvents, 1607
Corrigendum to Effect of solvent on the reaction of coordination complexes. Part 19.—Base hydrolysis of (αβ*S*)-(*o*-methoxybenzoato)-(tetraethylenepentamine)cobalt(III) in aquo-organic solvent media, 1715
Thermodynamic properties of a coarse-grained model of hydrocarbon polymers. Computer simulations on articulated chain structures, 2457
Thermodynamic properties of transfer RNA: A computational study, 2531
Interactions between cations and sugars. Part 8.—Gibbs energies, enthalpies and entropies of association of divalent and trivalent metal cations with xylitol and glucitol in water at 298.15 K, 2771
Corrigendum to IR studies of adhesion promoters. Part 3.—Adsorption and coupling of bifunctional silanes on silica at the solid/liquid interface, 3309
Steric solvent effect on small and large cations: Calorimetric study of halogeno and thiocyanato complexes of beryllium(II) and cadmium(II) in *N*,*N*-dimethylacetamide, 3851
Hydrodehalogenation of chlorosilanes in the presence of metal silicides: Experimental studies of gas and solid phase composition related to thermodynamic calculations, 3879
Thermodynamics of the interaction of 18-crown-6 with K^+, Tl^+, Ba^{2+}, Sr^{2+} and Pb^{2+} from 323.15 to 398.15 K, 4207
Equilibrium aspects of the extraction of caesium nitrate by dicyclohexano-21-crown-7, dibenzo-21-crown-7 and bis-[*tert*-alkylbenzo]-21-crown-7 in 1,2-dichloroethane, 4215
Thermodynamics of complexation of sodium, potassium, rubidium, caesium and ammonium ions with 18-crown-6 in acetonitrile and propylene carbonate, 4375
Simultaneous description of excess enthalpy and vapour–liquid equilibrium data of associated mixtures by means of a lattice–fluid model, 4381
Thermogravimetry
Transformation of cerium(III) hydroxycarbonate into ceria. Part 1.—Nucleation and growth rates of ceria, 4431
Thermokinetics
Kinetics by thermometry: An aldol condensation reaction, 991
Thiazylfluoroformate
Theoretical and experimental studies on the novel thiazylfluoroformate, FC(O)SN, 231
Thin film stability
Liquid droplets and solid particles at surfactant solution interfaces, 2681
Thiocyanate
Aggregation of alkaline-earth-metal thiocyanates in aprotic donor solvents, 4395
Mechanism of formation of copper thiocyanate on the copper anode, 4403
Thiocyanate dosimeter
Re-evaluation of the thiocyanate dosimeter for pulse radiolysis, 279
Thiourea
Simultaneous adsorption of thiourea and thiocyanate ions on mercury electrodes. Part 1.—Influence of thiourea on anion adsorption, 1005
Thiyl radical
Determination of absolute rate constants for the reversible hydrogen-atom transfer between thiyl radicals and alcohols or ethers, 1923
Three-component system
Comparison of activity coefficients in the three-component system sodium chloride–sucrose–water from independent isopiestic and emf measurements at 298.15 K, 1457
Three-phase system
Solvent composition dependence of the voltage generation and the electric pulse formation in the water–nitrobenzene–water liquid membrane system, 895
Threshold energy
Collision-induced desorption of water from Ru(001), 3655
Thymol blue
Kinetics and mechanism of the reaction between thymol blue and bromate in acidic medium, 1635
Tiling
Classification scheme for toroidal molecules, 4037
Time-domain reflectometry
Temperature- and frequency-dependent dielectric studies of *p*-fluorophenylacetonitrile–methanol mixtures using time-domain reflectometry, 623
Time-of-flight mass spectrometry
Formation and coalescence of fullerene ions from direct laser vaporization, 987
Time-resolved atomic emission spectroscopy
Kinetic investigation of energy pooling from $Sr[5s5p(^3P_J)]$ studied by time-resolved atomic emission following pulsed dye-laser excitation, 811
Time-resolved fluorescence spectroscopy
Characterisation of hydroxide complexes of uranium(VI) by time-resolved fluorescence spectroscopy, 2275
Time-resolved IR spectroscopy
Time-resolved IR studies of gas-phase photochemistry of $Co(CO)_3NO$, 847
Time-resolved microwave conductivity
Solvent-dependent switching between two dipolar excited states in a rigidly extended trichromophoric system, 2107
Titania
Surface chemistry of silica–titania-supported chromium oxide catalysts, 953
Investigations on hydrogen spillover. Part 1.—Electrical conductivity studies on titanium dioxide, 1091
Oxydehydrogenation of propane on V_2O_5/TiO_2 catalyst: Kinetic and mechanistic aspects, 2899
Acidic and basic properties of titania–alumina mixed oxides: Active sites for propan-2-ol dehydration, 2907
Characterisation of bandgap states in V-doped TiO_2 by high-resolution X-ray photoemission spectroscopy, 3495
Photogenerated chloride ion concentration near the surface of UV-irradiated titanium dioxide in the presence of aqueous 2,4-dichlorophenol probed using an ultramicroelectrode, 3893
Titania–silica mixed oxide
Effect of tetrahedral Ti in titania–silica mixed oxides on epoxidation activity and Lewis acidity, 1261
Titanium dopant
Mixed-valence formation in highly oriented Ti-doped iron oxide film, 2161
Titanium halide
Ab initio calculations of titanium NMR chemical shifts including the use of effective core potential basis sets, 1735
Titration spectrophotometry
Solvation and complexation equilibria of nickel(II) thiocyanato complexes in *N*,*N*-dimethylacetamide, 2313
TOF mass spectrometry
(1 + 1) Resonance-enhanced multiphoton ionization spectroscopy of jet-cooled C_2H_2, C_2HD and C_2D_2 in the range 46 400–48 400 cm^{-1}, 3327
Toroidal molecule
Symmetry extensions of Euler's theorem for polyhedral, toroidal and benzenoid molecules, 3089
Classification scheme for toroidal molecules,

4037
TPRS
Dehydrogenation, hydrogenation, exchange and combustion reactions of aromatic hydrocarbons on Pd(100), 3685
TPSSIMS
Mechanism of the conversion of ethene to ethylidyne on rhodium (111): Evidence for a vinylic intermediate, 3679
Trajectory calculation
Molecular dynamics of dissociative electron attachment in water, 2249
Zero-point energy problem in molecular dynamics caculations, and an improved method for sampling trajectories, 3747
Trajectory study
Quasiclassical trajectory studies of $N(^2D) + H_2$ reaction on a fitted *ab initio* potential-energy surface, 3771
Transfer activity coefficient
Stabilities in water of 1 : 1 lariat 16-crown-5 complexes with metal ions: Transfer activity coefficients from protic to aprotic solvents of 1 : 1 complexes of lariat and substituted 16-crown-5 derivatives with metal ions, 4079
Transfer RNA
Thermodynamic properties of transfer RNA: A computational study, 2531
Transfer thermodynamics
Thermodynamic study of the partitioning of organic compounds between water and octan-1-ol. Effects of water as cosolvent in the organic phase, 649
Transient species
High-resolution spectroscopic study of the oxidation of white phosphorus, 2993
Transition-metal catalyst
Surface science and catalysis of ethylene hydrogenation, 3671
Transition-metal ion dimers
Transition-metal ion dimers formed in CeO_2: An EPR study, 99
Translational diffusion constant
Simple EPR method for measuring translational diffusion constants, 887
Transmission electron microscopy
Studies of copper hydride. Part 2.—Transmission electron microscopy, 719
Trichromophoric system
Solvent-dependent switching between two dipolar excited states in a rigidly extended trichromophoric system, 2107
Trimer cluster
EPR spectrum of an acute-angled Na_3 cluster in an adamantane matrix, 3799
Triol
Volumetric study of mixed micelles of hexane-1,2-diol and some alkane-1,2,3-triols, 4105
Trioxane
Detection of the plastic-crystalline transition of trioxane by positron annihilation lifetime spectroscopy, 3185
Triplet state
The allene dication: Calculated and measured singlet-electronic-state energies, 1181
Combined experimental and computational investigation of the double ionization of $(CH_3)_4M$ molecules (M = Si, Ge, Sn and Pb), 1901
Laser flash photolysis studies on hydrogen atom abstraction from phenol by triplet naphthoquinones in acetonitrile, 2751
Tropospheric chemistry
High-level *ab initio* study of the reaction of OCS with OH radicals, 793
Tungsten
Temperature-dependent studies of the reaction of W(a ^5D_J, a $^7S_3$) with O_2, 3787
Tungsten hexacarbonyl
Chemiluminescence in 5 μm multiple-photon decomposition of $W(CO)_6$ in the presence of O_2, 597
Tunnel effect
Tunnel effects in oxidative addition reaction of methane to bare Pd atom, 3779
UHV technique
Surface chemistry of methyl groups adsorbed on Pt(111), 3619
Ultrasonic absorption
Specific micellar catalytic effects of the protolysis of *o*-benzoic acid derivatives studied by the ultrasonic absorption method, 3525
Ultrasonic absorption of nitrobenzene–isooctane mixtures of non-critical composition, 3889
Ultrasonic relaxation
Ultrasonic investigation of the viscosity dependence of the rate constants of rotational isomerism of dibromoethane and dibromopropane in solution, 445
Ultrasonic velocity
Volumetric properties of binary mixtures of water with methoxy(ethoxy)$_n$ ethanols, 2291
Ultrasonic velocity, conductivity, viscosity and calorimetric studies of copper(I) and sodium perchlorates in cyanobenzene, pyridine and cyanomethane, 2789
Corrigendum to Volumetric properties of binary mixtures of water with methoxy(ethoxy)$_n$ ethanols, 3553
Ultrasound
Investigation of the consumption of diphenylpicrylhydrazyl in solution in the absence and presence of ultrasound, 1067
Sonochemical dissolution of MnO_2 colloids, 2843
Ultra-thin film
Ultra-thin particulate films prepared from capped and uncapped reverse-micelle-entrapped silver particles, 673
UPS
Interaction of carbon dioxide with oxidised La/Cu(111), 3611
Uranium
Characterisation of hydroxide complexes of uranium(VI) by time-resolved fluorescence spectroscopy, 2275
Semiconductive properties of some uranium–antimony oxide phases used as catalysts in the mild oxidation of but-1-ene to butadiene, 2343
Urea
Effects of ureas on the kinetics of acid hydrolysis of 1-phenylethyl nitrite in water and in aqueous micellar solutions of sodium dodecyl sulfate, 1349
Effect of urea and surfactant on *p*-nitrophenol at the water surface: a surface second-harmonic generation study, 1769
Urethane polymer
Opposite electrorheological effects between urethane-based polymers having different terminal groups, 1051
UV absorption spectroscopy
Kinetics of reactions of primary, secondary and tertiary β-hydroxy peroxyl radicals. Application to isoprene degradation, 1911
A spectroscopic study of Cl_2O_3, 3027
UV excitation spectroscopy
Vacuum UV fluorescence excitation spectroscopy of BCl_3. Electronic spectroscopy of BCl_2, BCl_2^+, and BCl_3^+, 3073
UV–VIS absorption spectroscopy
Resonance Raman study of the chromophore-specific vibrational and electronic spectra of bilirubin, 1751
UV–VIS emission spectroscopy
Chemiluminescence in 5 μm multiple-photon decomposition of $W(CO)_6$ in the presence of O_2, 597
Valence bond
Model to study delocalization, 241
Modern valence-bond description of $(CH_3)_4Li_4$, 3363
Aromatic electrophilic substitution. A modern valence bond study, 4011
Vanadia
Oxydehydrogenation of propane on V_2O_5/TiO_2 catalyst: Kinetic and mechanistic aspects, 2899
FTIR studies of the interaction of aromatic hydrocarbons with vanadium oxide layered on ZrO_2 and TiO_2, 3505
Vanadium
Insertion of vanadium or molybdenum as oxides in LaNaY zeolite: Comparison with NaY, 1037
Vanadium complex
Ab initio MO study of the molecular structure, vibrational frequencies and bond dissociation energy of bis(2,4-pentanedionato-*O*,*O*') oxovanadium(IV), 2709
Vanadium pentoxide–tungsten trioxide
Phases in vanadium pentoxide–tungsten trioxide catalysts, 145
Vanadium phosphate catalyst
Electrical properties of doped vanadium phosphate phases and VPO catalysts used in the partial oxidation of *n*-butane to maleic anhydride, 3231
Vanadium phosphorus oxide
Redox interaction of ammonia with $(VO)_2P_2O_7$, 725
Vanadyl dimer
EPR of vanadium in $Ce_{0.25}H_3PVMo_{11}O_{40}$ catalyst. Formation of vanadyl dimers during the oxidative dehydrogenation of isobutyric acid, 1025
Vapour–liquid equilibrium
Vapour–liquid equilibrium of the ethanol–propanal system, 273
Influence of static electric field on the vapour–liquid coexistence of dipolar soft-sphere fluids, 889
VAPSO
Synthesis and characterization of VAPSO-44 and VAPSO-5, 1173
VEELS
Trapping of metastable oxygen species at Cu(111) surfaces, 2885
Velocity cross-correlation
Analysis of velocity cross-correlation and preferential solvation for the system *N*-methylpyrrolidone–water at 20 °C, 1339
Vesicle
Vesicle–surfactant interactions: Effects of added surfactants on the gel to liquid-crystal transition for two vesicular systems, 4275
Vibrational level
Chemiluminescence from the reactions of nitrogen and oxygen atoms with phosphorus vapour, 2989
Vibrational Raman optical activity
Vibrational Raman optical activity of lysozyme: Hydrogen–deuterium exchange, unfolding and ligand binding, 2087
Vibrational spectroscopy
Electronic spectroscopy of size-selected ionic complexes, 91
Derivation of accurate kinetic and potential-energy functions for several simultaneous large-amplitude vibrations: Application to acetaldehyde in the S_0 and T_1 states, 399
Vibrational structure
High-resolution IR spectrosopy of jet-cooled CF_3CH_2F, 1723
Vibration–rotational spectroscopy
Vibration–rotational spectra of GaF and molecular properties of diatomic fluorides of elements in Group 13, 3007
Vibration–rotation level
Millimetre-wave electronic spectrum of the D_2^+ ion, 1887
Vibration–rotation parameter
High-resolution spectroscopic study of $2\nu_1$, $2\nu_3$ and $\nu_1 + \nu_3$ stretching states: The local-mode effects of H_2Se, 13
Virial coefficient
Experimental determination of second density virial coefficients of xenon and chlorine at elevated temperatures, 1277
Viscoelasticity
Measurement of viscoelastic changes at electrodes modified with redox hydrogels with a quartz crystal device, 4083
Viscometry
Effect of temperature on poly(ethylene oxide) chains in aqueous solution. A viscometric, ^1H NMR and Raman spectroscopic study, 3897
Viscosity
Ultrasonic investigation of the viscosity dependence of the rate constants of rotational isomerism of dibromoethane and dibromopropane in solution, 445
Shear and extensional viscosity characteristics of a series of hydrophobically associating polyelectrolytes, 911
Studies of poly(styrene) solutions in an electric field: Viscosity and dynamic light scattering, 1357
Experimental determination of molecular radii using a microwave attenuation method, 2733
Partitioning of entropy of solvation: Single-ion

entropy of solvation in aqueous and non-aqueous solvents and the correlation of electrostatic entropy of solvation with electrostriction viscosity *B* and NMR *B'* coefficients, 3373
Mutual-diffusion coefficients and viscosities for the water–2-methylpropan-2-ol system at 15 and 25 °C, 4071
Effect of temperature and viscosity on intramolecular charge-transfer fluorescence of a 4-*p*-dimethylaminostyrylpyridinium salt in protic solvents, 4199
Voltage generation
Solvent composition dependence of the voltage generation and the electric pulse formation in the water–nitrobenzene–water liquid membrane system, 895
Voltammetry
Voltammetric and NMR studies of a bis(ferrocenecarboxamide)-substituted diaza 18-crown-6 receptor that simultaneously complexes and electrochemically recognises both cations and anions, 295
Imaging local mass-transfer rates within an impinging jet and studies of fast heterogeneous electron-transfer kinetics using the microjet electrode, 899
Volume
Volume properties of some linear and ring oligomer solutions, 2797
Vulcanization
Computer simulation of sulfur vulcanization, 2655
Water
Molecular dynamics of dissociative electron attachment in water, 2249
Comparison of the water perturbations induced by two small organic solutes: *Ab initio* calculations and molecular dynamics simulation, 3803
Preferential solvation controlled by clustering conditions of acetonitrile–water mixtures, 4063
Water–acetonitrile
Thermodynamic transfer properties for Na^+, Tl^+ and Ag^+ to water–acetonitrile mixtures, 875
Water-ice film
Optical effects in the IR reflection–absorption spectra of thin water-ice films on metal substrates, 4005
Wavefunction
Modern valence-bond description of the ground state of Li_2^-, 3751
Weakly bound complex
The bπ*ao* complex $C_2H_2\cdots Cl_2$ characterised by rotational spectroscopy as an intermediate in a reactive mixture of ethyne and chlorine, 1891
Wetting
Liquid droplets and solid particles at surfactant solution interfaces, 2681
Work function
CF_3I adsorption on InSb(001), 3603
Interaction of carbon dioxide with oxidised La/Cu(111), 3611
Xanthine derivative
Transformation reactions of the electron adducts of methyl derivatives of xanthine in aqueous solution by pulse radiolysis, 615
Xenon
Experimental determination of second density virial coefficients of xenon and chlorine at elevated temperatures, 1277
Xerogel
Fluorescence spectra of methyl salicylate during the sol–gel–xerogel transitions of mixed silicon–aluminium alkoxides, 4279
XPS
X-Ray photoelectron spectrum of glassy B_2S_3. Experimental and theoretical study, 93
Secondary ion mass spectroscopy and X-ray photoelectron spectroscopy of Na_2MoO_4/SiO_2 catalysts for methane oxidative coupling, 381
Effect of fluoride ions on the acidic and catalytic properties of beta zeolite, 539
Is the observed hydrogenation of formate the rate-limiting step in methanol synthesis?, 1267
Mixed-valence formation in highly oriented Ti-doped iron oxide film, 2161
XPS and LEED studies of 10,11-dihydrocinchonidine adsorption at Pt(111). Implications for the role of cinchona alkaloids in enantioselective hydrogenation, 2167
Optical absorption and X-ray photoelectron spectroscopic studies of thorium tetrabromide, 2767
Trapping of metastable oxygen species at Cu(111) surfaces, 2885
Surface composition, structural and chemisorptive properties of Raney nickel catalysts, 2891
Characterisation of bandgap states in V-doped TiO_2 by high-resolution X-ray photoemission spectroscopy, 3495
Effects of silicate ions on the formation and transformation of calcium phosphates in neutral aqueous solutions, 3499
Valence-band and core photoelectron spectroscopic studies of molybdenum aqueous oxidation and the influence of argon-ion etching, 3593
Interaction of carbon dioxide with oxidised La/Cu(111), 3611
Radiofrequency-induced plasma polymerisation of propenoic acid and propanoic acid, 3907
Spectroscopic investigation of the molybdenum active sites on Mo^{VI} heterogeneous catalysts for alkene epoxidation, 3969
Surface basicity of a new family of catalysts: Aluminophosphate oxynitride (AlPON), 4477
X-Ray absorption spectroscopy
Structure of Fe, Mn-promoted sulfated zirconia catalyst by X-ray and IR absorption spectroscopies, 1825
Studies on the pre-edge region of the X-ray absorption spectra of copper(I) oxide and the diamminecopper(I) ion, 3189
X-Ray crystallography
Structural and spectroscopic investigations of aminocyclopropenium cations, $[C_3(Nr_2)_3]^+$ (NR_2 = NMe_2, NEt_2, NC_5H_{10} or NC_4H_8O) and $[C_3(NPr^i_2)_2Cl]^+$, 1523
Variable-temperature X-ray crystallographic and magic-angle spinning NMR spectral studies on hexaethylbenzene, 2149
X-Ray diffraction
Intramolecular hydrogen bonding in *N*-salicylideneanilines. X-Ray diffraction and solid-state NMR studies, 77
Phases in vanadium pentoxide–tungsten trioxide catalysts, 145
Synthesis of faujasite zeolites with crown-ether templates, 167
Low-temperature single-crystal X-ray diffraction ^1H and ^{13}C solid-state NMR and ^{14}N NQR studies of 1,8-bis(dimethylamino) naphthalene, 3925
Studies of copper hydride. Part 1.—Synthesis and solid-state stability, 713
Characterization of precipitates formed from the tetraiodomercurate(II) anion and mercury(I) or silver(I) cations, 1217
Mixed-valence formation in highly oriented Ti-doped iron oxide film, 2161
X-Ray powder diffraction
Solid-state NMR and powder XRD studies of the structure of SAPO-40 upon hydration–dehydration cycles, 2213
Cation location and migration in lathanum-exchanged zeolite NaY studied by X-ray powder diffraction and MAS NMR spectroscopy, 1813
***P*-Xylene**
Analysis of bimodal frequency-response behaviour of *p*-xylene diffusion in silicalite-1, 2027
Yield stress
Theory and experiments for evaluating the number and the dimensions of solid particles dispersed in a liquid medium. Application to the system $Si_3N_4/H_2O(1)$, 323
Young's modulus
Auxetic two-dimensional polymer networks. An example of tailoring geometry for specific mechanical properties, 2671
Yttria
Alkene oxidation over the Au | yttria-stabilised zirconia | Ag system, 1111
Alkene oxidation over the (Pb,Bi)MoO_4/Au | yttria-stabilized zirconia | Ag system, 1125
Yttria-stabilized zirconia
Partial oxidation of CH_4 to synthesis gas using an Rh | YSZ | Ag electrochemical membrane reactor, 1655
Zeolite
Cadmium-exchanged Y zeolites studied with carbon monoxide and xenon as probes, 163
Synthesis of faujasite zeolites with crown-ether templates, 167
IR spectroscopic study of acid sites in mordenites fluorinated under mild conditions, 385
Atom pair potential for molecular dynamics simulations of structural and dynamical properties of aluminosilicates: Test on silicalite and anhydrous Na-A and Ca-A zeolites and comparison with experimental data, 525
Type III isotherms for the adsorption of ethanol–water mixtures on solid adsorbents, 535
Effect of fluoride ions on the acidic and catalytic properties of beta zeolite, 539
Effect of fluoride ions on the acidic and catalytic properties of beta zeolite, 539
Coadsorption of xenon and carbon monoxide in cadmium-exchanged zeolite Y studied with ^{129}Xe NMR spectroscopy, 555
^2H NMR studies of single-component adsorption in silicalite: A comparative study of benzene and *p*-xylene, 559
Effect of Pt particle size on H/D exchange of methane over alumina- and zeolite-supported catalysts, 569
Time-resolved diffuse reflectance of electron trapping by alkali-metal cation clusters in zeolites and clays following far-UV excitation, 759
Reversible and irreversible adsorption of nitrogen monoxide on cobalt ion-exchanged ZSM-5 and mordenite zeolites at 273–523 K, 767
^2H NMR studies of binary adsorption in silicalite, 963
Adsorbed phase composition in liquid-phase adsorption of organic compounds from aqueous solutions on hydrophobic zeolites, 971
Insertion of vanadium or molybdenum as oxides in LaNaY zeolite: Comparison with NaY, 1037
Frequency-response study of micro- and macro-pore diffusion in manufactured zeolite pellets, 1399
Propane conversion of dry-air-calcined HZSM-5 zeolite, 1689
Adsorption characteristics and reactions of propyne on microporous crystals, 1707
Cation location and migration in lathanum-exchanged zeolite NaY studied by X-ray powder diffraction and MAS NMR spectroscopy, 1813
In-situ IR monitoring of the acidic and structural variations of mordenite caused by pressure and temperature, 1835
Characterisation of the acidity of well defined Cu-ZSM-5 catalysts using pyridine as a probe molecule, 1841
FTIR study of the kinetics of solid-state ion exchange in zeolites using pyridine as a probe, 1845
Analysis of bimodal frequency-response behaviour of *p*-xylene diffusion in silicalite-1, 2027
Use of combination modes and overtones of metal carbonyls for the IR study of cation states in zeolites: Copper(I) carbonyls in reduced CuNaY zeolites, 2035
V–Ti and V–Al silicate molecular sieves of MFI topology: Synthesis and characteristics, 2217
Cationic mobility in MgX zeolite: An FTIR study, 2961
Selective catalytic reduction of nitric oxide with ammonia on MFI-type ferrisilicate, 3275
Reversible interaction of NH_3 with the framework of template-free zeolite-type SAPO-34, 3281
Formation of $Cu^I—N_2$ adducts at 298 and 77 K in Cu^I-ZSM-5: An FTIR investigation, 3285

Formation of $Cu^{I}-N_2$ adducts at 298 and 77 K in Cu^{I}-ZSM-5: An FTIR investigation, 3285
Comparison of $Pd(NH_3)_4^{2+}$ decomposition and Pd^{2+} reduction in zeolites NaY, NaX and CsX, 3291
Synthesis, characterisation and catalytic performance of the solid acid DAF-1, 3537
Multinuclear MAS NMR spectroscopic study of the zeolite, MCM-22, 3549
Catalysed cyclotrimerisation of acetylene: A computational study, 3975
Nickel ion-exchanged zeolite-4A: Reduction behaviour of nickel and structure stability, 3983
Adsorbate interactions of paramagnetic palladium species in Pd^{II}-exchanged H-rho zeolite characterized by EPR and electron spin echo modulation spectroscopies, 3987
^{29}Si MAS NMR study of a highly siliceous EUO-type material, 4309
Computer simulation studies on the role of templating organic molecules in the synthesis of ZSM-5, 4313
Computer simulation studies on the role of templating organic molecules in the synthesis of ZSM-5, 4313

Zeolite crystallization
A simple model for the kinetic evaluation of zeolite crystallization processes, 549

Zeotype
Reduction of copper(II) with subsequent disproportionation of copper(I) during the hydrothermal syntheses of microporous silicoaluminium phosphates SAPO-5 and -11, 3529

Zero-point energy
Zero-point energy problem in molecular dynamics caculations, and an improved method for sampling trajectories, 3747

Zinc oxide
Diversity of the kinetics of carbon monoxide oxidation on differently prepared zinc oxides, 1391
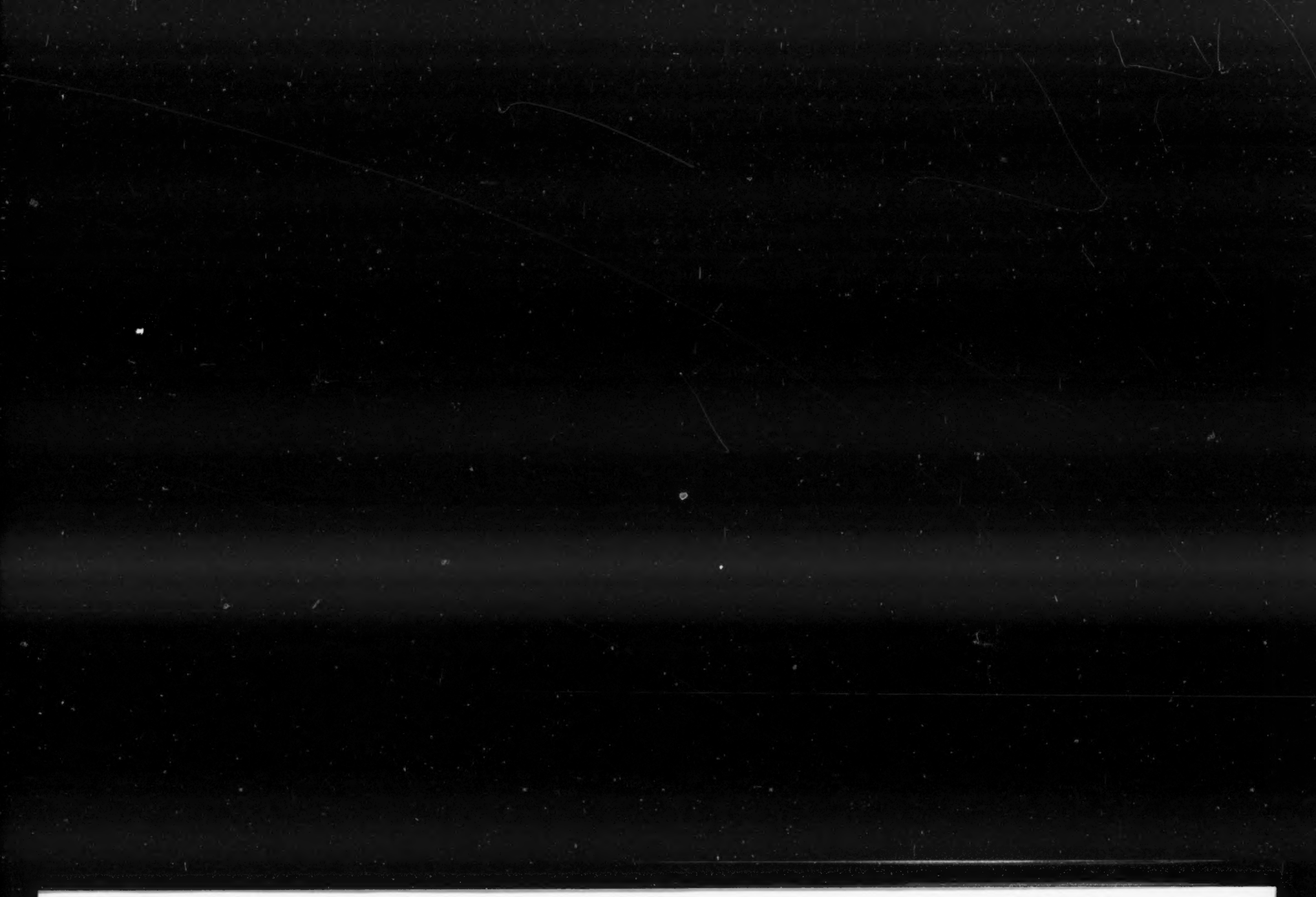
Zirconia
Surface characterisation of yttria-stabilized tetragonal ZrO_2. Part 2.— Adsorption of CO, 113
Surface characterization of yttria-stabilized tetragonal ZrO_2. Part 3.—CO_2 adsorption and the CO_2–CO interaction, 125
Alkene oxidation over the Au | yttria-stabilised zirconia | Ag system, 1111
Alkene oxidation over the (Pb,Bi) MoO_4/Au | yttria-stabilized zirconia | Ag system, 1125
Structure of Fe, Mn-promoted sulfated zirconia catalyst by X-ray and IR absorption spectroscopies, 1825
Effects of citrate adsorption on the interactions between zirconia surfaces, 2921
Dehydration of 4-methylpentan-2-ol over zirconia catalysts, 3263
In situ FTIR studies of high-temperature adsorption of hydrogen on zirconia, 4441